

# **N**uclear Power Plant Components and Structures under Severe Accident Loading (COSSAL)

Final Report



**NUCLEAR ENERGY AGENCY  
COMMITTEE ON THE SAFETY OF NUCLEAR INSTALLATIONS**

**Nuclear Power Plant Components and Structures under Severe Accident Loading  
(COSSAL): Final Report**

This document is available as PDF only.

**JT03450315**

## ORGANISATION FOR ECONOMIC CO-OPERATION AND DEVELOPMENT

The OECD is a unique forum where the governments of 36 democracies work together to address the economic, social and environmental challenges of globalisation. The OECD is also at the forefront of efforts to understand and to help governments respond to new developments and concerns, such as corporate governance, the information economy and the challenges of an ageing population. The Organisation provides a setting where governments can compare policy experiences, seek answers to common problems, identify good practice and work to co-ordinate domestic and international policies.

The OECD member countries are: Australia, Austria, Belgium, Canada, Chile, the Czech Republic, Denmark, Estonia, Finland, France, Germany, Greece, Hungary, Iceland, Ireland, Israel, Italy, Japan, Korea, Latvia, Lithuania, Luxembourg, Mexico, the Netherlands, New Zealand, Norway, Poland, Portugal, the Slovak Republic, Slovenia, Spain, Sweden, Switzerland, Turkey, the United Kingdom and the United States. The European Commission takes part in the work of the OECD.

OECD Publishing disseminates widely the results of the Organisation's statistics gathering and research on economic, social and environmental issues, as well as the conventions, guidelines and standards agreed by its members.

## NUCLEAR ENERGY AGENCY

The OECD Nuclear Energy Agency (NEA) was established on 1 February 1958. Current NEA membership consists of 33 countries: Argentina, Australia, Austria, Belgium, Canada, the Czech Republic, Denmark, Finland, France, Germany, Greece, Hungary, Iceland, Ireland, Italy, Japan, Korea, Luxembourg, Mexico, the Netherlands, Norway, Poland, Portugal, Romania, Russia, the Slovak Republic, Slovenia, Spain, Sweden, Switzerland, Turkey, the United Kingdom and the United States. The European Commission and the International Atomic Energy Agency also take part in the work of the Agency.

The mission of the NEA is:

- to assist its member countries in maintaining and further developing, through international co-operation, the scientific, technological and legal bases required for a safe, environmentally sound and economical use of nuclear energy for peaceful purposes;
- to provide authoritative assessments and to forge common understandings on key issues as input to government decisions on nuclear energy policy and to broader OECD analyses in areas such as energy and the sustainable development of low-carbon economies.

Specific areas of competence of the NEA include the safety and regulation of nuclear activities, radioactive waste management and decommissioning, radiological protection, nuclear science, economic and technical analyses of the nuclear fuel cycle, nuclear law and liability, and public information. The NEA Data Bank provides nuclear data and computer program services for participating countries.

This document, as well as any data and map included herein, are without prejudice to the status of or sovereignty over any territory, to the delimitation of international frontiers and boundaries and to the name of any territory, city or area.

Corrigenda to OECD publications may be found online at: [www.oecd.org/about/publishing/corrigenda.htm](http://www.oecd.org/about/publishing/corrigenda.htm).

### © OECD 2019

You can copy, download or print OECD content for your own use, and you can include excerpts from OECD publications, databases and multimedia products in your own documents, presentations, blogs, websites and teaching materials, provided that suitable acknowledgement of the OECD as source and copyright owner is given. All requests for public or commercial use and translation rights should be submitted to [neapub@oecd-nea.org](mailto:neapub@oecd-nea.org). Requests for permission to photocopy portions of this material for public or commercial use shall be addressed directly to the Copyright Clearance Center (CCC) at [info@copyright.com](mailto:info@copyright.com) or the Centre français d'exploitation du droit de copie (CFC) [contact@cfcopies.com](mailto:contact@cfcopies.com).

---

## *COMMITTEE ON THE SAFETY OF NUCLEAR INSTALLATIONS*

The Committee on the Safety of Nuclear Installations (CSNI) is responsible for the Nuclear Energy Agency (NEA) programmes and activities that support maintaining and advancing the scientific and technical knowledge base of the safety of nuclear installations.

The Committee constitutes a forum for the exchange of technical information and for collaboration between organisations, which can contribute, from their respective backgrounds in research, development and engineering, to its activities. It has regard to the exchange of information between member countries and safety R&D programmes of various sizes in order to keep all member countries involved in and abreast of developments in technical safety matters.

The Committee reviews the state of knowledge on important topics of nuclear safety science and techniques and of safety assessments, and ensures that operating experience is appropriately accounted for in its activities. It initiates and conducts programmes identified by these reviews and assessments in order to confirm safety, overcome discrepancies, develop improvements and reach consensus on technical issues of common interest. It promotes the co-ordination of work in different member countries that serve to maintain and enhance competence in nuclear safety matters, including the establishment of joint undertakings (e.g. joint research and data projects), and assists in the feedback of the results to participating organisations. The Committee ensures that valuable end-products of the technical reviews and analyses are provided to members in a timely manner, and made publicly available when appropriate, to support broader nuclear safety.

The Committee focuses primarily on the safety aspects of existing power reactors, other nuclear installations and new power reactors; it also considers the safety implications of scientific and technical developments of future reactor technologies and designs. Further, the scope for the Committee includes human and organisational research activities and technical developments that affect nuclear safety.

## *Table of contents*

<b>Executive summary .....</b>	<b>8</b>
<b>List of abbreviations and acronyms.....</b>	<b>10</b>
<b>1. Background.....</b>	<b>12</b>
<b>2. Survey.....</b>	<b>14</b>
2.1. Objectives and participation .....	14
2.2. Summary of answers.....	14
<b>3. Benchmark study on a large-scale test .....</b>	<b>17</b>
3.1. Problem statement on the large-scale test.....	17
3.1.1. Geometry.....	17
3.1.2. Material data.....	18
3.1.3. Loading conditions.....	23
3.1.4. Test results.....	26
3.1.5. Task matrix.....	30
3.2. Comparison of analysis results on the large-scale test.....	30
3.2.1. Radial and axial displacements .....	32
3.2.2. Wall thickness reduction close to failure .....	39
3.2.3. Comparison of failure times .....	40
<b>4. Benchmark study on pressurised water reactor components.....</b>	<b>42</b>
4.1. Problem statement on pressurised water reactor components.....	42
4.1.1. Objective .....	42
4.1.2. Geometry and boundary conditions of the components .....	42
4.1.3. Material data.....	44
4.1.4. Loading conditions.....	48
4.1.5. Task matrix.....	49
4.2. Comparison of analysis results on pressurised water reactor components .....	50
4.2.1. Main tasks .....	53
4.2.2. Tasks of parametric studies .....	60
4.2.3. Conclusion.....	62
<b>5. Benchmark study on boiling water reactor components .....</b>	<b>64</b>
5.1. Problem statement on boiling water reactor components .....	64
5.1.1. Motivation .....	64
5.1.2. Geometry, loads and boundary conditions .....	64
5.1.3. Material data.....	68
5.1.4. Task matrix.....	69
5.2. Comparison of analysis results on boiling water reactor components .....	69
5.2.1. Local failure of a flange connection.....	69
5.2.2. Local failure of a reactor core instrumentation pipe .....	79

<b>6. Evaluation of the COSSAL workshop.....</b>	<b>81</b>
<b>7. Summary and conclusions .....</b>	<b>84</b>
<b>8. References .....</b>	<b>87</b>

### List of tables

Table 1.1.	Participating countries/organisations in COSSAL activities.....	13
Table 3.1.	Chemical composition of the test pipe material 20 MnMoNi 55 .....	18
Table 3.2.	Elastic modulus of the test material 20 MnMoNi 55 dependent on temperature .....	18
Table 3.3.	Norton parameters .....	21
Table 3.4.	Garofalo parameters .....	22
Table 3.5.	Thermal expansion coefficient (TEC) of the test material 20 MnMoNi 55 dependent on temperature (reference temperature 20 °C).....	22
Table 3.6.	Thermal conductivity .....	23
Table 3.7.	Decrease of wall thickness at different axial/circumferential positions .....	30
Table 3.8.	Reconstruction of the average permanent circumferential strain at different axial/circumferential positions using the distance increment between two markers.....	30
Table 3.9.	Task matrix of the COSSAL benchmark on the large-scale test.....	30
Table 3.10.	Participants and employed simulation methodology.....	31
Table 3.11.	MT3 – Determination of the wall thickness reduction close to failure .....	40
Table 3.12.	MT4 – Determination of failure time .....	40
Table 3.13.	Dependence of failure times on pressure load variation (PS-P).....	41
Table 3.14.	Dependence of failure times on wall thickness variation (PS-W).....	41
Table 4.1.	Geometry data of the simplified components.....	43
Table 4.2.	Linear-elastic data .....	44
Table 4.3.	Norton parameters according to formula (1).....	45
Table 4.4.	Isotropic secant coefficient of thermal expansion .....	45
Table 4.5.	Linear-elastic material data .....	46
Table 4.6.	Norton parameters according to formula (1).....	47
Table 4.7.	Isotropic secant coefficient of thermal expansion .....	48
Table 4.8.	Task matrix of the COSSAL benchmark on a severe accident .....	50
Table 4.9.	Participants and employed simulation methodology.....	51
Table 4.10.	Employed symmetry properties for steam generator tube models (180°).....	51
Table 4.11.	Participants and employed load conditions .....	52
Table 4.12.	Participants and employed boundary conditions of models (main tasks) .....	52
Table 4.13.	Comparison of failure times and temperatures of main tasks MT1 (MCL), MT2 (SL) and MT4 (SGT).....	53
Table 4.14.	Comparison of failure times and temperatures of Main Task 1 (Main coolant line, straight).....	53
Table 4.15.	Comparison of failure times and temperatures of main tasks MT1 (main coolant line, elbow).....	56
Table 4.16.	Comparison of failure times of main tasks 2 (surge line, elbow).....	58
Table 4.17.	Minimum wall thickness of steam generator tube (reference wall thickness 1.23 mm) during accident without failure.....	60
Table 4.18.	Comparison of failure times and temperatures of main task MT4.....	60
Table 4.19.	Comparison of failure times and temperatures of PS-A.....	61
Table 4.20.	Minimum wall thickness of steam generator tube during accident without failure (original wall thickness: 1.23 mm) .....	61
Table 4.21.	Comparison of failure times of PS-C (MT4, SGT, elbow) .....	62

Table 5.1.	Flange data.....	65
Table 5.2.	Bolt data.....	66
Table 5.3.	Gasket data.....	66
Table 5.4.	Task matrix of the third COSSAL benchmark.....	69
Table 5.5.	Overview about different/important boundary conditions.....	70
Table 5.6.	Failure times defined by arising outer gap.....	76
Table 5.7.	Calculated failure times .....	80
Table 6.1.	Organisations that participated in the Workshop.....	81

## List of figures

Figure 3.1.	Geometry of the test specimen.....	17
Figure 3.2.	True stress-strain curves of test material 20 MnMoNi 55 up to uniform elongation and linear extrapolation dependent on temperature .....	19
Figure 3.3.	Load controlled creep curves of test material 20 MnMoNi 55 .....	19
Figure 3.4.	Secondary creep rates .....	21
Figure 3.5.	Internal pressure difference during the experiment .....	24
Figure 3.6.	Positions of temperature sensors at the inside (rectangle marker) and outside (circle marker) of the assembly.....	25
Figure 3.7.	Measured temperatures at selected sensors during the experiment .....	26
Figure 3.8.	Positions of displacement transducers on the outer surface of the test specimen, for radial deformation (empty circle markers) and for axial deformation (filled circle markers) .....	27
Figure 3.9.	Radial displacement of transducers at different positions of the assembly and corresponding average circumferential strain .....	28
Figure 3.10.	Axial displacement of transducers and corresponding average axial strain.....	28
Figure 3.11.	Test specimen after failure .....	29
Figure 3.12.	Cross section of the test specimen at different axial positions close to the time of failure.....	29
Figure 3.13.	Radial displacements during the whole testing time (MT1, PS-F) .....	32
Figure 3.14.	Radial displacements during the period before failure (MT1, PS-F).....	33
Figure 3.15.	Axial displacements during the whole testing time (MT2, PS-F).....	34
Figure 3.16.	Axial displacements during first phase (MT2, PS-F).....	34
Figure 3.17.	Axial displacements during the period before failure(MT2, PS-F).....	35
Figure 3.18.	Radial displacements during the whole testing time (PS-P) .....	35
Figure 3.19.	Radial displacements during the period before failure (PS-P).....	36
Figure 3.20.	Axial displacements during the whole testing time (PS-P).....	36
Figure 3.21.	Axial displacements during the period before failure (PS-P) .....	37
Figure 3.22.	Radial displacements during whole testing time (PS-W).....	37
Figure 3.23.	Radial displacements during last phase of testing (PS-W) .....	38
Figure 3.24.	Axial displacements during whole testing time (PS-W) .....	38
Figure 3.25.	Axial displacements during the period before failure (PS-W).....	39
Figure 4.1.	Drawing of an idealised generic piece representing the components .....	42
Figure 4.2.	Geometry of the coolant loop .....	43
Figure 4.3.	True stress-strain curves .....	44
Figure 4.4.	Secondary creep rates .....	45
Figure 4.5.	True stress-strain rates .....	46
Figure 4.6.	Secondary creep rates .....	47
Figure 4.7.	Component temperatures during transient .....	48



Figure 4.8. Primary and secondary pressure during transient .....	49
Figure 4.9. Equivalent stresses of simulations (MT1, straight).....	54
Figure 4.10. Accumulated plastic strains of simulations (MT1, straight) .....	55
Figure 4.11. Accumulated creep strains of simulations (MT1, straight).....	55
Figure 4.12. Equivalent stresses of simulations (MT1, elbow).....	56
Figure 4.13. Accumulated plastic strains of simulations (MT1, elbow) .....	57
Figure 4.14. Accumulated creep strains of simulations (MT1, elbow) .....	57
Figure 4.15. Equivalent stresses of simulations (MT2, elbow).....	58
Figure 4.16. Accumulated plastic strains of simulations (MT2, elbow) .....	59
Figure 4.17. Accumulated creep strains of simulations (MT2, elbow) .....	59
Figure 5.1. Schematic drawing of the flange /KTA13/ .....	65
Figure 5.2. Schematic drawing of bolt [4].....	66
Figure 5.3. Schematic drawing of the gasket after arising of a gap [4].....	66
Figure 5.4. CAD model of the assembly.....	67
Figure 5.5. Schematic view of a reactor core instrumentation pipe .....	68
Figure 5.6. Example of an FEM model.....	68
Figure 5.7. FE models from Participant 1 (top left), Participant 2 Model A (top right), Model B (bottom left) and Participant 3 (bottom right).....	<b>Error! Bookmark not defined.</b>
Figure 5.8. Inner thermal boundaries from Participant 1 (top left), Participant 2 Model A (top right), Model B (bottom left) and Participant 3 (bottom right).....	72
Figure 5.9. Outer thermal boundaries from Participant 1 (top left), Participant 2 Model A (top right), Model B (bottom left) and Participant 3 (bottom right).....	73
Figure 5.10. History of the outer temperature, measured at the gasket-near edge .....	74
Figure 5.11. History of the radial difference temperature over the flange .....	74
Figure 5.12. History of the outer gap (maximum gap along gasket outer edge) .....	75
Figure 5.13. History of the inner gap (maximum gap along gasket inner edge) .....	76
Figure 5.14. History of the bolt force .....	77
Figure 5.15. History of the clamping force .....	77
Figure 5.16. History of the inner gap during the load application phase.....	78
Figure 5.17. History of the bolt force during the load application phase .....	78

## Executive summary

In the face of severe accident scenarios with melted core material, such as those that occurred at Three Mile Island-2 in 1979 and at Fukushima Daiichi in 2011, the integrity assessment of primary circuit components requires special consideration. The Nuclear Energy Agency (NEA) Working Group on Integrity and Ageing of Components and Structures (WGIAGE) thus established an international initiative to investigate the integrity of Components and Structures under Severe Accident Loading (COSSAL), which is led by Gesellschaft für Anlagen- und Reaktorsicherheit (GRS). The objective of the COSSAL project is to compare structure mechanical analysis methods for integrity assessment of metallic components under severe accident loading, especially under high temperatures, which may occur during core melt scenarios. The two main safety-related issues to be treated from a generic point of view are: i) which metallic component of the pressure boundary loaded by selected severe accident scenarios with high temperatures will fail first, and ii) what are the uncertainties for the integrity assessment and the quantification of safety margins against failure.

The main tasks within the COSSAL project were as follows:

- a survey of analysis methods, material properties and failure criteria;
- a benchmark on a large-scale test with a pipe;
- benchmarks on components of selected pressurised water reactor (PWR) and boiling water reactor (BWR) pressure boundaries;
- a workshop at GRS in Cologne in February 2018.

The results of the survey presented in this report<sup>1</sup> provide an overview of the knowledge and the work that has been performed in the participating organisations.

The analysis results of the benchmark on the large-scale test show that sufficient accuracy in the simulations can be achieved if special numerical boundary conditions (e.g. consideration of large deformations by geometric non-linear calculation) and material models that consider non-linear material properties, especially creep and plasticisation effects, are selected. Finite-Element (FE) models (2D/3D) and analytical models were successfully used to predict the failure time.

The analysis results regarding the benchmark tasks given for PWR components under a station blackout scenario show that all participants concluded that in this case, the main coolant line will fail first, prior to the surge line and the steam generator tubes, without pre-existing damage. The steam generator tube will fail if there is pre-existing wall thinning to less than about 15 % of the original wall thickness. If a modified scenario with heating by circulating gas flow (countercurrent circulation flow) is considered, an early failure of the steam generator tube becomes more probable.

---

<sup>1</sup> Appendices 1 to 7 can be found on the [NEA website](#).

In the benchmark of BWR, components failure of a safety valve with flange connection was investigated under a scenario with increasing temperature and constant pressure derived from best estimate thermal-hydraulic calculations of the Fukushima Daiichi unit 3. The most relevant measures, which influence the differences between the analysis results of the participants concerning failure of the flange connection, are:

- the procedure within the FE code to interpolate creep data dependent on stress and temperature;
- the application of the specified bolt preload;
- the consideration of frictional contact between the bolts and the flange;
- the definition of the distance between the boundaries of the FE model and the region of interest.

The workshop in Cologne allowed participants to discuss the main factors leading to differences in the calculated results on the benchmark tasks. Furthermore, the plenary lectures of the workshop gave an international overview concerning the state of the art on component behaviour under severe accident loading, including interdisciplinary aspects.

Based on the COSSAL results, the overall conclusion is that FE methods for assessment of global failure are precise and robust whereas simplified methods can be partly adequate. These simplified methods may give accurate predictions in failure time, if properly used and application limits are considered.

Future research activities are needed on the assessment of the local failure and integrity of complex components, the size quantification of early leaks, and the consideration of ageing effects/pre-existing damage as well as uncertainties. The accuracy of the failure assessment of the pressure boundary is strongly dependent on the amount of available short-term creep data of the pressure boundary steels. The available databases and public sources of material data are partly incomplete and should be extended to reduce the influence of data approximation/interpolation procedures on the failure assessment.

The assessment of components under severe accident loading is important for the simulation of scenarios by system codes. The structure mechanical behaviour of components, especially the failure of components, has consequences for the thermal-hydraulic behaviour and the dispersion of aerosols in a plant during a severe accident. Therefore, the determination of failure times and modes of components (global/local) is important. In system codes, simplified analysis models for the assessment of component failure are usually implemented. It is important to know the application limits and the accuracies of such models as well as recommendations on proper use. Furthermore, the main factors with their uncertainties should be specified to allow the sensitivities of the results to be investigated. Future interdisciplinary activities between the NEA WGIAGE and the Working Group on Analysis and Management of Accidents (WGAMA) would be useful in assessing the simplified component failure models.

## List of abbreviations and acronyms

BfE	Bundesamt für kerntechnische Entsorgungssicherheit (Federal Office for the Safety of Nuclear Waste Management, Germany)
BWR	Boiling water reactor
CAD	Computer-aided design
COSSAL	Components and Structures under Severe Accident Loading (NEA)
CRIEPI	Central Research Institute of Electric Power Industry (Japan)
CSNI	Committee on the Safety of Nuclear Installations (NEA)
DN	Nominal diameter
EU	European Union
FAD	Failure assessment diagram
FE	Finite-Element
FEM	Finite-Element Method
FORM	First Order Reliability Method
GRS	Gesellschaft für Anlagen- und Reaktorsicherheit (Germany)
IRSN	Institut de Radioprotection et de Sûreté Nucléaire (France)
IVMR	In-vessel melt retention
JAEA	Japan Atomic Energy Agency
JRC	Joint Research Centre
KR	Khachanov-Rabotnov Law
MCL	Main coolant line
MCS	Monte Carlo simulation
MPA	Materialprüfungsanstalt Universität Stuttgart (Germany)
MG	Modified Garofalo Equation
MT	Main task
NEA	Nuclear Energy Agency equation
NRA	Nuclear Regulation Authority (Japan)
NRC	Nuclear Regulatory Commission (United States)
OECD	Organisation for Economic Co-operation and Development
PS	Parametric study

---

PVA	Civil and structural engineering firm (South Africa)
PWR	Pressurised water reactor
RPV	Reactor pressure vessel
SGT	Steam generator tube
SGTR	Steam generator tube rupture
SL	Surge line
SSM	Strålsäkerhetsmyndigheten (Radiation Safety Authority of Sweden)
SÚJB	State Office for Nuclear Safety (Czech Republic)
TEC	Thermal expansion coefficient
WGIAGE	Working Group on Ageing and Integrity of Components and Structures (NEA)
WWER	Water-Water Energetic Reactor (Russia)

## 1. Background

In face of severe accident scenarios with melted core material, such as those that occurred in 1979 at Three Mile Island-2 and in 2011 at Fukushima Daiichi, the integrity assessment of primary circuit components is of special concern. The Nuclear Energy Agency (NEA) Working Group on Integrity and Ageing of Components and Structures (WGIAGE) established an international initiative to investigate the integrity of Components and Structures under Severe Accident Loading (COSSAL). The COSSAL project was approved by the Committee on the Safety of Nuclear Installations (CSNI) in June 2014. The objective of the COSSAL project is to compare structure mechanical analysis methods for integrity assessment of metallic components of selected pressurised and boiling water reactors under severe accident loading, especially under high temperatures which may occur during core melt scenarios. The two main safety-related issues to be treated from a generic point of view are:

- Which metallic component of the pressure boundary loaded by selected severe accident scenarios with high temperatures fails first in selected pressurised and boiling water reactors with/without consideration of ageing aspects?
- What are the uncertainties for the integrity assessment of the metallic components and the quantification of safety margins against failure?

The main tasks within the COSSAL project were:

- a survey on analysis methods, material properties and failure limits/criteria (Task 2);
- a benchmark on a large-scale test with a pipe (Task 3);
- benchmarks on components of selected pressurised water reactor (PWR) and boiling water reactor (BWR) pressure boundaries (Task 4.1 and 4.2);
- a workshop in February 2018 at GRS in Cologne.

The participating teams of the COSSAL activities are from the organisations listed in Table 1.1.

**Table 1.1. Participating countries/organisations in COSSAL activities**

<b>Country</b>	<b>Organisation</b>
Czech Republic	ÚJV Řež
EU	JRC Petten
Finland	PVA
France	IRSN
Germany	GRS / BMWi, MPA Univ. Stuttgart, IWM Freiburg, BfE
Japan	JAEA / NRA, CRIEPI
Slovak Republic	VUJE
Sweden	Kiwa Inspecta / SSM
United States	NRC

## 2. Survey

### 2.1. Objective and participation

The aim of the COSSAL survey was to review analysis methods, material properties and failure limits/criteria used for integrity assessment of steel components under severe accident loading. The survey was conducted by means of a questionnaire given to the participants to complete. The seven participating teams are from the organisations PVA (Finland), GRS (Germany), IWM Freiburg (Germany), MPA University of Stuttgart (Germany), JAEA/NRA (Japan), Kiwa Inspecta/SSM (Sweden) and VUJE (Slovak Republic). The questions were arranged in four parts (general aspects, analysis methods, material properties and failure criteria/failure limits), containing eight questions each.

### 2.2. Summary of answers

The questionnaire on “Engineering Models, Material Properties and Failure Criteria” has been answered by participants of seven teams representing nine organisations from five countries.

Selected results on “General Aspects” are:

- All participants have done assessments of metallic components under transient thermomechanical loading due to design basis accidents in the past, three participants considered beyond-design loads due to core melt scenarios.
- The following components were investigated:
  - reactor pressure vessels or pressure vessels in general (7);
  - piping (5);
  - other components (2).
- Two participants considered components under cyclic loading.
- One participant considered complex models containing more than one component.
- Small-scale experiments were performed by two participants, one performed also large-scale experiments.
- All participants used deterministic approaches (e.g. FEM, ASME XI, R5, R6, API579, BS7910), four used also probabilistic approaches (e.g. FAD, FORM, MCS, Monte Carlo) and four participants carried out sensitivity analyses.

Selected results on “Analysis Methods” are:

- The FEM Codes ABAQUS (3), ANSYS (3), ADINA (3), MSC.Marc (1), Code\_Aster (1) and FINAS (1) were used.
- Reasons stated for the choice of the FEM code were:



- the ability to include user defined material models or elements;
- a broad use in research and industry;
- the capability for simulation of fluid structure interaction;
- licence related reasons.
- All participants used elastic-plastic material models, five considered creep and four used continuum damage models.
- Four participants used a direct or indirect nodal release technique.
- Three participants also used simplified methods (e.g. analytical limit load, net section collapse, failure assessment diagram).
- Five participants validated their analysis methods on experiments.
- Six participants used linear elastic and elastic-plastic fracture mechanics, three used high temperature fracture mechanics, e.g. based on the  $C^*$ -concept.

Selected results on “Material Properties” are:

- The Steels used by participants are: 20MnMoNi55, 16MND5, 22NiMoCr37, Alloy 600, Alloy617B, Alloy 800H, 304H, 316HP, 316SS, 321HTB, C-Mn, 2.25Cr1Mo, 1Cr0.5Mo, A533B-1, X6CrNiNb18-10, 10CrMo9-10, 14MoV6-3, X20CrMoV12-1, P91, X10CrNiNb18-9, 15MnNi6-3, SA533B1.
- Two participants considered the development of material models as a main task of their work.
- Both displacement controlled and force controlled tests were used as basis.
- Ageing effects are considered by the participants in the frame of design basis accidents like embrittlement in the integrity assessment of reactor pressure vessels, fatigue and stress corrosion cracking. Up to now, no participant considered ageing effects in beyond-design accidents like core melt scenarios.
- The extrapolation beyond test data was done in several different ways:
  - full plasticity above the limit load;
  - extrapolation using a Manson-Haferd relations;
  - linear extrapolation;
  - comparison with a similar steel;
  - Arrhenius equation.

Selected results on “Failure Criteria / Failure Limits” are:

- Examples for failure criteria are: limit stress, limit strain, Rousselier, Kachatov-Rabotnov, Larson Miller parameter, plastic instability.
- Six participants used plastic instability, five creep fracture, four brittle fracture and four ductile fracture as failure criterion in their analyses.
- Two participants investigated the microscopic material behaviour in detail.
- Four participants implemented their failure criteria into a code.

- Two participants divided their criteria into an upper bound and a lower bound conservative criterion.
- In most criteria for failure due to plasticity/creep only the dependence of stress and local triaxiality is recognised, some consider also temperature, history of triaxiality, load history, load type and size effects.

The detailed answers of the participants are given in Appendix 1.<sup>2</sup>

---

<sup>2</sup> Appendices 1 to 7 can be found on the [NEA website](#).

### 3. Benchmark study on a large-scale test

The main objective of the first COSSAL benchmark study (Task 3 of the COSSAL project) was to quantify uncertainties in determination of failure time due to creep/plasticisation” of a pipe (DN 700) tested under high temperature and pressure load.

The participants of the benchmark are PVA Engineering Services (Finland), GRS (Germany), JAEA (Japan), Kiwa Inspecta (Sweden) and VUJE (Slovak Republic).

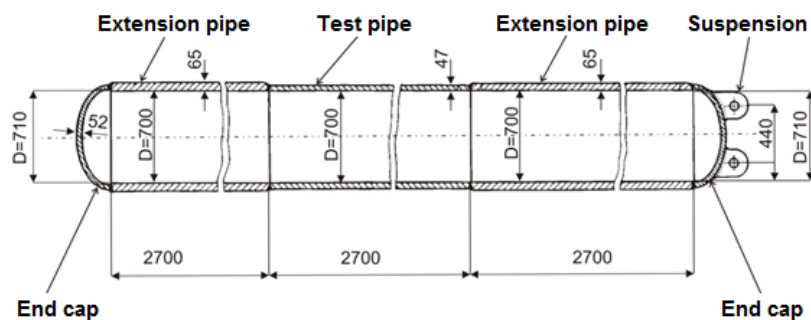
MPA University of Stuttgart performed a large-scale experiment to investigate the creep rupture behaviour of the main coolant line in a high-pressure core melt scenario in 1988 /MPA90/, /MPA88/. A test specimen with similar geometry and material as a straight section of a German PWR main coolant line was assembled together with auxiliary parts to a 10 t heavy test body. The inner pressure was simulated by compressed air and the temperature was applied in three phases using inductive coils. The instrumentation consisted of a manometer, several temperature sensors inside and outside the test body, accelerometers as well as radial and axial displacement transducers. Because of the destructive capacity of the experiment it was conducted at a military test terrain in Meppen (Germany).

#### 3.1. Problem statement on the large-scale test

##### 3.1.1. Geometry

Figure 3.1 shows the geometrical configuration of the test specimen. The actual test pipe was a straight pipe with an inner diameter of 700 mm, a wall thickness of 47 mm and a length of 2 700 mm. The dimensions of the test pipe corresponded to those of a German PWR main coolant line. Ultrasonic wall thickness measurements showed deviations up to +0.3 mm. Extension pipes with an equal inner diameter, a wall thickness of 65 mm and a length of 2 700 mm each were welded to both ends to increase the test volume. The assembly was completed by a top and bottom end cap.

Figure 3.1. Geometry of the test specimen



Via eyelets at the top of the assembly and a chain it was fixed in an upright position and freely suspended to a stiff structure.

### 3.1.2. Material data

The material of the test specimen was the reactor steel 20 MnMoNi 55 (material number 1.6310), a ferritic steel that is used for RPV and piping of German PWR. The upper shelf energy was about 150 J. Chemical analysis of a specimen of the same charge as the test pipe revealed the following proportion of alloying metals (Table 3.1).

**Table 3.1. Chemical composition of the test pipe material 20 MnMoNi 55**

Element	C	Si	Mn	P	S	Cr	Mo	Ni	Cu	Sn	Al	N	V	As
Share	.21	.24	1.48	.008	.005	.20	.52	.80	.07	.005	.015	.007	.02	.02

Before the test pipe and the extension pipes were assembled, a tempering treatment was applied (6.5 h at 920 °C, 7.5 h at 640 °C and 8 h at 660 °C). Ultrasound and surface crack testing revealed no recordable cracks.

The material of the test specimen was characterised by small-scale tensile and creep tests performed at MPA University of Stuttgart /MPA88/ (see sections 2.2.2 and 2.2.3). The raw data are given in Appendix 2.

#### 3.1.2.1 Linear-elastic material data

The data for the linear-elastic behaviour was extracted from tensile tests (Table 3.2).

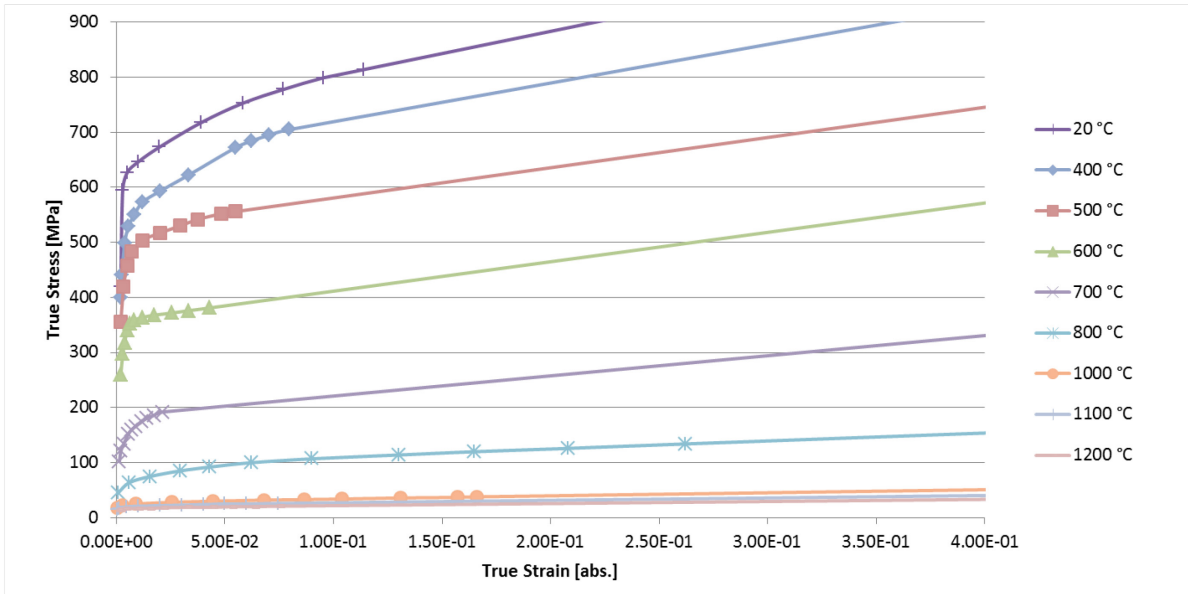
**Table 3.2. Elastic modulus of the test material 20 MnMoNi 55 dependent on temperature**

T (°C)	E (MPa)	Poissons Ratio
20	210 000	0.3
400	200 000	0.3
500	178 000	0.3
600	130 000	0.3
700	75 000	0.3
800	50 000	0.3
1 000	30 000	0.3
1 100	20 300	0.3
1 200	15 600	0.3

#### 3.1.2.2 Tensile tests

The material can be described by temperature-dependent true stress-strain curves, especially beyond the linear-elastic regime (Figure 3.2). The last data points of the solid lines mark the uniform elongations, i.e. the beginning of necking. A linear extrapolation of the lines is suggested due to the lack of data during necking. The raw data of the stress-strain curves in Figure 3.2 are available in Appendix 2.

**Figure 3.2. True stress-strain curves of test material 20 MnMoNi 55 up to uniform elongation and linear extrapolation dependent on temperature**



### 3.1.2.3 Creep tests

Small-scale creep tests had been conducted load controlled. The specimens had a diameter of 10 mm and a length of 50 mm. The test material 20 MnMoNi 55 showed an almost negligible primary creep (Figure 3.3). The raw data of the figures are available in Appendix 2. In addition to the “raw” creep test data additional material data sets were made available which could be used within parametric studies concerning the sensitivity on creep curve approximations.

**Figure 3.3. Load controlled creep curves of test material 20 MnMoNi 55**

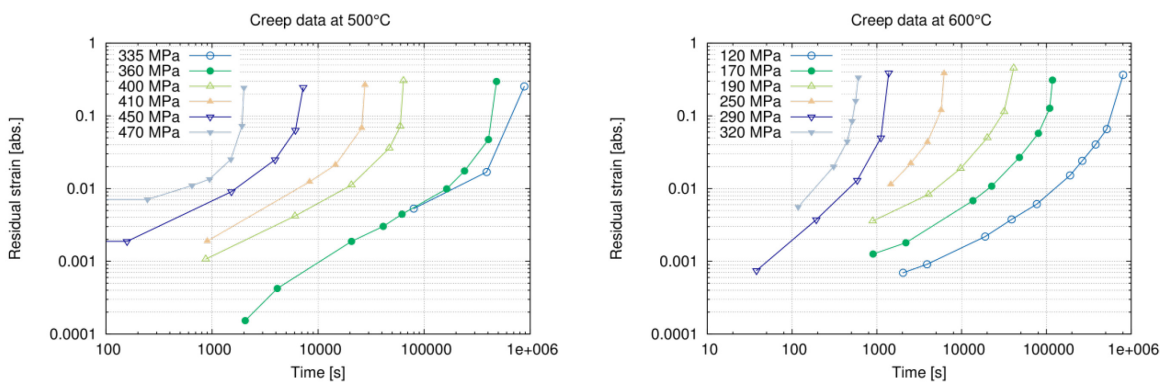
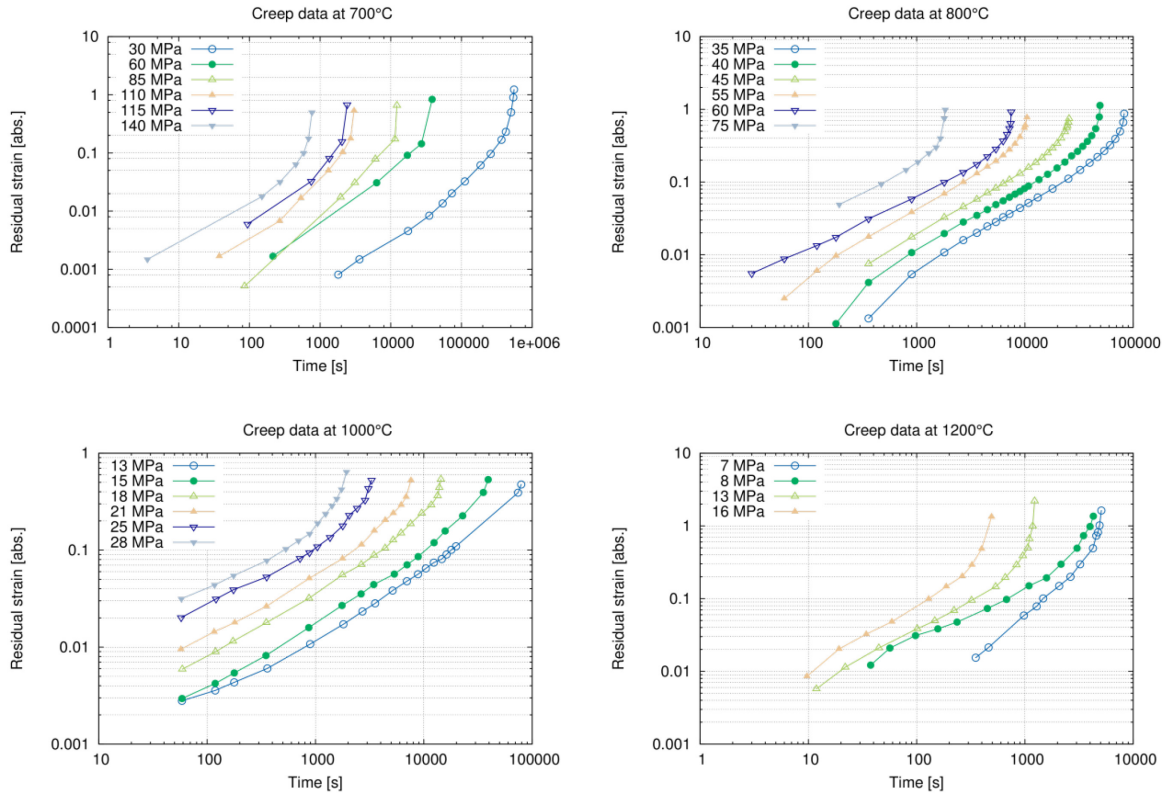
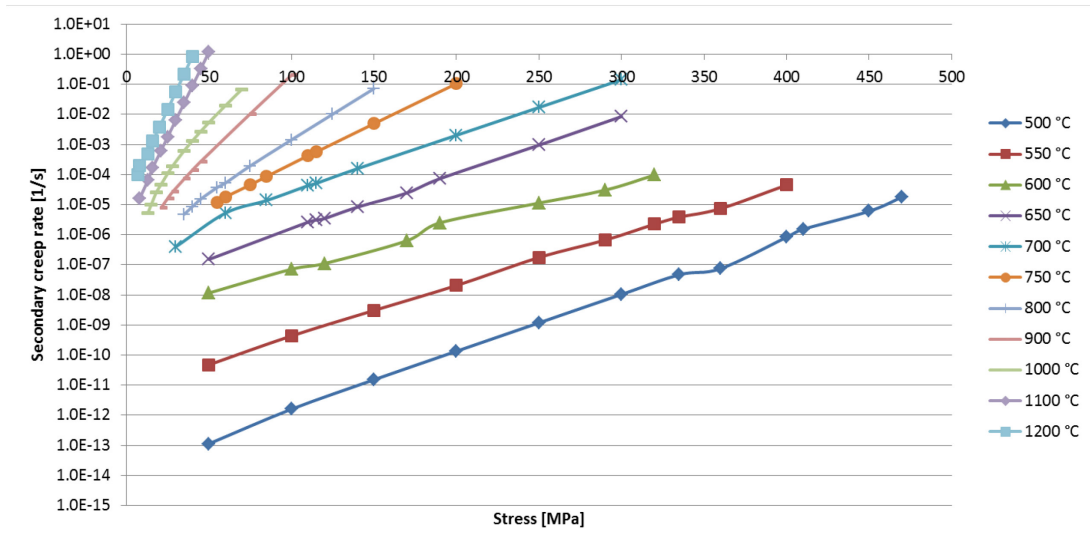


Figure 3.4. Load controlled creep curves of test material 20 MnMoNi 55 (Continued)



While the “raw” creep test data include representation of primary and tertiary creep the additional data sets are based on an extraction of the secondary creep rates from the test data (see Figure 3.4). The creep rates of the additional data sets are only a function of stress and temperature; i. e. the corresponding curves of creep strains are linearly increasing with time. Primary creep and the part of tertiary creep that does not origin from geometric changes are neglected.

Figure 3.5. Secondary creep rates



Due to gaps in the test data, interpolation and extrapolation especially concerning stress dependence are necessary. For the description of the creep strain rates two fittings according to the Norton approach given in formula (1) and the Garofalo approach given in formula (2) were made available.

$$\dot{\epsilon}_{creep} = C_1 \sigma^{C_2} \quad (1)$$

$$\dot{\epsilon}_{creep} = C_1 [\sinh(C_2 \sigma)]^{C_3} \quad (2)$$

The derived parameters are listed in Table 3.3 and Table 3.4 with unit of the stresses is MPa, while the creep strain rate is given in 1/s.

Table 3.3. Norton parameters

T [°C]	C1	C2
500	1.88722E-56	19.0602021
550	8.36453E-35	11.35313377
600	3.78999E-22	6.882836435
650	3.07578E-18	5.812863796
700	1.4062E-12	3.674336439
750	7.74566E-15	5.243964287
800	2.19135E-13	4.740518772
900	5.7015E-12	4.620320954
1 000	3.05842E-11	4.69268647
1 100	5.02839E-09	3.774803925
1 200	5.21031E-07	2.741854798

**Table 3.4. Garofalo Parameters**

T [°C]	C1	C2	C3
500	1.4545E-13	0.016321752	2.660024476
550	4.2715E-11	0.018397043	2.07115078
600	8.5850E-09	0.02049577	1.584948809
650	3.1848E-08	0.048928343	0.894029139
700	1.9953E-06	0.018688294	2.27704201
750	2.9461E-06	0.023958788	2.56119478
800	5.0701E-06	0.02527638	3.088180666
900	1.5172E-05	0.035814148	3.289833198
1 000	3.5049E-04	0.028059538	4.227139562
1 100	1.3169E-05	0.114652622	2.263988589
1 200	2.1676E-05	0.660479839	0.411879972

#### 3.1.2.4 Thermophysical data

While the heat distribution can be assumed as quasi-stationary, the temperature expansion may have induced geometry changes and thermal stresses.

**Table 3.5. Thermal expansion coefficient (TEC) of the test material 20 MnMoNi 55 dependent on temperature (reference temperature 20 °C)**

Temperature [°C]	TEC [1/K]
20	1.1200E-05
400	1.4013E-05
500	1.4335E-05
600	1.4593E-05
700	1.4688E-05
800	1.0501E-05
1 000	1.2669E-05
1 100	1.3583E-05
1 200	1.4420E-05



**Table 3.6. Thermal conductivity**

Temperature [°C]	$\lambda$ [W/mm K]
20	4.28E-02
400	3.68E-02
500	3.51E-02
600	3.22E-02
700	2.96E-02
800	3.25E-02
1 000	2.45E-02
1 100	2.47E-02
1 200	2.48E-02

### 3.1.3. Loading conditions

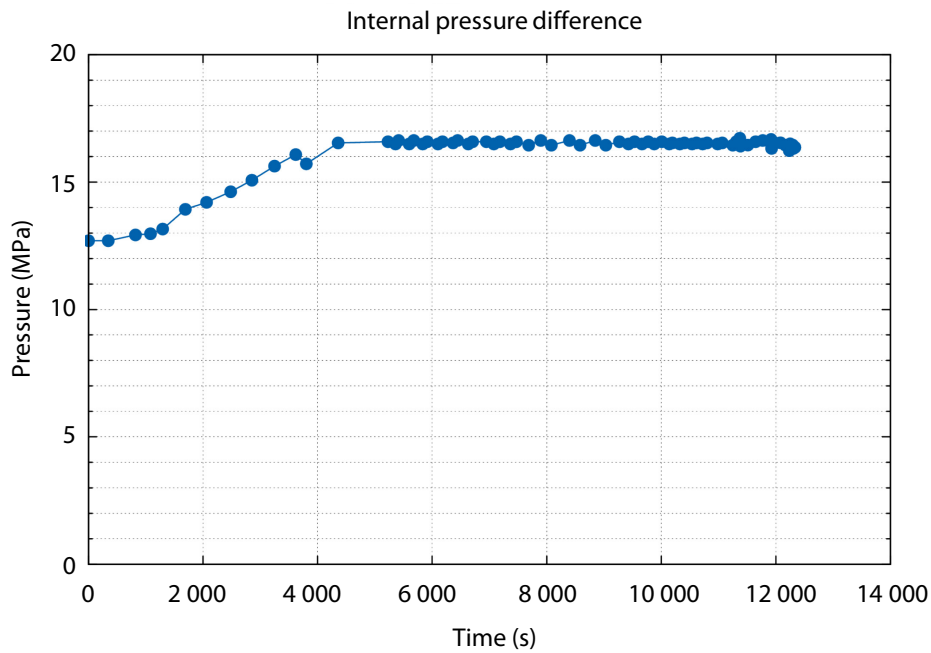
The loading conditions were chosen after typical values that might occur during a high-pressure core melt scenario.

#### 3.1.3.1 Pressure

The pressure was applied using air as medium, high-pressure compressors and a compressed air tank to account for fast volume changes. The inlet nozzle was positioned at the bottom of the assembly. A controller was connected to valves at the compressed air tank and at an exhaust pipe, which accounted for the expansion of the air with increasing temperature.

At  $t = 0$  s, the test body was at room temperature with an inner difference pressure of 12.70 MPa. The difference pressure was increased to about 16.54 MPa within 4 357 s and kept constant with a deviation of +0.13/-0.31 MPa (Figure 3.5). The raw data are available in Appendix 2.

Figure 3.6. Internal pressure difference during the experiment



### 3.1.3.2 Temperature

Heating was accomplished by induction coils attached from the outside with a maximum heating power of 1 120 kW in total. An insulation layer reduced the temperature gradient along the pipe wall. The power of the heating coils was controlled manually. The temperature was raised with a temperature gradient of approximately 4 K/min (phase I, until 7 892 s), later with 7 K/min (phase II, until 11 249 s) and then kept constant until failure (phase III, until 12 476 s).

Several temperature sensors are installed along the test pipe on the inner and outer surface. The accuracy of the temperature sensors is specified with  $\pm 2$  °C. Figure 3.6 shows the positions of the temperature sensors with help of the virtually sliced and unrolled pipe. The angular position is specified by a clock face scheme, the axial position is given relatively to the symmetry plane of the assembly. Rectangle markers indicate sensors at the inside, circle marker at the outside of the pipe. For the red underlined sensors data is available. The green cross marks the position where the crack leading to failure is initiated.

Figure 3.7. Positions of temperature sensors at the inside (rectangle marker) and outside (circle marker) of the assembly

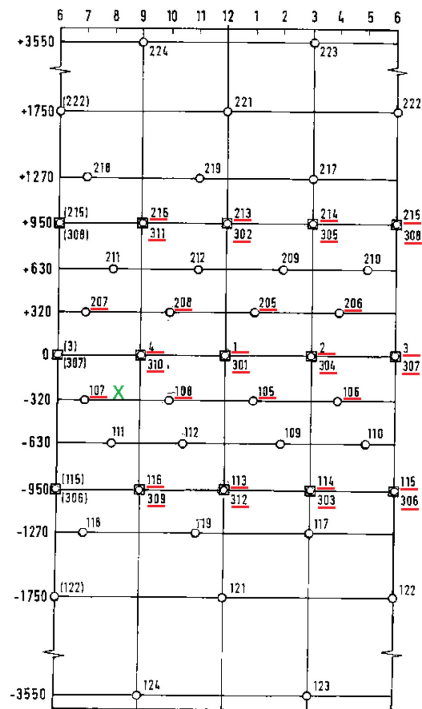
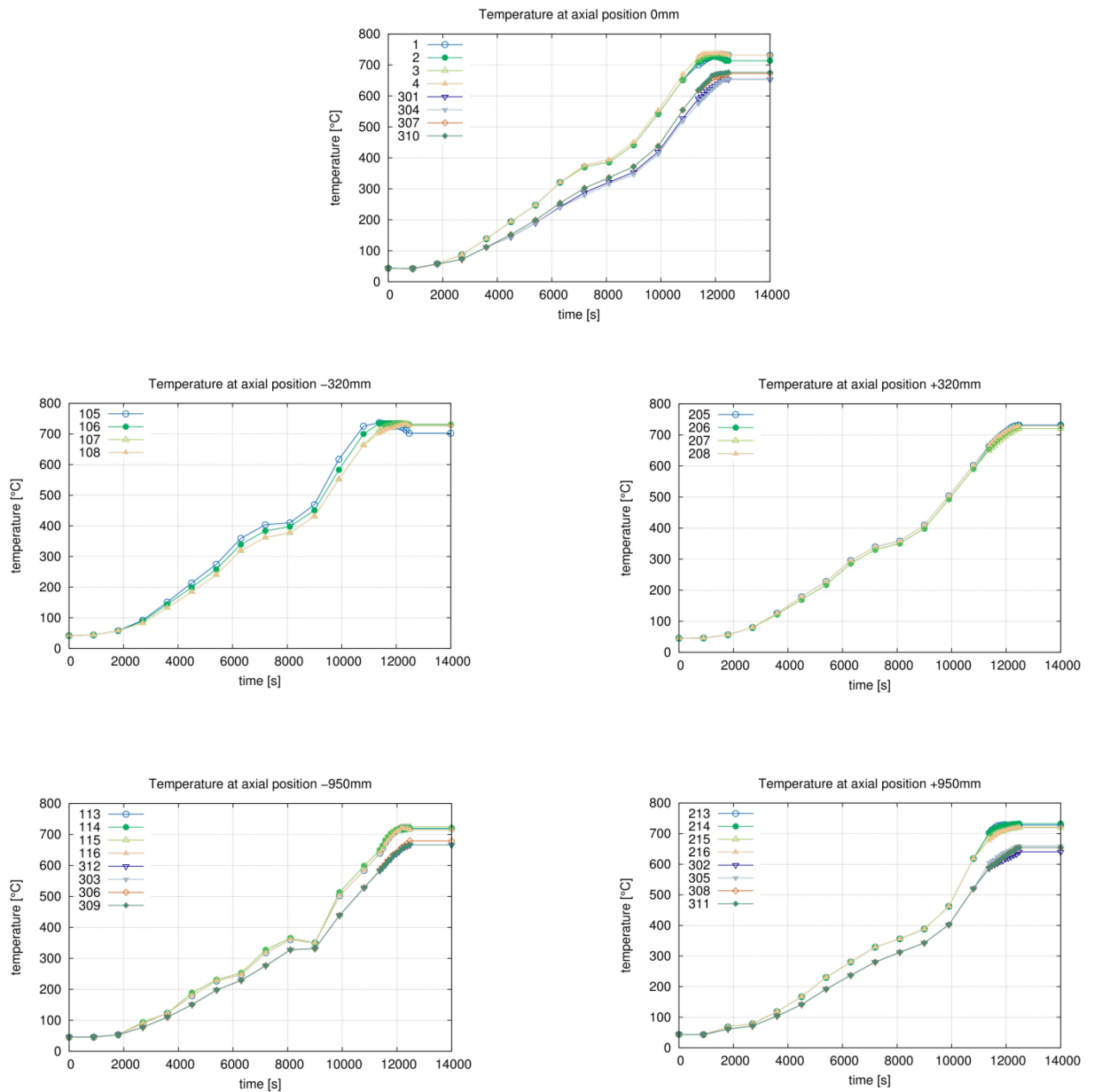


Figure 3.7 shows the temperature profile at five different axial positions. For the positions -320 mm and +320 mm sensors were available only at the outer surface. The raw data are available in Appendix 2.

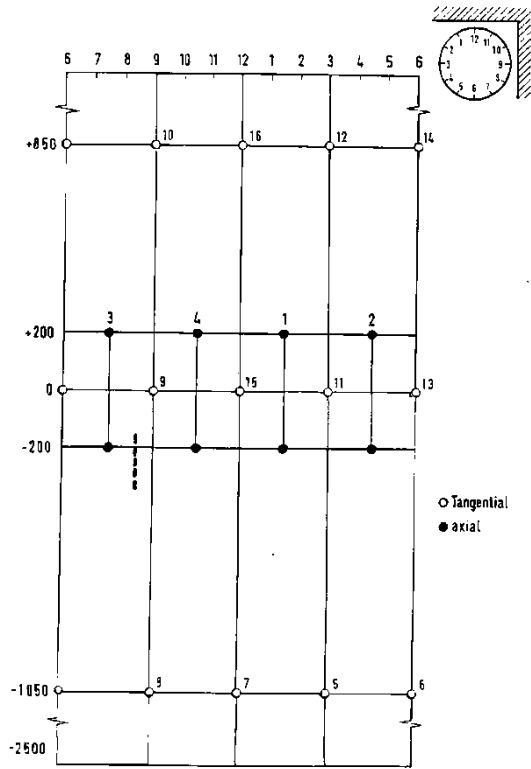
Figure 3.8. Measured temperatures at selected sensors during the experiment



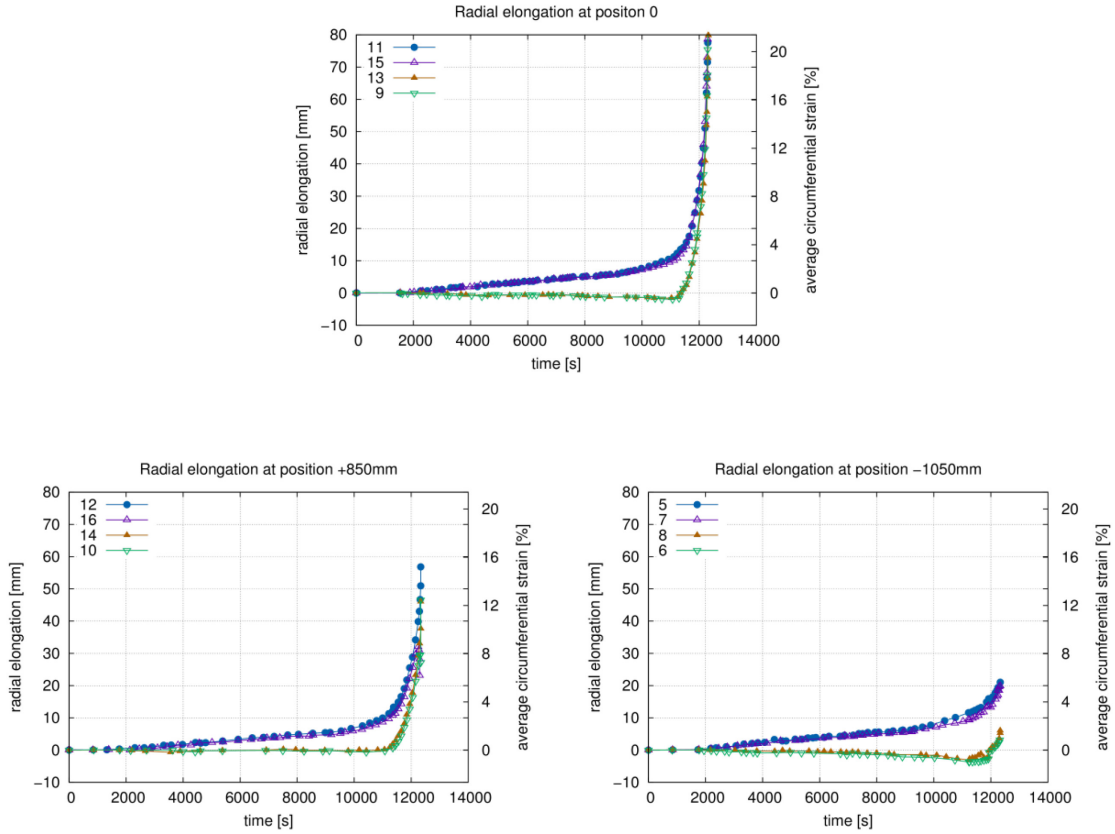
### 3.1.4. Test results

Significant deformation took place only during the last period phase III, when pressure and temperature were constant. Figure 3.8 shows the positions of the displacement transducers on the outer surface of the test specimen and Figure 3.9 and Figure 3.10 selected test results. The raw data are available in Appendix 2. The axial elongation was measured relative to a length of 400 mm. Thus, an average axial strain can be calculated. The same applies for the radial displacement using the original radius as a basis length. The dashed line in Figure 3.8 marks the offspring location of failure.

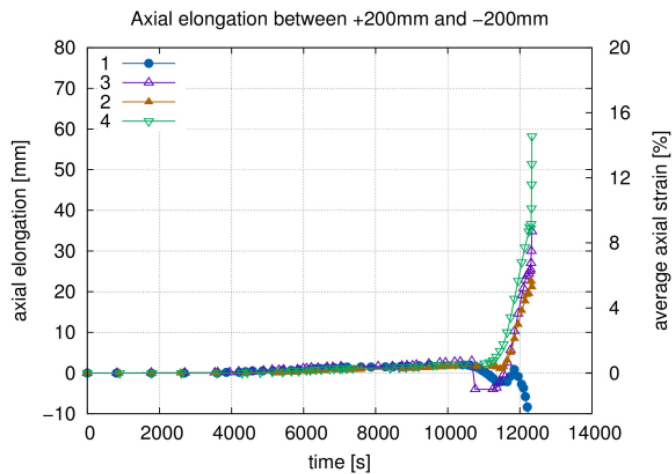
Figure 3.9. Positions of displacement transducers on the outer surface of the test specimen, for radial deformation (empty circle markers) and for axial deformation (filled circle markers)



**Figure 3.10. Radial displacement of transducers at different positions of the assembly and corresponding average circumferential strain**

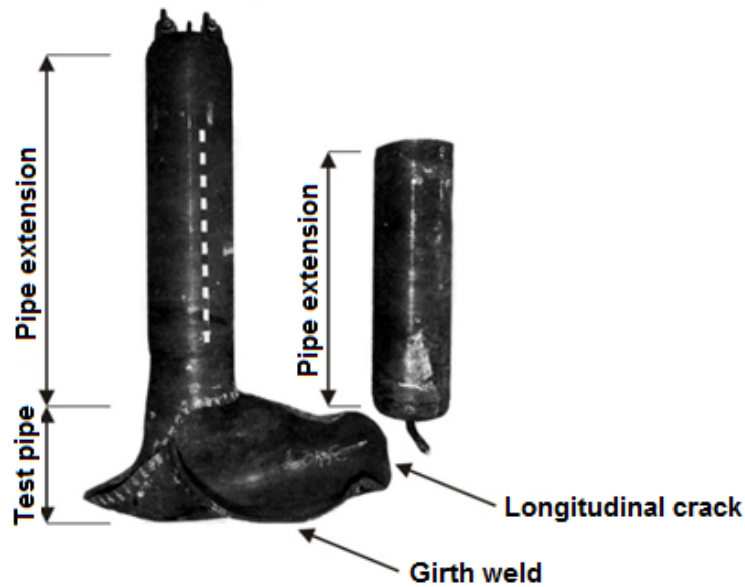


**Figure 3.11. Axial displacement of transducers and corresponding average axial strain**



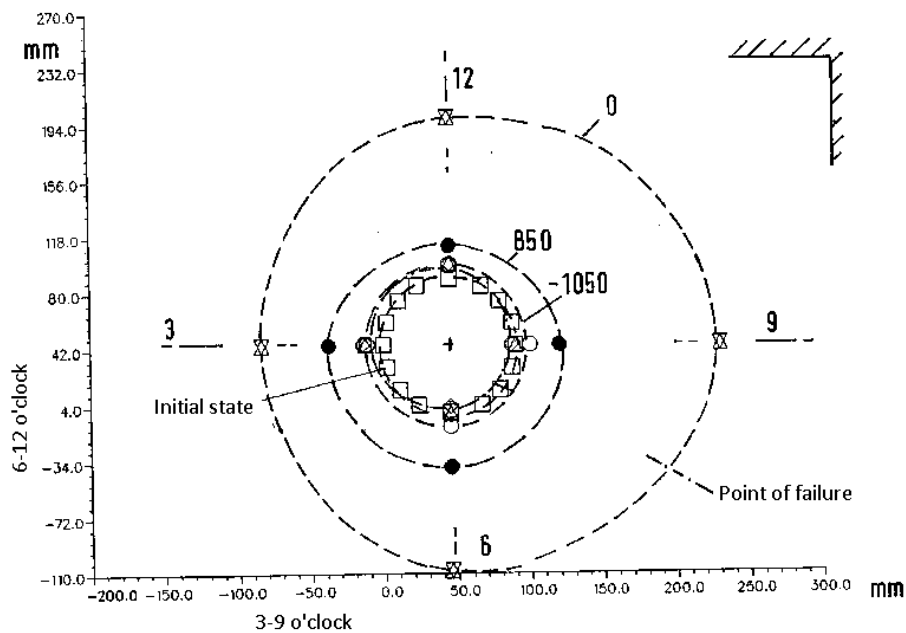
The test specimen failed in form of a break at time 12 476, i.e. 1 085 s after start of phase III. Prior to the break a longitudinal crack was formed, which propagated first axially and was deflected when it reached the lower welding between the test pipe and the extension pipe, leading to a complete separation (Figure 3.11).

Figure 3.12. Test specimen after failure



In Figure 3.12, the status shortly before failure is depicted. It can be seen that the expansion is not entirely symmetric. After the experiment the wall thickness reduction was measured at different axial positions of the test specimen (Table 3.7). Markers on the wall surface allowed to reconstruct the average permanent circumferential strain within a segment (Table 3.8). Nevertheless, the peak strain at the location of failure may be significantly larger than the so reconstructed average strain.

Figure 3.13. Cross section of the test specimen at different axial positions close to the time of failure



**Table 3.7. Decrease of wall thickness at different axial/circumferential positions**

Position	Decrease of wall thickness [%]				
	750 mm	250 mm	-250 mm	-750 mm	-1 250 mm
7:51	11.8	15.2	34.2	26.4	7.0
9:45	27.2	22.2	34.6	27.2	17.3
0:05	12.3	19.5	37.9	22.1	18.6
2:07	6.8	15.8	31.9	22.3	7.9
3:50	10.0	14.2	33.0	20.7	9.5
5:44	10.0	12.6	30.4	19.4	3.3

**Table 3.8. Reconstruction of the average permanent circumferential strain at different axial/circumferential positions using the distance increment between two markers**

Position	Average permanent circumferential strain [%]					
	1 250 mm	750 mm	250 mm	-250 mm	-750 mm	-1 250 mm
6:47	1.7	-1.7	9.0	33.1	19.2	0.2
8:39	1.0	8.4	30.7	64.0	36.6	4.5
10:50	4.1	10.8	22.4	55.8	27.9	-5.6
0:58	2.0	-3.3	12.3	39.7	17.8	-1.7
2:50	2.0	4.9	7.8	23.6	13.7	-2.9
4:36	2.9	8.6	12.9	49.3	25.7	-2.2

### 3.1.5. Task matrix

The tasks of the COSSAL benchmark on the large-scale test with a pipe (DN 700) under high temperature and pressure load with failure due to creep/ plasticisation are summarised in Table 3.9.

**Table 3.9. Task matrix of the COSSAL benchmark on the large-scale test**

Main tasks (MT)
<ul style="list-style-type: none"> <li>• MT 1 Determination of the time history of the radial elongations and circumferential strains at the axial positions given in Figure 3.9.</li> <li>• MT 2 Determination of the time history of the axial elongations and the axial strains at the position given in Figure 3.10.</li> <li>• MT 3 Determination of the wall thickness reduction at different positions given in Table 3.7.</li> <li>• MT 4 Determination of the failure time.</li> </ul>



**Table 3.10. Task matrix of the COSSAL benchmark on the large-scale test (Continued)**

Tasks of parametric studies (PS)	
• PS-W	Main tasks for wall thickness deviation of $\pm 5\%$ , i.e. wall thickness of the test specimen should be 44.65 mm or 49.35 mm instead of 47 mm.
• PS-P	Main tasks for pressure load variation of $\pm 5\%$ , i.e. the load time history given in Figure 3.5 should be increased / decreased by 5%.
• PS-F	Main tasks with different assessment criteria to simulate failure due to creep and plasticisation..

### 3.2. Comparison of analysis results on the large-scale test

In the following the participants' contributions to the COSSAL large-scale test with a pipe (DN 700) are summarised. The documentations provided by the participants (/JAE15/, /GRS15/, /PVA15/, /VUJE15/, /INS15/) are attached in Appendix 3. These documents include details on the analysis models and applied boundary conditions.

As shown in Table 3.9 the Task matrix is subdivided into two main categories, the main tasks (MT) and the tasks of parametric studies (PS). In chapter 3.2.1 the calculated and measured radial and axial displacements are compared, in chapter 3.2.2 the wall thickness reductions and in chapter 3.2.3 the failure times. Due to a high number of simulations selected results of each participant of the 2D and 3D FE models were used for the diagram plot. Otherwise the progression of the curves could be hardly identified due to the overlapping of curves. Table 3.10 gives an overview of all participants' simulations, employed material laws and failure criteria used in the analyses.

**Table 3.11. Participants and employed simulation methodology**

Participant Number	FE-Code	2D/3D	Material Law	Failure criterion
1	Nastran Abaqus	3D 3D	Norton	Numeric instability
2	Ansys Mech.	2D 3D	mod. Garofalo	Numeric instability
3	Abaqus	2D 3D	Norton mod. Garofalo Khachanov- Rabotnov	20 % creep strain 35 % creep strain
4	Ansys Mech.	3D	Linear- elastic Norton	10 % strain Stress criterion
5	MSC Marc	2D 3D	Linear-elastic Norton	n/a

### 3.2.1. Radial and axial displacements

In Figure 3.13, radial displacements of the test and the simulations are compared. Figure 3.14 shows different progressions of the radial displacements around time of failure. The radial displacement curves of the participants 1 (3D Abaqus), 2 (2D and 3D), 3 (2D and 3D) and 4 (3D) are in good accordance with the experimental results. The results of the participants 1 (3D-Nastran) and 5 (2D and 3D) show a trend which differs significantly from the measured test data. A reason might be that the change of the kinematic situation due to large deformations is not sufficiently regarded; hence the progressive character of the failure process is not reproduced correctly. 3D and 2D FE models with selected boundary conditions may show a good coincide with the test results. Norton's Law, a modified Garofalo formulation and a Khachanov-Rabotnov Law were successfully used to describe creep properties of the employed material. The results show a high sensitivity on the assumed temperature distribution in the test specimen, which influences the creep process significantly.

Figure 3.14. Radial displacements during the whole testing time (MT1, PS-F)

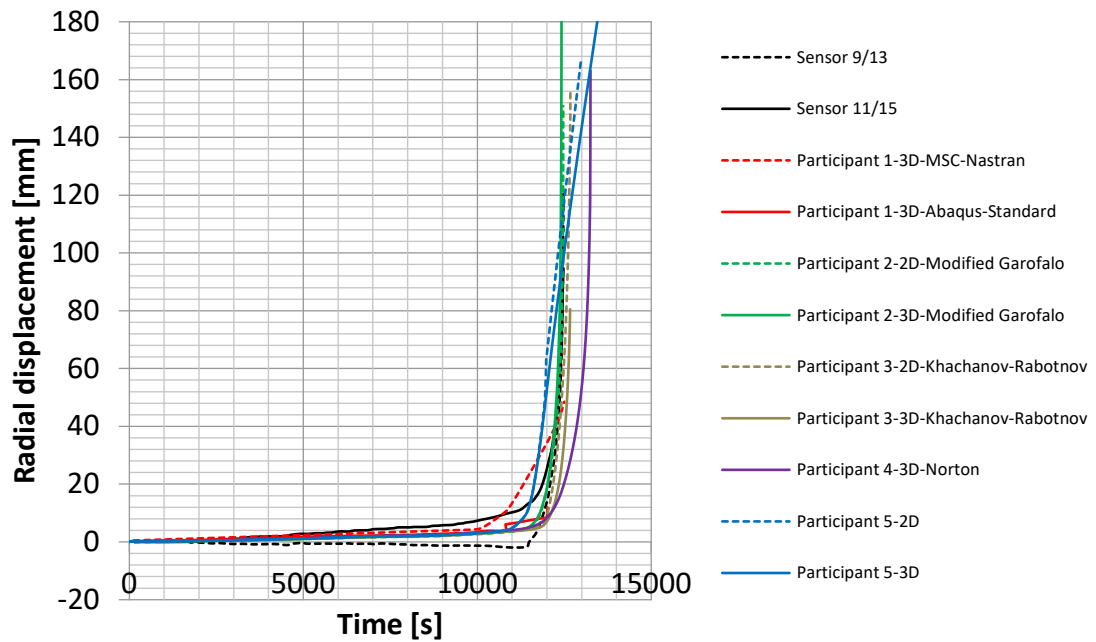
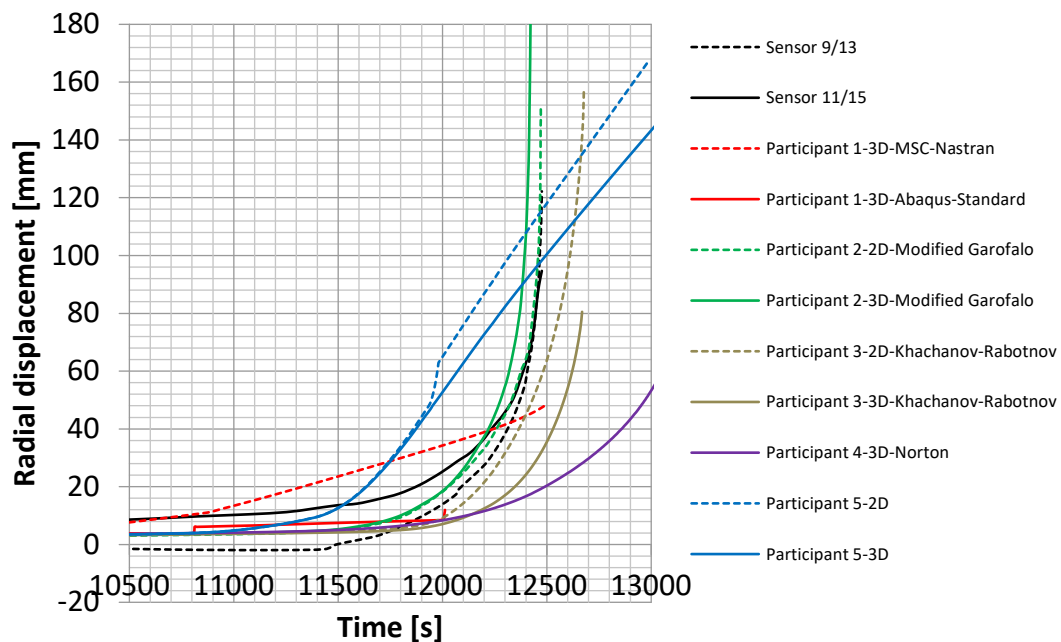


Figure 3.15. Radial displacements during the period before failure (MT1, PS-F)



After about 10 500 s, when the pipe starts to buckle, a slightly asymmetric deformation behaviour of the pipe structure occurs (see Figure 3.12). None of the 3D models were able to simulate this behaviour, which might be due to small unknown local deviations in geometry or temperatures or rigid body motion of the whole assembly, not considered in the simulations.

Figure 3.15 shows the measured and calculated axial displacements of the participants' simulations during the whole testing time. Up to 10 500 s all simulations overestimate the axial displacement slightly (see Figure 3.16), The discrepancy may be traced to the measurement method with wires, which shows uncertainties especially for extensions below 1 mm, potentially due to missing tension of the wires in the beginning. The 3D simulation of participant 1 overestimates the axial displacements to a larger extent.

A significant axial deformation can be only observed in the last 2 000 s before failure (Figure 3.17). After about 10 500 s the results of sensors 2, 3 and 4 (positions see Figure 3.8) show positive axial displacements (relative elongation of a length of 400 mm), while sensor 1 measures negative axial displacement, i.e. a relative contraction. A reason might be the radially asymmetric deformation (Figure 3.12) which might have influence on the axial displacement transducers because they were not directly attached to the specimen surface. The results of the 3D-simulation of participant 2 denoted with S1, S2, S3 and S4 represent the sensor positions 1, 2, 3 and 4. They coincide with the measured results of sensor 1 (see Figure 3.17).

Figure 3.16. Axial displacements during the whole testing time (MT2, PS-F)

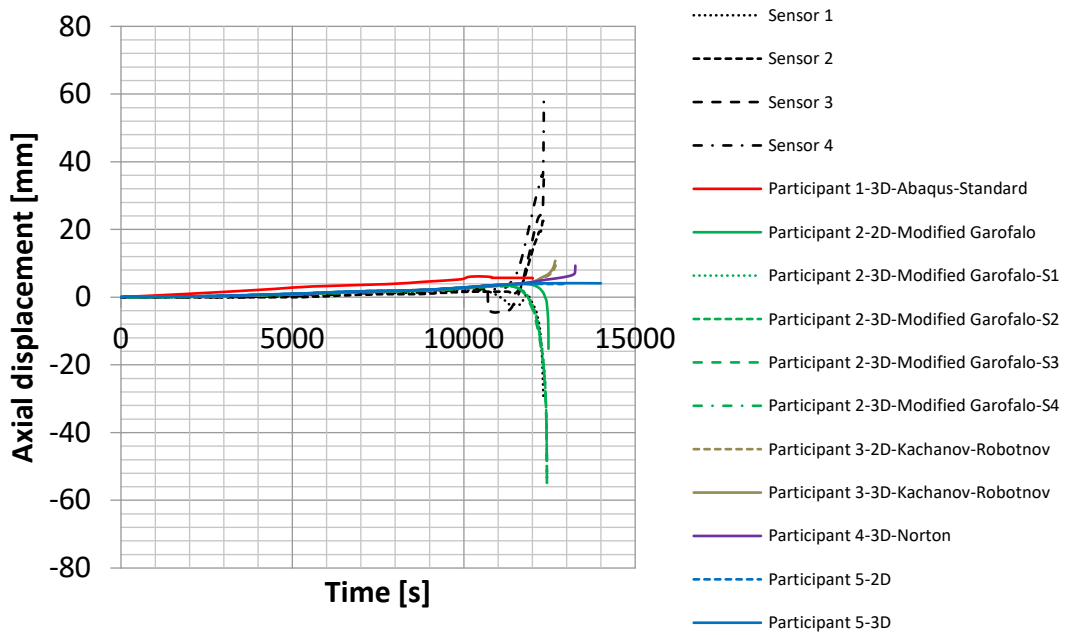


Figure 3.17. Axial displacements during first phase (MT2, PS-F)

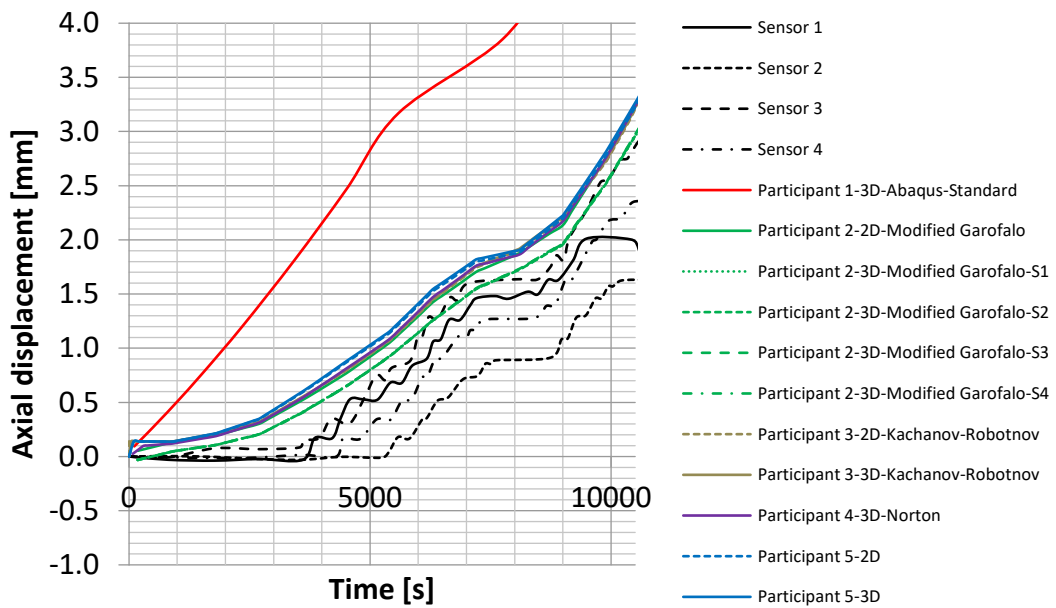


Figure 3.18. Axial displacements during the period before failure (MT2, PS-F)

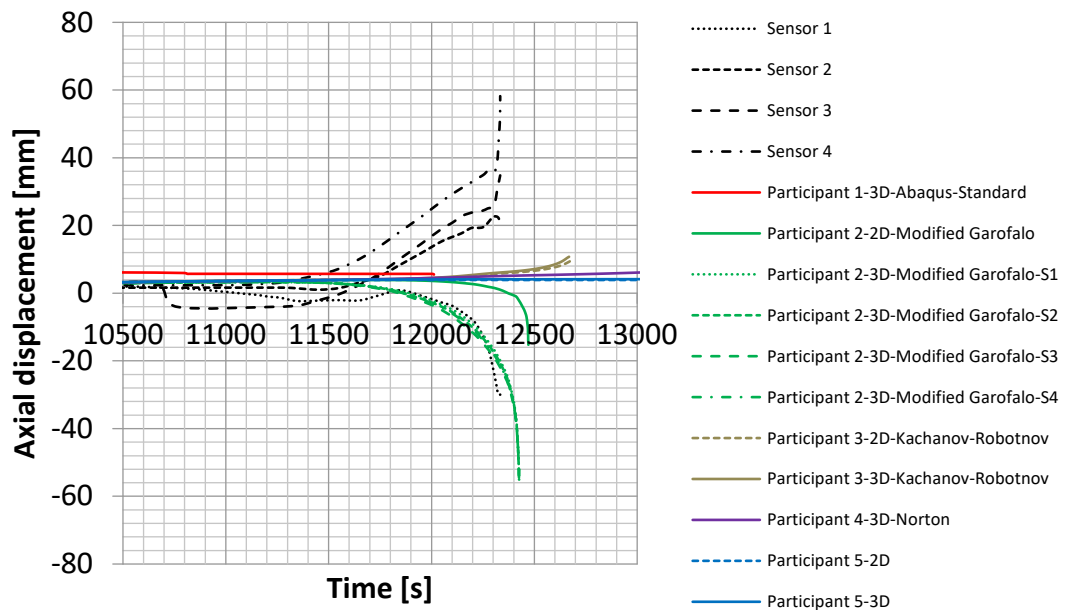


Figure 3.18, Figure 3.19, Figure 3.20 and Figure 3.21 display the results of the main tasks MT1 and MT2 with the variation of the pressures transient by  $\pm 5\%$  (PS-P). As expected an increased pressure load shifts the radial and axial displacement curves to lower times while a decreased pressure load shifts the curves to higher times. The influence of the load variation is evidently significant.

Figure 3.19. Radial displacements during the whole testing time (PS-P)

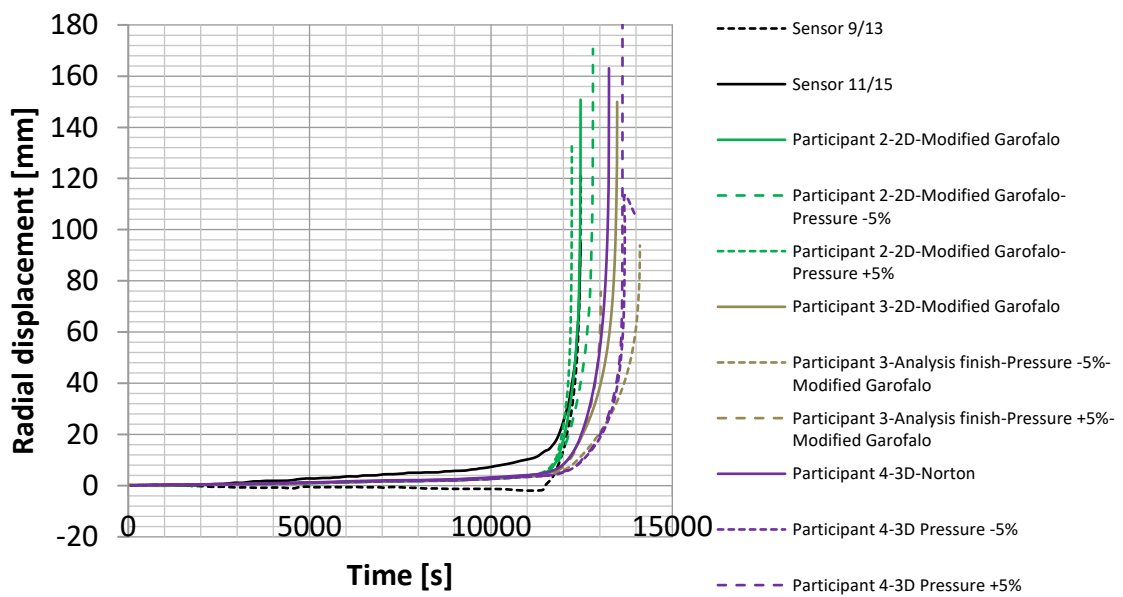


Figure 3.20. Radial displacements during the period before failure (PS-P)

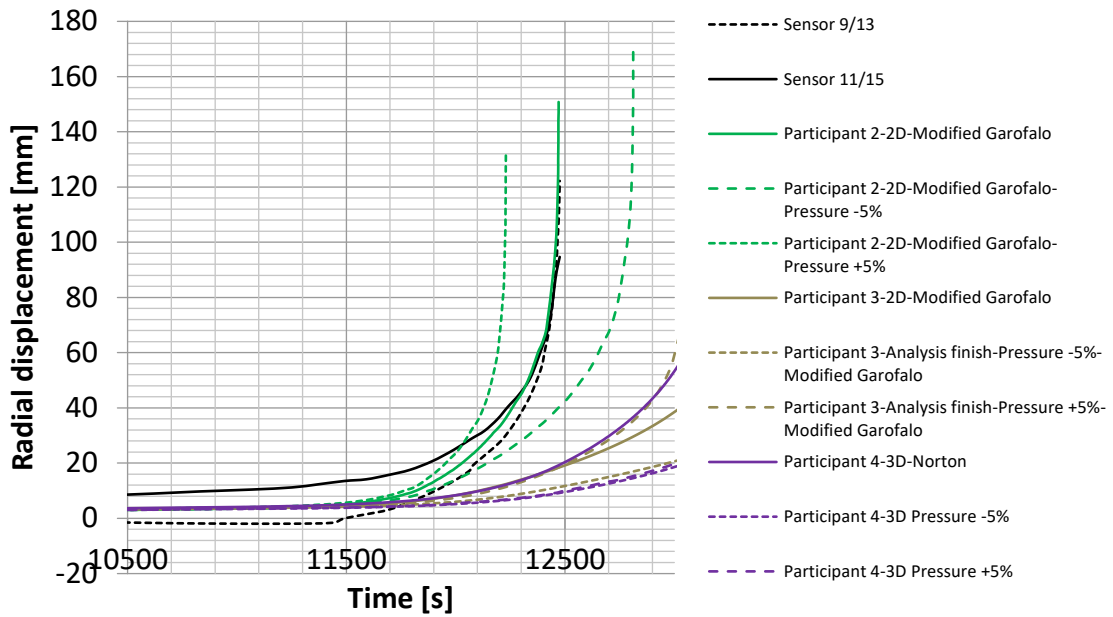


Figure 3.21. Axial displacements during the whole testing time (PS-P)

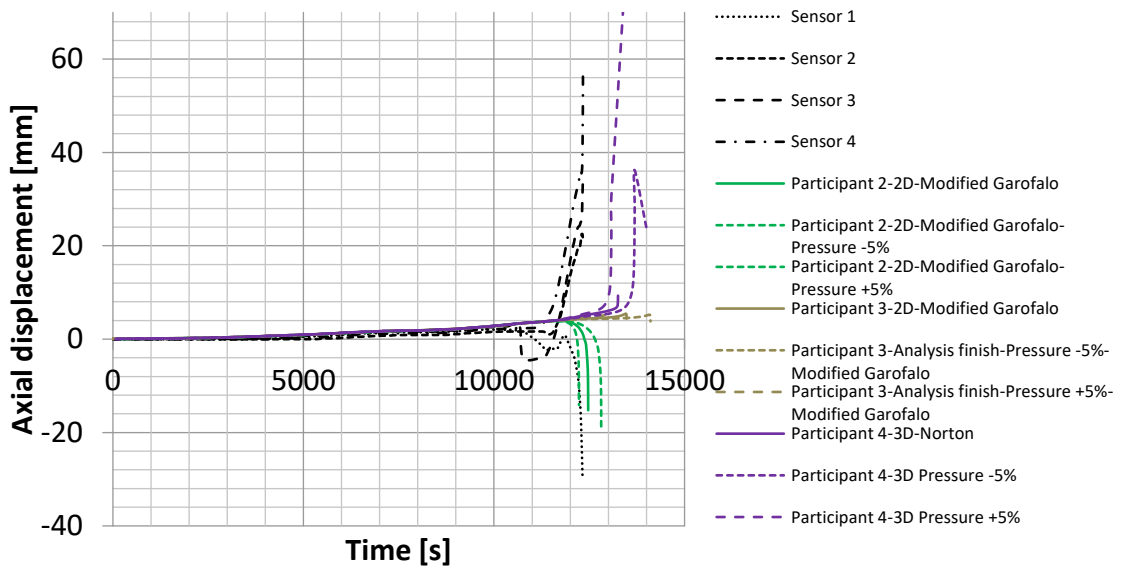


Figure 3.22. Axial displacements during the period before failure (PS-P)

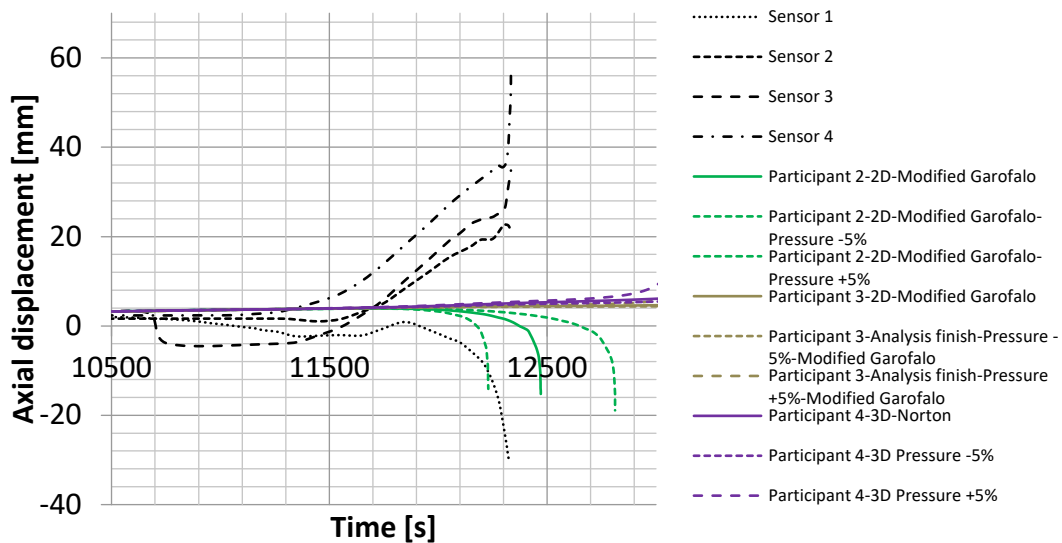


Figure 3.22, Figure 3.23, Figure 3.24 and Figure 3.25 display the results of the main tasks MT1 and MT2 with the variation of the wall thickness by  $\pm 5\%$  (PS-W), i.e. the wall thickness is assumed as 44.65 mm (-5 %) or 49.35 % (+5 %) instead of 47 mm. As expected an increased wall thickness shifts the radial and axial displacement curves to higher times while a decreased wall thickness shifts the curves to lower times. The influence of the wall thickness variation is also significant. The explanation is that both wall thickness and pressure contribute linearly to the stress level. Only in the geometrically deformed situation there might be a slightly different behaviour.

Figure 3.23. Radial displacements during whole testing time (PS-W)

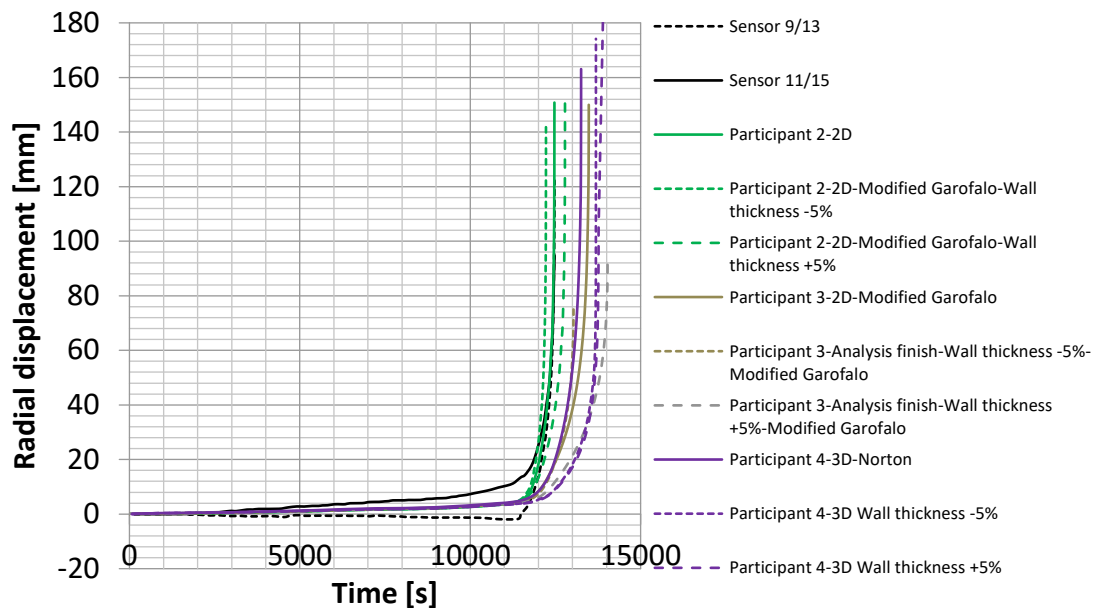


Figure 3.24. Radial displacements during last phase of testing (PS-W)

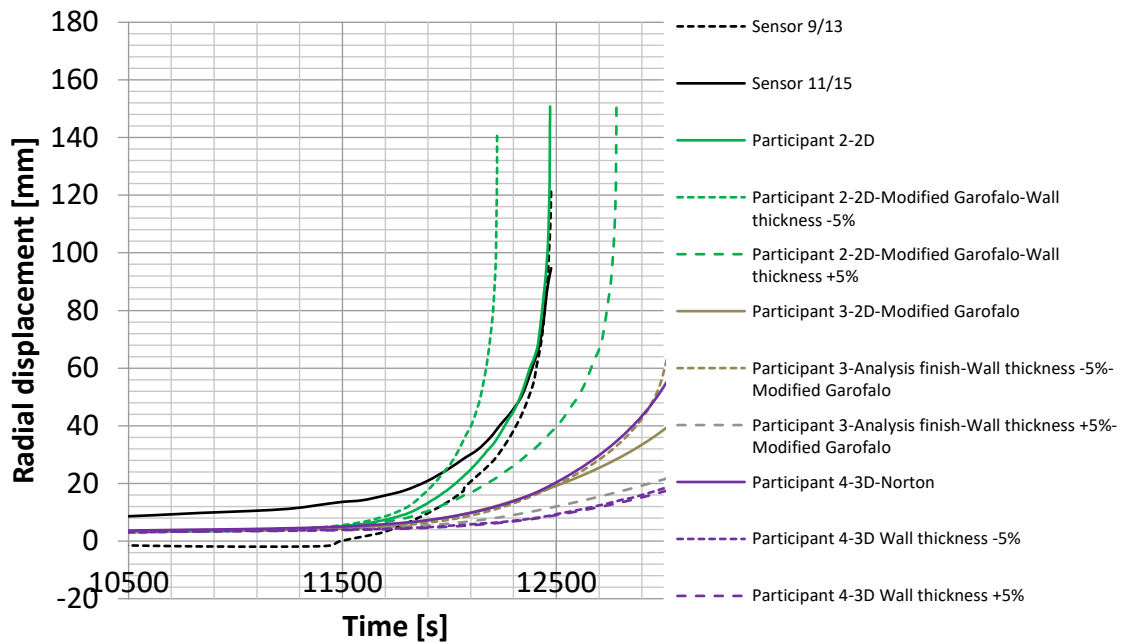


Figure 3.25. Axial displacements during whole testing time (PS-W)

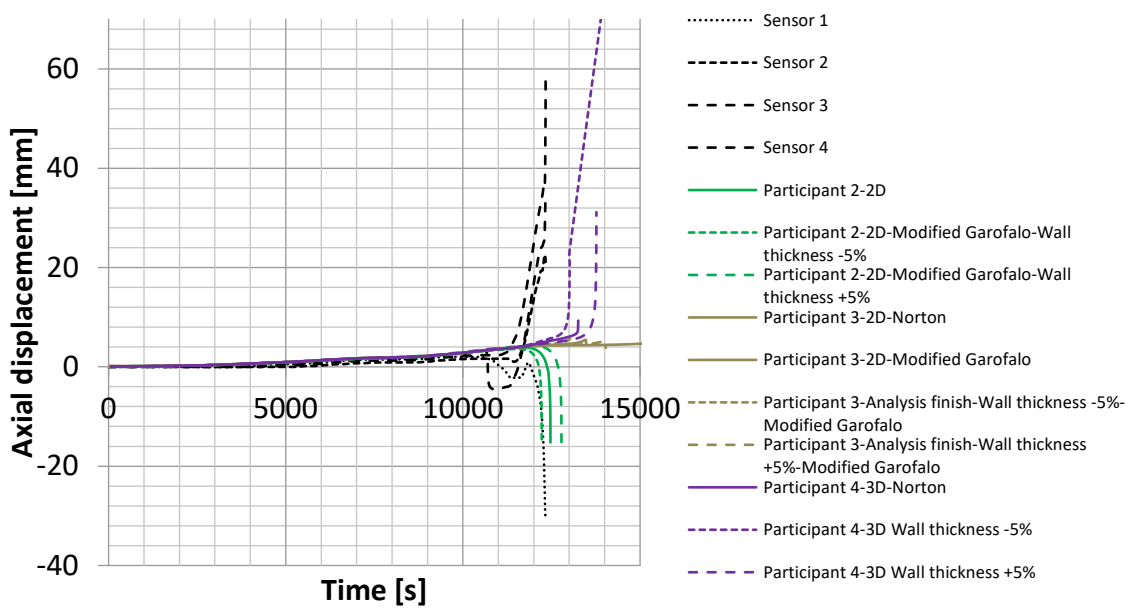
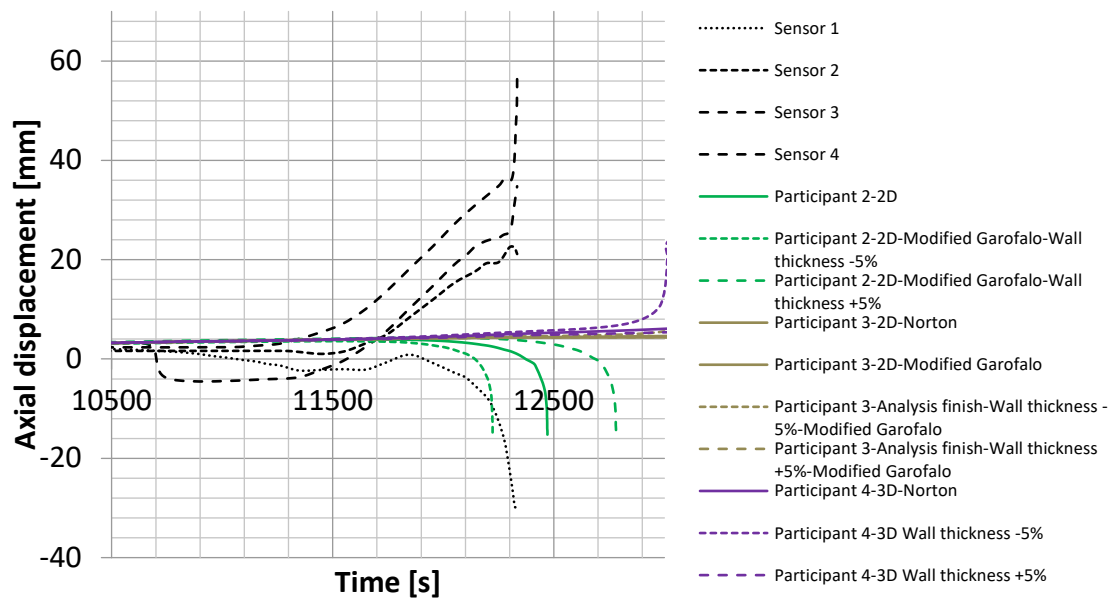




Figure 3.26. Axial displacements during the period before failure (PS-W)



### 3.2.2. Wall thickness reduction close to failure

In Table 3.11, the simulation results of MT 3 (determination of the wall thickness reduction close to failure) are summarised.  $w_t$  is an arithmetic mean of the measured thickness reductions at all positions listed in Table 3.7. The deviations between calculated and measured results are quantified. The calculated values of participants 3 and 4 are average values from different positions. They underestimate the wall thickness reduction by about 10 % to 16 %. Participant 2 overestimates the averaged wall thickness reduction by about 3 %.

In this context it should be noted that the maximum local wall thickness reduction measured after failure could not be reliably simulated. This might be due to the fact that the highly dynamic rupture process after reaching instability is not accessible to quasistatic simulation.

**Table 3.12. MT3 – Determination of the wall thickness reduction close to failure**

Participant	FE-Code	2D/3D	Creep Law	Failure criterion	Averaged measured wall thickness reductions $w_t$ [%]	Simulated wall thickness reduction $w_s$ [%]	$w_s - w_t$ [%]
2	Ansys Mech.	2D	mod. Garofalo	Plastic Instability	19.4	23.0	+3.6
2	Ansys Mech.	3D	mod. Garofalo	Plastic Instability	19.4	22.0	+2.6
3	Abaqus	2D	Khachanov-Rabotnov	20 % creep strain	19.4	6.4	-13.0
3	Abaqus	2D	mod. Garofalo	20 % creep strain	19.4	10.1	-9.3
4	Ansys Mech.	3D	Norton	10 % strain	19.4	3.2	-16.2

### 3.2.3. Comparison of failure times

In Table 3.12, the results of MT 4 (determination of failure time) are summarised and compared to the test. Four results show deviations in failure time by less than  $\pm 50$  s (participant 1 / Nastran 3D with creep law “Norton”, participant 2 / Ansys Mech. 2D and 3D with creep law “mod. Garofalo”, participant 3 / Abaqus 2D with creep law “Khachanov-Rabotnov”). Three results show larger deviations up to 807 s (participant 1 / Abaqus 3D with creep law “Norton”, participant 3 / Abaqus 2D with creep law “mod. Garofalo”) and participant 4 / Ansys Mech. with creep law “Norton”).

**Table 3.13. MT4 – Determination of failure time**

Participant	FE-Code	2D/3D	Creep Law	Failure criterion	Measured failure time $t_t$ [s]	Simulated failure time $t_s$ [s]	Delta $t_s - t_t$ [s]
1	Nastran	3D	Norton	Numeric instability	12 476	12 500	24
1	Abaqus	3D	Norton	Numeric instability	12 476	12 012	-464
2	Ansys Mech.	2D	mod. Garofalo	Plastic Instability	12 476	12 471	-50
2	Ansys Mech.	3D	mod. Garofalo	Plastic Instability	12 476	12 426	-50
3	Abaqus	2D	Kachanov-Robotnov	20 % creep strain	12 476	12 468	-8
3	Abaqus	2D	mod. Garofalo	20 % creep strain	12 476	13 283	+807
4	Ansys Mech.	3D	Norton	10 % strain	12 476	12 760	+284

Table 3.13 summarises the failure times of the parametric studies PS-P (pressure load variation) calculated by participants 2, 3 and 4. It can be observed that the -5 % deviation causes a later time of failure in the range of 1.6 % to 4.1 %. The +5% deviation causes an earlier time of failure in the range of -1.2 % to -3.4 %.

**Table 3.14. Dependence of failure times on pressure load variation (PS-P)**

Participant	Pressure variation	FE-Code	2D/3D	Creep Law	Failure criterion	Simulated failure time $t_s$ [s]	Delta [%]
2	0 %	Ansys Mech.	2D	mod. Garofalo	Plastic Instability	12 471	0
	-5 %					12 812	+2.7
	+5 %					12 229	-2.0
3	0 %	Abaqus	2D	mod. Garofalo	20 % creep strain	13 283	0
	-5 %					13 833	+4.1
	+5 %					12 833	-3.4
4	0 %	Ansys Mech.	3D	Norton	10 % strain	12 760	0
	-5 %					12 967	+1.6
	+5 %					12 608	-1.2

Table 3.14 summarises the failure times of the parametric studies PS-W (wall thickness variation) calculated by participants 2, 3 and 4. It can be observed that the -5 % deviation causes an earlier time of failure in the range of -1.5 % to -2.6 %. The +5 % deviation causes a later time of failure in the range of +2.0 % to +3.4 %.

**Table 3.15. Dependence of failure times on wall thickness variation (PS-W)**

Participant	Thickness variation	FE-Code	2D/3D	Creep Law	Failure criterion	Simulated failure time $t_s$ [s]	Delta [%]
2	0 %	Ansys Mech.	2D	mod. Garofalo	Plastic Instability	12 471	0
	-5 %					12 223	-2.0
	+5 %					12 781	+2.5
3	0 %	Abaqus	2D	modified Garofalo	20 % creep strain	13 283	0
	-5 %					12 933	-2.6
	+5 %					13 733	+3.4
4	0 %	Ansys Mech.	3D	Norton	10 % strain	12 760	0
	-5 %					12 570	-1.5
	+5 %					13 019	+2.0

Different failure criteria have been used, especially numerical instability (participant 1), plastic instability (participant 2) and fixed strain values (participants 3 and 4). Due to the progressive late phase the failure criteria generally have only minor influence.

A material law which considers non-linear material properties. i.e. creep and plasticisation effects and the consideration of large deformation effects are necessary for an accurate simulation and prediction of the time of failure.

## 4. Benchmark study on pressurised water reactor components

### 4.1. Problem statement on pressurised water reactor components

#### 4.1.1. Objective

The main objective of the pressurised water reactor (PWR) benchmark (Task 4.1 of the COSSAL project) was to analyse the behaviour of selected components of a generic PWR primary loop during a typical high-pressure core melt scenario and to determine the component which fails first. The location of failure has large impact on the further progression of the accident scenario. The failure of the main coolant line or the surge line may lead to a depressurisation of the primary circuit even before the reactor pressure vessel is seriously heated. The early failure of steam generator tubes on the other hand could lead to a serious containment bypass, especially when the tubes are weakened by ageing and damage effects.

#### 4.1.2. Geometry and boundary conditions of the components

For this benchmark task, only main coolant line, surge line and steam generator tube of a generic PWR coolant loop as the components likely to fail were investigated. For the main tasks, in a first approach, the geometry of the components was represented by a simplified generic component which includes both a straight part and an elbow (Figure 4.1). The geometry of the generic piece could be characterised by outer diameter, wall thickness, bend radius and elbow angle. Specific data for each component is included in Table 4.1.

For the hot leg of the main coolant line two generic pieces represented both an elbow piece and a piece of the slightly thinner straight part. The austenitic cladding was neglected and its thickness of 5 mm is added to the thickness of the ferritic body.

**Figure 4.1. Drawing of an idealised generic piece representing the components**

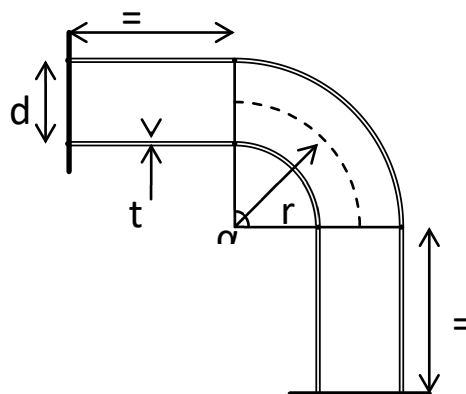


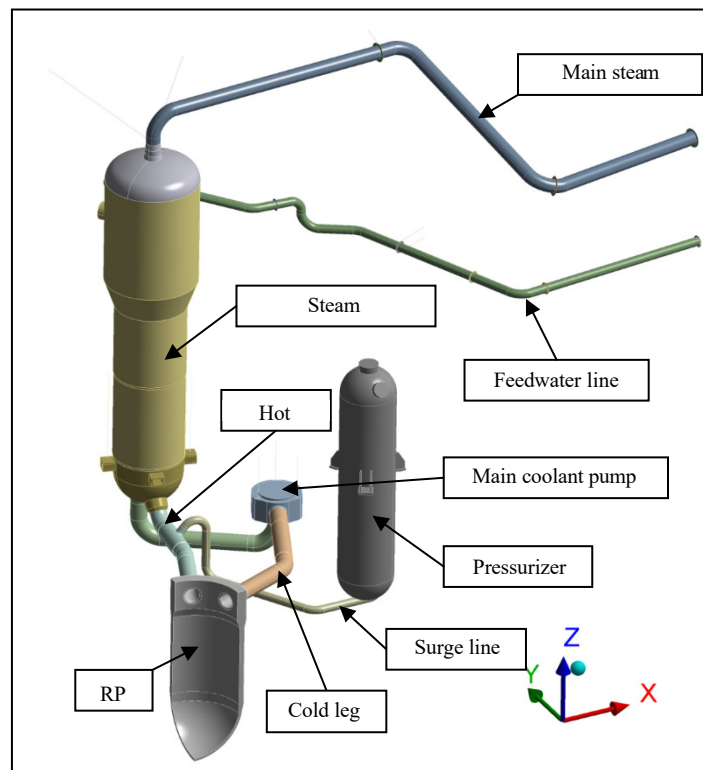
Table 4.1. Geometry data of the simplified components

Component	Material	$d_o$	$t_w$	$r_m$	$\alpha$
Main coolant line elbow	20MnMoNi5-5	874 mm	62 mm	1 125 mm	50 °
Main coolant line straight	20MnMoNi5-5	864 mm	57 mm		0 °
Surge line	X10CrNiNb18-9	428 mm	40 mm	645 mm	140 °
Steam generator tube	Alloy 800 (mod.)	22 mm	1.23 mm	193 mm	180 °

The real boundary conditions of the components are complex. A cooling loop of a PWR is supported in such a way, thermal expansion can be compensated to a certain degree. Nevertheless, displacements and momenta are induced into the components, which is more or less relevant depending on the position. In a first approach, one end of the generic piece should be fixed in all degrees of freedom and the other end were asked to be modelled freely movable and sealed with a pressurised end cap or an auxiliary reaction force. In the parametric study PS-A, both ends should be fixed to allow a coarse qualitative insight in the effects of thermal elongation and restraints, especially on stresses and failure time.

A deeper insight in the effects of the real boundary conditions and the effects of gravitation on the failure of the main coolant line and the surge line should be done in the parametric study PS-B using a geometry model of a full PWR-loop (or parts of it with defined boundary conditions), available as step-file (Figure 4.2). Appendix 4 gives some hints how to implement the model.

Figure 4.2. Geometry of the coolant loop



### 4.1.3. Material data

In this section material data of the ferritic steel (main coolant line), the austenitic steel (surge line) and the nickel-based alloy (steam generator tubes) are presented.

#### 4.1.3.1 Ferritic steel 20MnMoNi5-5

The data of the ferritic steel 20MnMoNi5-5, which characterises the material of the main coolant line, was already described in the first benchmark of the COSSAL activities (see chapter 3.1.2)

#### 4.1.3.2 Austenitic steel X10CrNiNb18-9

In the following, similar data as in chapter 3.1.2 are given for the austenitic steel X10CrNiNb18-9, which characterises the material of the surge line.

**Table 4.2. Linear-elastic data**

T (°C)	E (MPa)	Poissons Ratio
20	196 000	0.277
400	176 000	0.3
500	168 000	0.306
600	157 000	0.312
700	145 000	0.318
800	130 000	0.324
900	98 000	0.33
1 000	55 000	0.336

**Figure 4.3. True stress-strain curves**

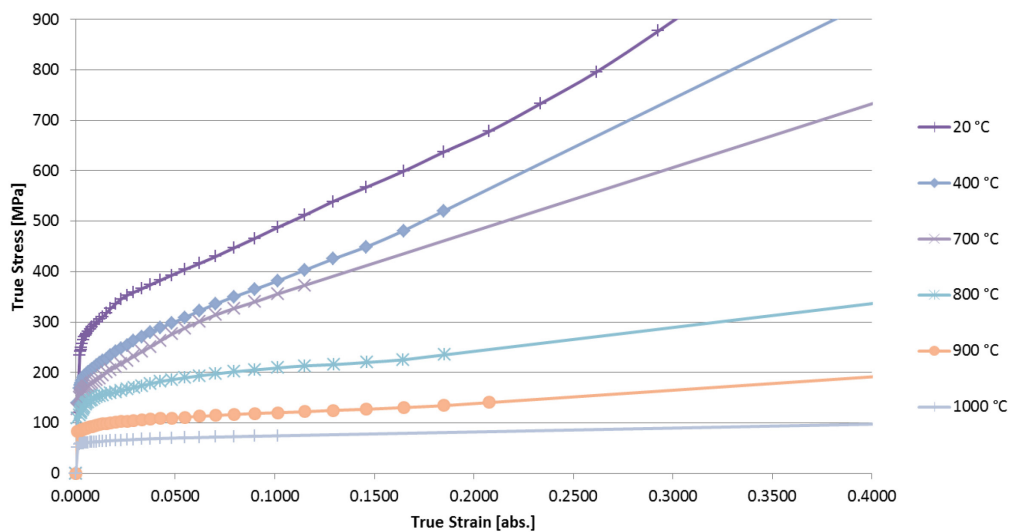


Figure 4.4. Secondary creep rates

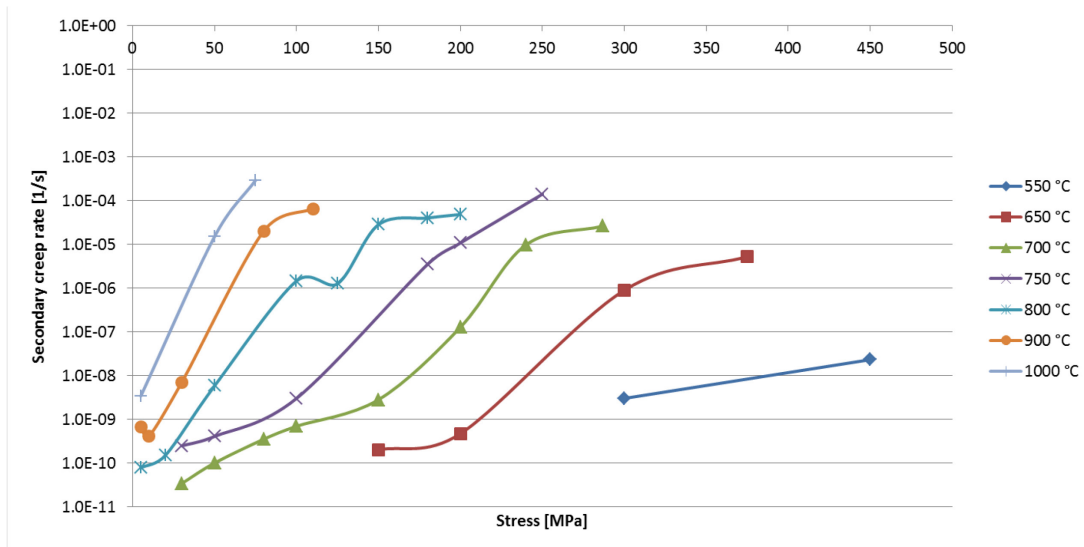


Table 4.3. Norton parameters according to formula (1)

T [°C]	C1	C2
650	3.11849E-21	5.909656168
700	3.12943E-21	6.478440657
750	6.52277E-22	7.220746474
800	1.10658E-12	3.332233954
900	1.77091E-12	3.705680534
1 000	9.81909E-18	7.183910016

Table 4.4. Isotropic secant coefficient of thermal expansion

Temperature [°C]	CTE <sub>secant</sub> [1/K]
20	1.65E-05
400	1.85E-05
500	1.89E-05
600	1.02E-05
700	1.95E-05
800	1.96E-05
900	1.97E-05
1 000	1.98E-05

4.1.3.3 Nickel-based Alloy 800 (mod.)

In the following, similar data as in chapter 3.1.2 are given for the nickel base alloy known as Alloy 800 (mod.), which characterises the material of the steam generator tubes and is related to the common nickel-based alloys *Alloy 800* and *Alloy 800H*.

Table 4.5. Linear-elastic material data

T (°C)	E (MPa)	Poissons Ratio
20	196 500	0.339
500	165 000	0.367
600	157 700	0.373
700	150 100	0.381
800	141 300	0.394
900	132 500	0.394
1 000	123 700	0.394

Figure 4.5. True stress-strain rates

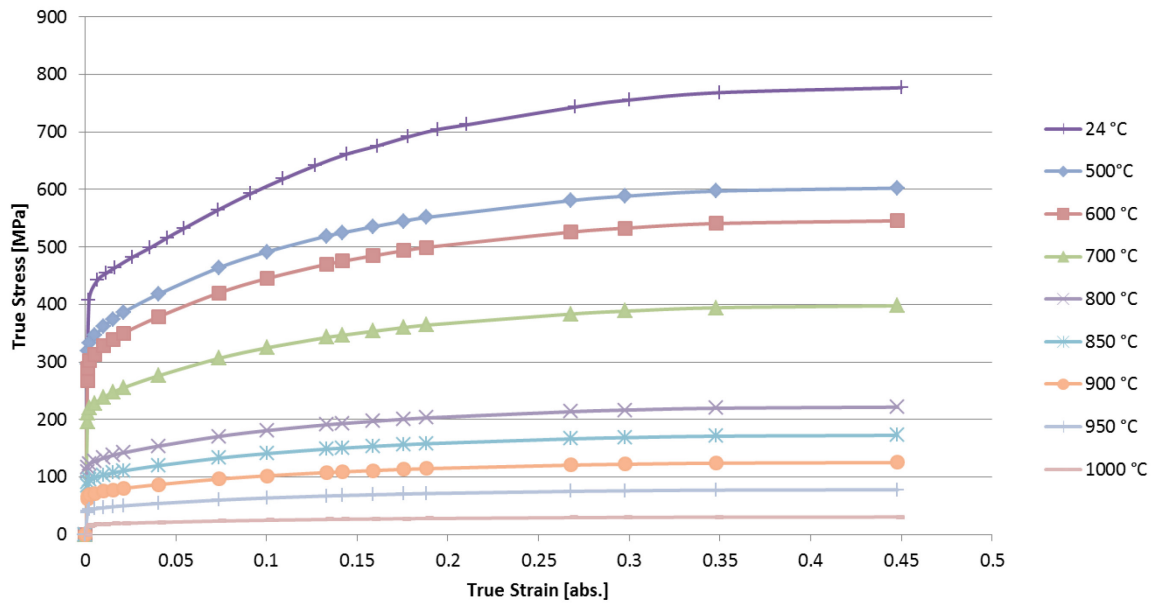




Figure 4.6. Secondary creep rates

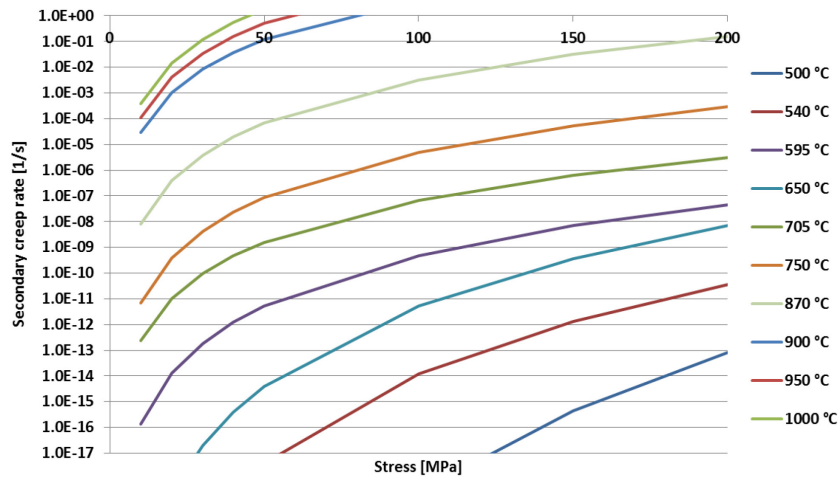


Table 4.6. Norton Parameters according to formula (1)

T [°C]	C1	C2
500	3.00E-55	18.003
540	1.00E-37	11.539
595	4.00E-23	6.5422
650	1.00E-32	10.361
705	8.00E-19	5.4684
750	9.00E-18	5.8717
870	2.00E-14	5.6079
900	2.00E-10	5.1608
950	6.00E-10	5.2516
1 000	2.00E-09	5.2725

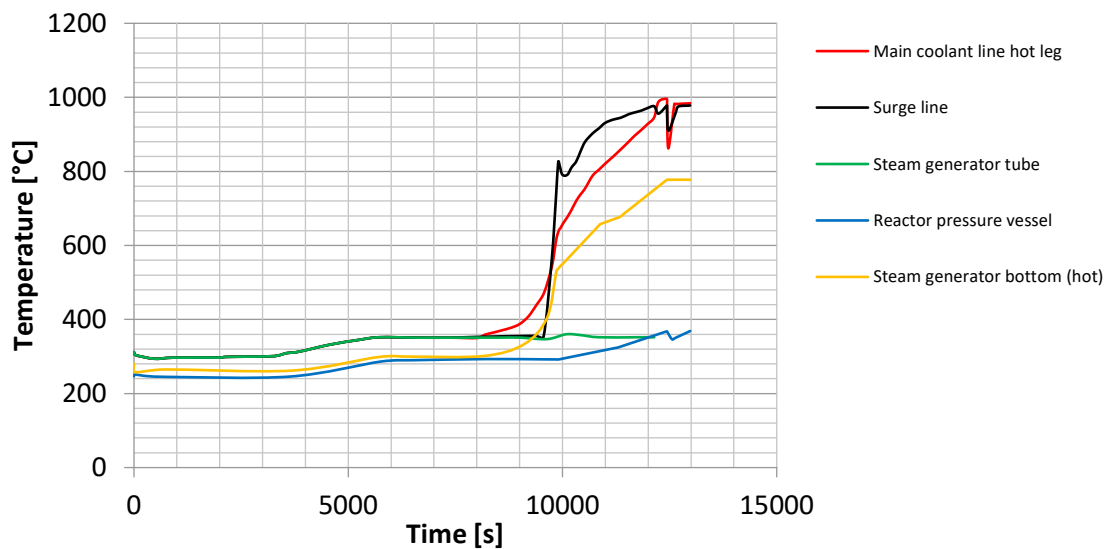
Table 4.7. Isotropic secant coefficient of thermal expansion

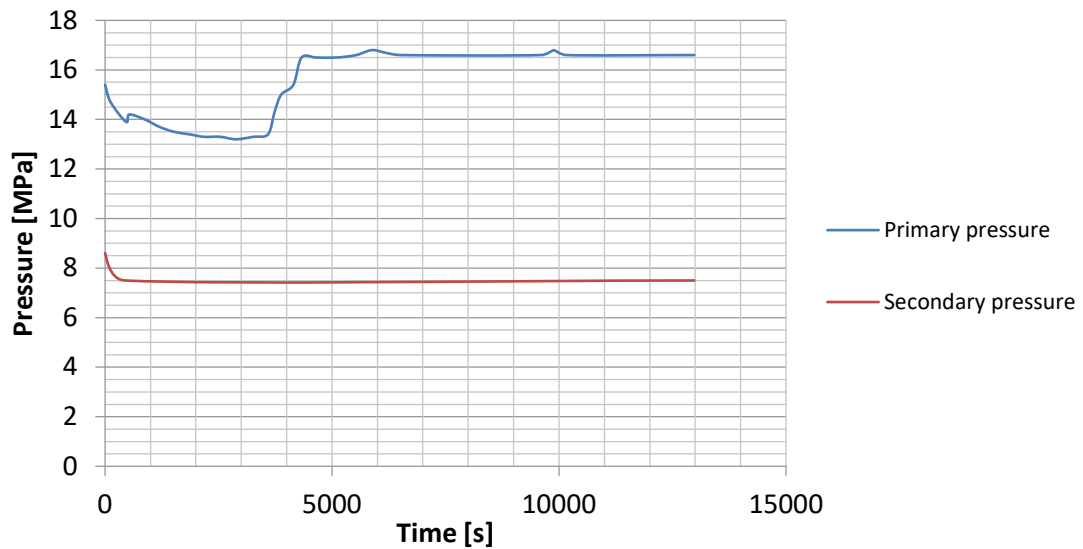
Temperature [°C]	CTE <sub>secant</sub> [1/K]
20	1.44E-05
500	1.68E-05
600	1.71E-05
700	1.75E-05
800	1.8E-05
900	1.8E-05
1 000	1.8E-05

#### 4.1.4. Loading conditions

The components described in chapter 4.1.2 are loaded by a severe accident scenario due to a total station blackout. The background on the exemplary transient is described in Appendix 4.1. Figure 4.7 shows selected component temperatures during the transient and Figure 4.8 the time history of the primary and the secondary pressure. Thermal gradients in the walls of the components are neglected here due to assumed ideal insulation or small wall thickness, so that the piping components can be attributed to one global temperature profile for each piping component.

Figure 4.7. Component temperatures during transient



**Figure 4.8. Primary and secondary pressure during transient**

An additional scenario shall be investigated, in which the steam generator tubes are significantly heated by circulating gas flow (reflux condenser). Depending on the type of reactor this may be possible under special circumstances (see Appendix 4). In the frame of main task MT 4 the temperature history of the hot leg of the main coolant line should be used for the steam generator tube.

#### **4.1.5. Task matrix**

The tasks of the COSSAL benchmark on a severe accident of a generic PWR are summarised in Table 4.8.

**Table 4.8. Task matrix of the COSSAL benchmark on a severe accident**

<b>Main tasks (MT)</b>
<ul style="list-style-type: none"> <li>• MT-1 Structural behaviour of the main coolant line (generic piece) during the given severe accident scenario. Requested output: Time history of equivalent stress, equivalent elastic/plastic/creep/total strain at the position of maximum values; failure time and temperature, if applicable; used failure criteria.</li> <li>• MT-2 Structural behaviour of the surge line (generic piece) during the accident. Requested output: see MT 1.</li> <li>• MT-3 Minimum wall thickness of the steam generator tube (generic piece) during the severe accident scenario without failure. Due to the low temperature level no time-dependent creep will take place. The minimum wall thickness is related to maximum damage of steam generator tubes due to ageing approximated by wall thinning.</li> <li>• MT-4 Structural behaviour of the steam generator tube for a reflux-condenser scenario. For this investigation the temperature history of the hot leg of the main coolant line shall be used for the steam generator tube. Requested output: see MT 1.</li> </ul>
<b>Tasks of parametric studies (PS)</b>
<ul style="list-style-type: none"> <li>• PS-A For the components defined in MT1-4 calculations should be performed while fixing the movement of both ends of the generic pieces instead of only one end to allow a coarse qualitative insight in the effects of thermal elongation and restraint.</li> <li>• PS-B MT1 and MT 2 shall be performed using the geometry model of a loop (or parts of it with defined boundary conditions) available as step-file. Appendix 4 gives some hints how to implement the model.</li> <li>• PS-C MT 3 and MT 4 shall be performed assuming a depressurisation of the secondary circuit (<math>p = 0</math> MPa).</li> </ul>

#### 4.2. Comparison of analysis results on pressurised water reactor components

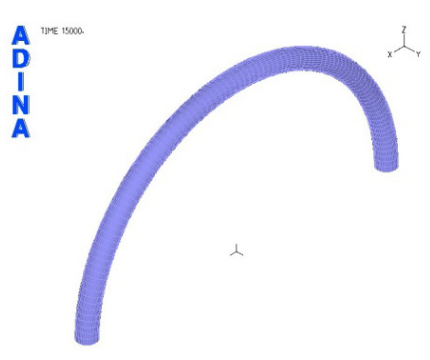
In the following the participants' contributions to the COSSAL PWR Benchmark are summarised and compared. The documentations provided by the participants (/INS 17a/, /GRS17a/) are attached in Appendix 5. These documents include details on the analysis models and applied boundary conditions. In Table 4.9 details of the participants' simulations are compared.

**Table 4.9. Participants and employed simulation methodology**



Part.	FE-Code	Transient therm. Sim.	2D/3D	Number of Elements	Large strain	Creep Law	Failure criterion
2	Adina	No	2D	MT1-st.: 45	Yes	Norton	Numerical instability
			3D	MT1-el.: 3 600-7 200 MT2-el.: 2 880-5760 MT4-el.: 6 000-12 000			
3	Abaqus	Yes (?)	3D	MT1-st.: 31 416	?	Norton	Numerical instability (20 % creep strain)
				MT1-el.: 23 392	?	Mod. Garofalo (MG)	20 % creep strain
				MT2-el.: 45 370	?	Khachanov- Rabotnov (KR)	Damage parameter (D = 1)
4	Ansys Mech.	Yes (?)	3D	?	?	Norton	10 % total strain

In Table 4.10, the employed symmetry properties of the FE models are displayed.

**Table 4.10. Employed symmetry properties for steam generator tube models (180°)**

Participant	Symmetry properties of FE model	steam generator tube models
2	No symmetry used	

**Table 4.11. Employed symmetry properties for steam generator tube models (180°)  
(Continued)**

3	No symmetry used	
4	Longitudinal half symmetry	

In Table 4.11, the loading conditions of the participants' FE models are shown.

**Table 4.12. Participants and employed load conditions**

Participant	Temperature load	Pressure load	Auxiliary axial force
2	Homogenously on all elements	On inner surface	Axial force due to pressure on cross section
3	?	?	?
4	On inner surface	On inner surface and end cap	-

In Table 4.12 (main tasks), the boundary conditions of the participants' simulations are compared. Participant 2 used a separate 2D model for the straight pipe, where the lower nodes are fixed in axial direction and the upper nodes coupled on a horizontal line.

**Table 4.13. Participants and employed boundary conditions of models (main tasks)**

Participant	"Left" surface fixation	"Right" surface fixation
2	Direction normal to the surface is fixed	-
3	?	?
4	Direction normal to the surface is fixed	Direction normal to the surface is fixed

#### 4.2.1. Main tasks (MT)

In Table 4.13, the failure times of the main tasks MT1 (main coolant line), MT2 (surge line) and MT4 (steam generator tube) of the participants results are displayed to give an overview. Details are given in the following sub-chapters.

**Table 4.14. Comparison of failure times and temperatures of main tasks MT1 (MCL), MT2 (SL) and MT4 (SGT)**

Participant	Failure Criterion	MT1-MCL-elbow	MT1-MCL-straight	MT2-SL-elbow	MT4-SGT-elbow
2	Numerical instability	10 800 s 799 °C	10 424 s 740 °C	11 100 s 937 °C	11 880 s 916 °C
3	20 % creep strain (Norton)	10 569 s 762 °C	10 551 s 758 °C	11 411 s 948 °C	11 243 s 847 °C
	20 % creep strain (MG)	10 534 s 755 °C	10 539 s 756 °C	*	11 021 s 823 °C
	Damage value (D = 1) (KR)	10 247 s 704 °C	10 360 s 727 °C	10 435 s 858 °C	11 491 s 874 °C
4	10 % total strain	10 590 s 768 °C	10 779 s 795 °C	12 107 s 974 °C	10 798 s 798 °C
<b>Mean value</b>		10 548 s 758 °C	10 531 s 755 °C	11 263 s 929 °C	11 287 s 852 °C

\*Calculation shows significant increase of creep strains already after 9 862 s

##### 4.2.1.1 Main task 1 – Main coolant line (straight)

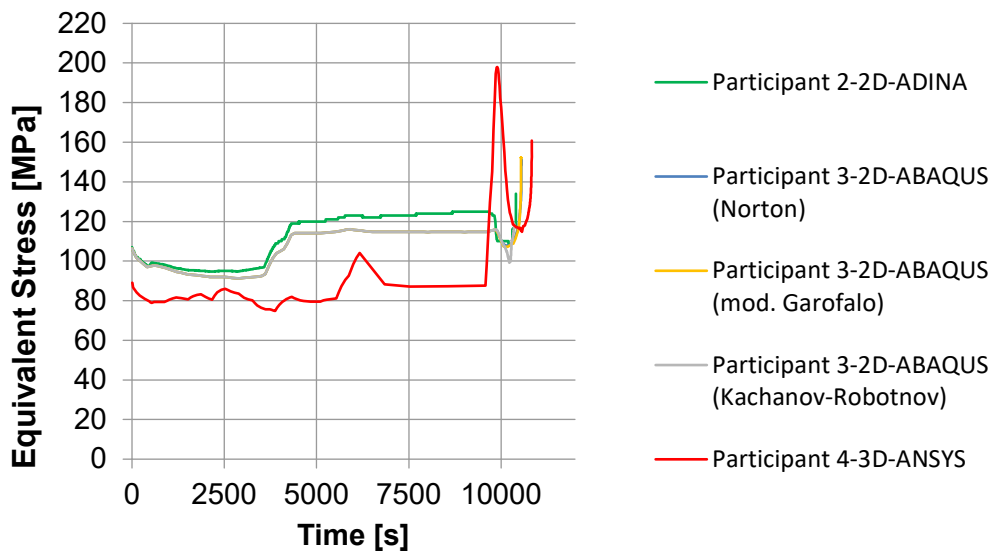
In Table 4.14, the failure times and the corresponding temperatures of the main coolant line (straight piece) during a postulated accident scenario are compared. The failure times of all participants are within a scatterband of -170 s up to +284 s around the mean value (10 531 s). The failure time of participant 4 based on a failure strain of 10 % shows the largest value and the calculation of participant 3 based on the damage parameter in the Khachanov-Rabotnov creep law gives the most conservative failure time.

**Table 4.15. Comparison of failure times and temperatures of Main Task 1 (Main coolant line, straight)**

Participant	Failure Criterion	Failure Time	$\Delta t$ to mean value	Failure Temperature	$\Delta T$ to mean value
2	Numerical instability	10 424 s	-107 s	740 °C	-15 K
3	20 % creep strain (Norton)	10 551 s	20 s	758 °C	3 K
	20 % creep strain (MG)	10 539 s	8 s	756 °C	1 K
	Damage value (D = 1) (KR)	10 360 s	-171 s	727 °C	-28 K
4	10 % total strain	10 779 s	248 s	795 °C	40 K

In Figure 4.9 the equivalent stresses of the participants' simulations are compared. The simulation results of participant 2 and participant 3 are in good agreement while the result of participant 4 underestimates the stress until it rises sharply at 9 572 s. Possibly, geometry issues of the FE model of participant 4 are responsible for lower stress level at the beginning. The reason for the peak of participant's 4 stress curve is possibly due to thermal stresses by a thermal gradient, since thermal boundaries were applied only at the inner surface.

Figure 4.9. Equivalent stresses of simulations (MT1, straight)



The following figures display the accumulated plastic strain (Figure 4.10) and the accumulated creep strain (Figure 4.11) show a typical pattern of failure which is related to piping under pressure and high temperature as described in the large-scale test (see chapter 3. ). Large deformations caused by progressive rising creep strains start before relevant plastic strains occur. At a point of high creep strain abruptly plastic strain rises until failure caused by plastic instability. The deviations in the strain plots may be partly due to different interpolation methods in the employed material formulations of the used FE codes.



Figure 4.10. Accumulated plastic strains of simulations (MT1, straight)

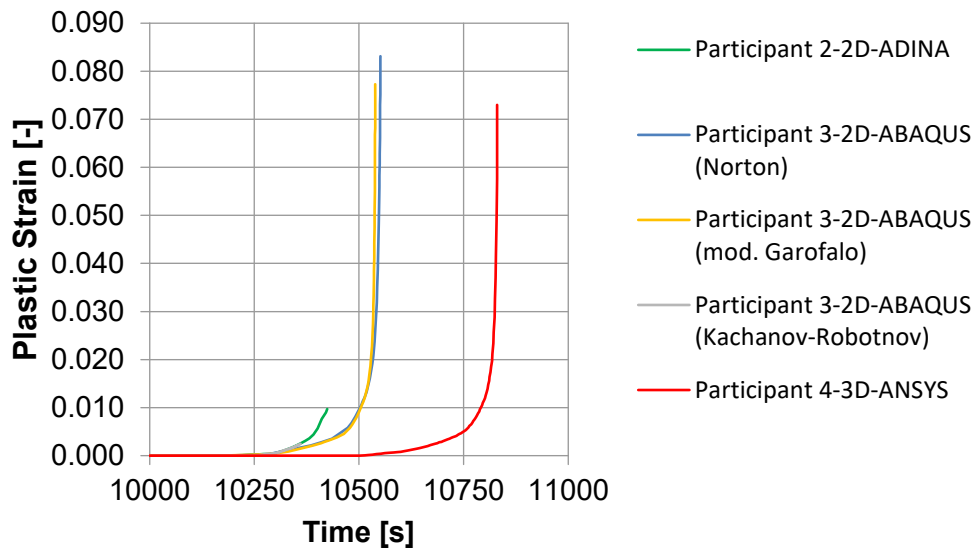
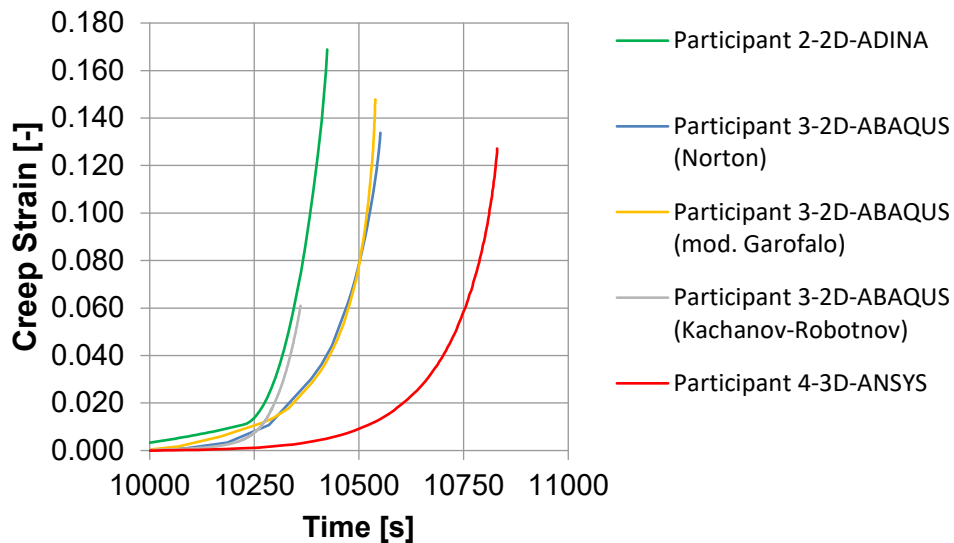


Figure 4.11. Accumulated creep strains of simulations (MT1, straight)



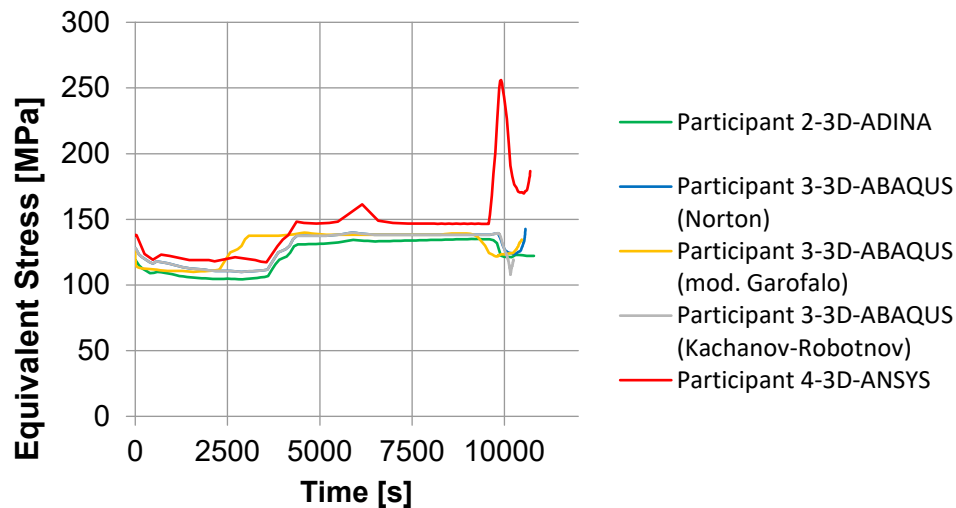
#### 4.2.1.2 Main task 1 – Main coolant line (elbow)

In Table 4.15 the failure times and the corresponding temperatures of the main coolant line (elbow piece) are compared to the mean values (10 548 s / 758 °C). In this case the failure time of participant 2 based on numerical instability shows the largest value and similar to the MCL straight line the calculation of participant 3 based on the damage parameter in the Khachanov-Rabotnov creep law gives the most conservative failure time.

**Table 4.16. Comparison of failure times and temperatures of main tasks MT1 (main coolant line, elbow)**

Participant	Failure	Failure Time	$\Delta t$ to mean value	Failure Temperature	$\Delta T$ to mean value
2	Numerical instability	10 800 s	252 s	799 °C	41 K
3	20 % creep strain (Norton)	10 569 s	21 s	762 °C	4 K
	20 % creep strain (MG)	10 534 s	-14 s	755 °C	-3 K
	Damage value (D = 1) (KR)	10 247 s	-301 s	704 °C	-54 K
4	10 % total strain	10 590 s	42 s	768 °C	10 K

In Figure 4.12 the equivalent stresses of the participants' simulations are compared. The simulation results of all participants are inside a scatter band of ca. 28 MPa up to about 9 000 s. The reason for the peak of participant's 4 stress curve at 9 572 s is possibly due to thermal stresses by a thermal gradient, since in this calculation thermal loads are applied only at the inside (see chapter 0).

**Figure 4.12. Equivalent stresses of simulations (MT1, elbow)**

The following figures display the accumulated plastic strains (Figure 4.13) and the accumulated creep strains (Figure 4.14). The strain histories of all participants show significant increase which leads to failure prediction within about 250 s. Only the calculation of participant 3 based on the damage parameter in the Khachanov-Rabotnov creep law predicts failure at creep strain values of about 2 %, which is very conservative.

Figure 4.13. Accumulated plastic strains of simulations (MT1, elbow)

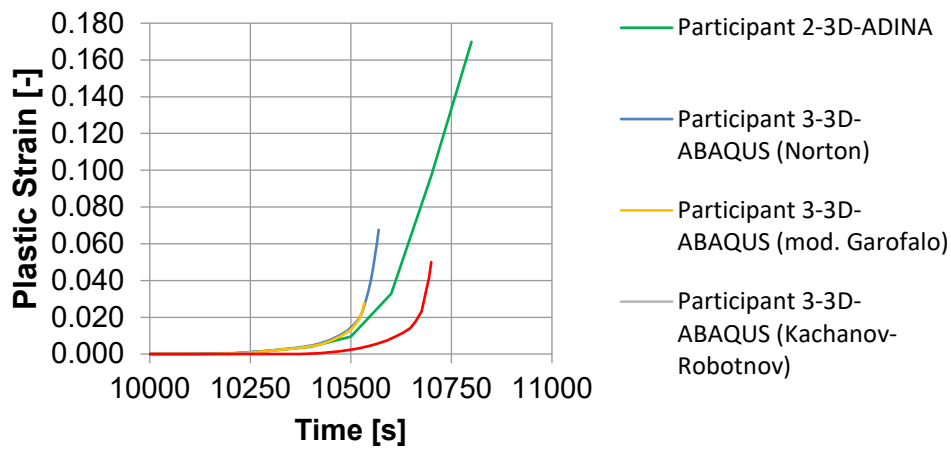
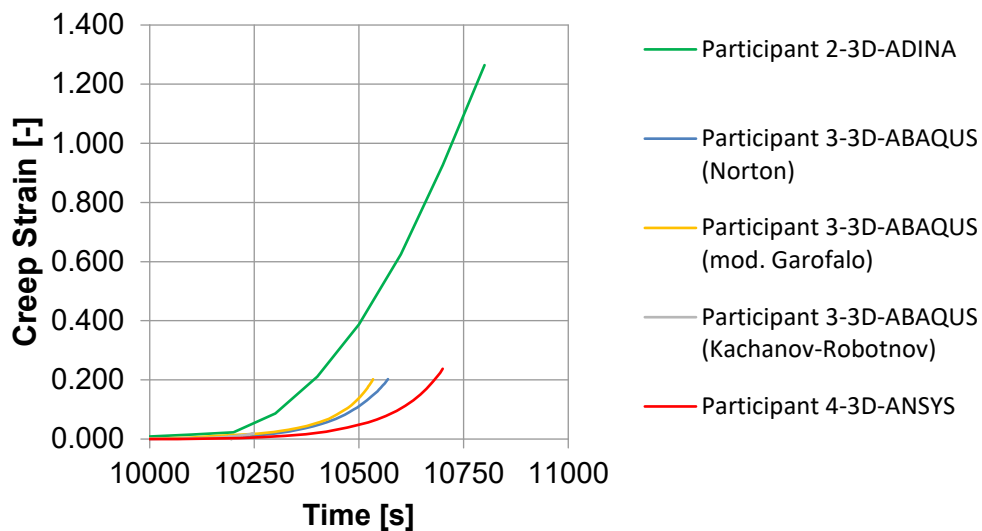


Figure 4.14. Accumulated creep strains of simulations (MT1, elbow)



#### 4.2.1.3 Main task 2 – Surge line

In Table 4.16, the failure times and the corresponding temperatures of the surge line (elbow piece) are compared. The mean failure time (11 263 s, without the calculation of participant 3 based on the modified Garofalo creep law) is about 715 s larger than the failure time of the MCL elbow.

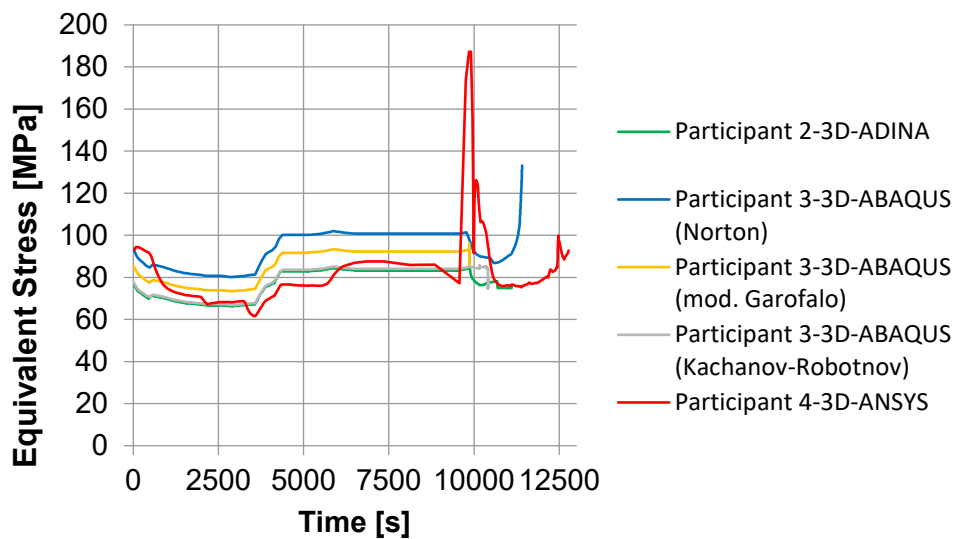
Table 4.17. Comparison of failure times of main tasks 2 (surge line, elbow)

Participant	Failure Criterion	Failure Time	$\Delta t$ to mean value	Failure Temperature	$\Delta T$ to mean value
2	Numerical instability	11 100 s	-163 s	937 °C	8 K
3	20 % creep strain (Norton)	11 411 s	148 s	948 °C	19 K
	20 % creep strain (MG)	*			
	Damage value (D = 1) (KR)	10 435 s	-828 s	858 °C	-71 K
4	10 % total strain	12 107 s	844 s	974 °C	45 K

\*Calculation shows significant increase of creep strains already after 9 862 s

In Figure 4.15, the equivalent stresses of the participant's simulations are compared. The simulation results of all participants are inside a scatter band of ca. 20 MPa up to about 9 000 s.

Figure 4.15. Equivalent stresses of simulations (MT2, elbow)



The following figures display the accumulated plastic strains (Figure 4.16) and the accumulated creep strain (Figure 4.17). The creep strain curves show significant discrepancies. The calculation of participant 3 based on the modified Garofalo (MG) creep law shows significant increase of creep strains already after 9 862 s which may be attributed to the participant's determination of Garofalo creep law parameters and corresponding interpolation techniques. Participant 2's calculation is aborted at about 11 000 s due to unphysical boundary effects.

Figure 4.16. Accumulated plastic strains of simulations (MT2, elbow)

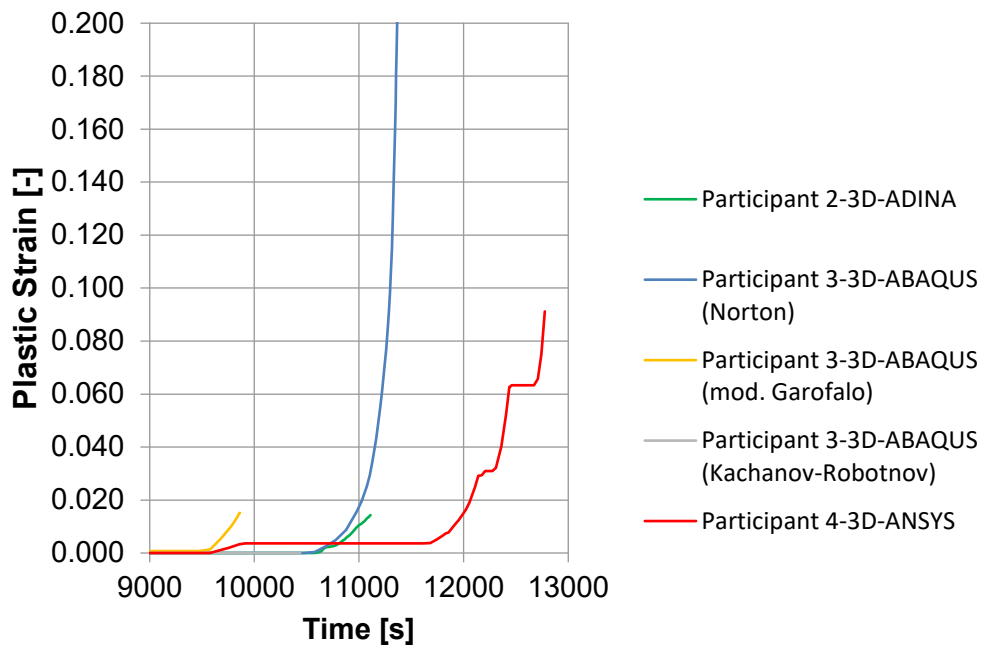
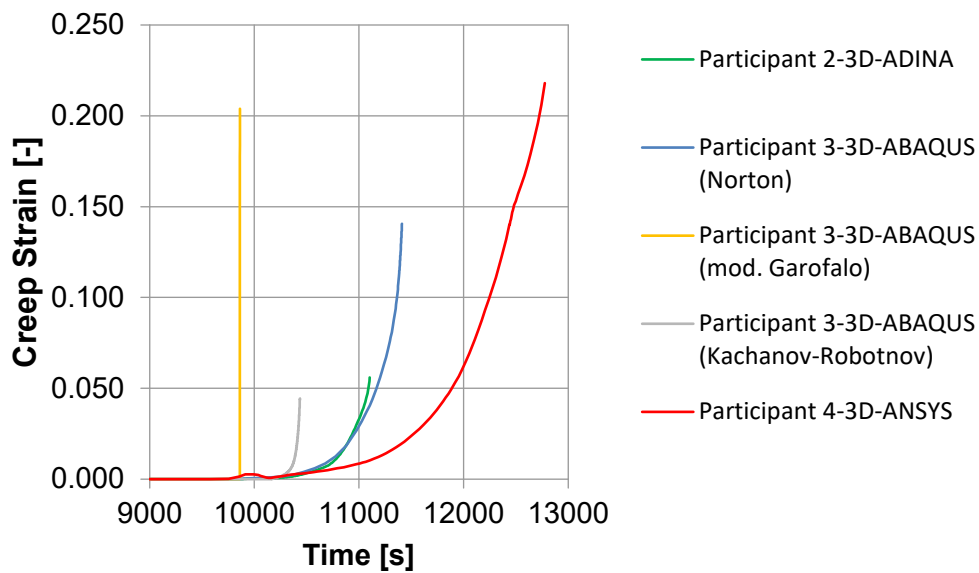


Figure 4.17. Accumulated creep strains of simulations (MT2, elbow)



As already noticed in the calculations on MT1, deviations in the strain plots may be also partly due to different interpolation methods in the employed material formulations of the used FE codes.

#### 4.2.1.4 Main task 3 – Steam generator tube with wall thinning

The minimum wall thickness of the steam generator tube (generic piece with wall thickness of 1.23 mm) during the accident without failure is identified by a sequence of single simulations. The results of the participants show that for the specified loading failure occurs if the wall thickness is less than 16 – 20 % of the original wall thickness (see Table 4.17), i. e. SGT with more than 80 % wall thinning due to damage mechanisms may fail. All results are inside a band of 5.5 %.

**Table 4.18. Minimum wall thickness of steam generator tube (reference wall thickness 1.23 mm) during accident without failure**

	Participant 2	Participant 3	Participant 4
$t_{\min}$ (mm / %)	0.215 / 17.5	0.246 / 20	0.2 / 16.3
Reduction (%)	85.5	80	83.7

#### 4.2.1.5 Main task 4 – Steam generator tube with reflux-condenser scenario

In Table 4.18, the failure times and the corresponding temperatures of steam generator tube (elbow piece) in a reflux-condenser scenario are compared. The mean failure time (11 287 s) is 739 s larger than the corresponding value of the MCL elbow.

**Table 4.19. Comparison of failure times and temperatures of main task MT4**

Participant	Failure Criterion	Failure Time	$\Delta t$ to mean value	Failure Temperature	$\Delta T$ to mean value
2	Numerical instability	11 880 s	593 s	916 °C	64 K
3	20 % creep strain (Norton)	11 243 s	-44 s	847 °C	-5 K
	20 % creep strain (MG)	11 021 s	-266 s	823 °C	-29 K
	Damage value (D = 1) (KR)	11 491 s	204 s	874 °C	22 K
4	10 % total strain	10 798 s	-489 s	798 °C	-54 K

### 4.2.2. Tasks of parametric studies (PS)

#### 4.2.2.1 Parametric studies A (PS-A)

In parametric study A the boundary conditions from the main tasks (MT) are modified, so that both ends of the pipes are fixed. In Table 4.19 the failure times of the main tasks 1 (main coolant line), 2 (surge line) and 4 (steam generator tube) with modified boundary conditions are given. The influence of the modified boundary conditions on e. g. the mean failure time of MT1-MCL straight is only 142 s.

**Table 4.20. Comparison of failure times and temperatures of PS-A**

Participant	Failure Criterion	MT1-MCL-elbow	MT1-MCL-straight	MT2-SL-elbow	MT4-SGT-elbow
2	Numerical instability	10 320 s 720 °C	10 800 s 799 °C	*	11 540 s 880 °C
3	20 % creep strain (Norton)	10 529 s 767 °C	10 569 s 762 °C	11 423 s 948 °C	11 473 s 873 °C
	20 % creep strain (MG)	10 524 s 753 °C	10 562 s 761 °C	**	11 270 s 850 °C
4	20 % creep strain	10 589 s 768 °C	10 762 s 795 °C	12 140 s 976 °C	10 783 s 797 °C
<b>Mean value</b>		10 491 s 752 °C	10 673 s 780 °C	11 781 s 962 °C	11 267 s 850 °C

\* Simulation run aborted after 9 500 s due to convergence problems

\*\* Calculation shows significant increase of creep strains already after 9 862 s

#### 4.2.2.2 Parametric studies C (PS-C)

In parametric study C the loading conditions of main tasks 3 and 4 were modified so that due to a depressurised secondary side, the difference pressure on the steam generator tube is increased. The results of the participants on the minimum wall thickness of the steam generator tube (PS-C-MT3) are given in Table 4.20. The results show that for the modified loading condition failure occurs if the wall thickness is less than 33 – 40 % of the original wall thickness, i. e. SGT with more than 60 % wall thinning due to damage mechanisms may fail.

**Table 4.21. Minimum wall thickness of steam generator tube during accident without failure (original wall thickness: 1.23 mm)**

	Participant 2	Participant 3
<b>t<sub>min</sub> (mm / %)</b>	0.4 / 32.5	0.49 / 39.8
<b>Reduction (%)</b>	67.5	60.2

In Table 4.21, the failure times and the corresponding temperatures of steam generator tube (elbow piece) in a reflux-condenser scenario with depressurised secondary side (PS-C-MT4) are given. The mean failure time (10 822 s) is about 465 s smaller than the corresponding value in MT4 and 274 s larger than the value of MCL elbow.

**Table 4.22. Comparison of failure Times of PS-C (MT4, SGT, elbow)**

Participant	Failure Criterion	Failure Time	$\Delta t$ to mean value	Failure Temperature	$\Delta T$ to mean value
2	Numerical instability	11 170 s	348 s	838 °C	40 K
3	20 % creep strain (Norton)	10 652 s	-170 s	779 °C	-19 K
	20 % creep strain (MG)	10 644 s	-178 °s	777 °C	-21 K

### 4.2.3. Conclusion

The participants' results indicate a common sequence of failure during the assumed core melt scenario. The main coolant line fails first, the surge line second and the steam generator tube last. For the specified loading SGT failure occurs if the wall thickness is less than 16 – 20 % of the original wall thickness, i. e. SGT with more than 80 % wall thinning due to damage mechanisms may fail. Early failure of steam generator tube with heating by circulating gas flow (reflux condenser) becomes more probable.

The main influence factors concerning differences in calculated results are:

- Creep data were provided for a set of stress / temperature values. Some participants used interpolation measures for values in between by the tools of the used codes, others used an Arrhenius type approximation.
- Boundary conditions at the pipe end may have significant influence if not properly defined.
- The comparison of same stress values is important (specified location/global maximum, inside/outside, vector/equalised scalar, maximum/averaged).
- Nonphysical effects at the boundaries preventing a solution convergence or leading to a nonphysical rise in values confused with failure.
- Method of thermal load application is crucial. Some participants used homogeneous temperature distributions, some calculated transient distributions with thermal gradients, which effect stress gradients.

The general key findings from the participants' results are:

- It has been shown that a geometric non-linear calculation is necessary to account for the changed kinematic properties due to large deformations during the progressive failure process.
- A material law which considers non-linear material properties, i.e. creep and plasticisation effects is necessary for an accurate simulation and prediction of the time of failure. Norton's Law, a modified Garofalo formulation and a Khachanov-Rabotnov Law were successfully used to describe creep properties of the employed materials.
- The choice of a failure criterion may have a minor influence on the time of failure, if high rise of strains occur.



In conclusion, therefore, the COSSAL results on PWR components show that Finite-Element methods for assessment of component failure are reliable and robust. To get an appropriate failure analysis of PWR components it is important to employ suitable boundary and load conditions as well as a fitting material law which considers creep effect well.

## 5. Benchmark study on boiling water reactor components

### 5.1. Problem statement on boiling water reactor components

#### 5.1.1. Motivation

While the first two benchmarks focused on global/catastrophic failure of components in form of an experiment recalculation (see chapter 3. ) and an application to a severe accident analysis of a PWR (see chapter 4. ), the third COSSAL benchmark (Task 4.2 of the COSSAL project) addressed early local failure resulting in leaks of limited size. Investigations on the behaviour of the pressure boundary of unit 1 of Fukushima Daiichi during the 2011 accident showed a significant effect of early leaks on thermal-hydraulic calculations and thus the importance of taking local failure into account. Local failure can occur in a wide variety of situations, e.g. in connection with spot-like loads or local weaknesses of components.

In this benchmark, two representative cases were derived from the investigations on the Fukushima Daiichi accident and presented in a generic manner:

- The first task addressed the behaviour of safety valves in the region of the flange connection under high temperature and pressure loading.
- The second task addressed a possible buckling failure of a reactor core instrumentation pipe under high temperature and external pressure.

While in the main tasks all specifications were given in detail, in the parametric studies participants were free to vary suggested or any other parameters to investigate sensitivities and to identify relevant factors of influence.

#### 5.1.2. Geometry, loads and boundary conditions

##### 5.1.2.1 Local failure of a flange connection

In this task, a local failure and subsequent leak of a flange connection of a safety valve should be investigated. Therefore, a coupled (unidirectional) thermomechanical calculation was required.

The connection was made of two DN150 / 6'' flanges. With respect to the available material characterisation data, the material of the flanges was assumed to be 20MnMoNi5-5. The flange was internally heated by hot steam with an increasing temperature of 0.2 K/s starting from 300 °C. This temperature course was based on best estimate thermal-hydraulic calculations of Fukushima Daiichi unit 3 /NEA15/. The heat transfer from the steam at the inside of the flanges could be assumed as "very good", so that for the calculation a heat transfer coefficient of 10 000 W/m<sup>2</sup>K could be used. Alternatively, the inner surface of the flanges could be set to the steam temperature. At the outer surface, natural convection and radiation to the environment of 50 °C could be assumed (heat transfer coefficient of 10 W/m<sup>2</sup>K, emissivity of 0.5). The thermal calculation could be done quasistatic, since the temperature change is rather slow. The inner (differential) pressure  $p_i$  was assumed to be constant at 7.1 MPa.

The geometry of the flange was given in the schematic drawing Figure 5.1 and in Table 5.1. The simulated length of the pipe attached to the flange should be chosen sufficiently long

since creep deformation of the pipes can have an effect on the flange. A minimum of  $4 \cdot h_F$  was suggested. A suitable fixation of the pipe ends, e.g. allowing radial deformation, should be implemented. For the FEM model, a 3D-representation was suggested. Note that due to the number of 8 bolts, a  $45^\circ$  or  $22.5^\circ$  pattern-symmetry can be used.

Figure 5.1. Schematic drawing of the flange /KTA13/

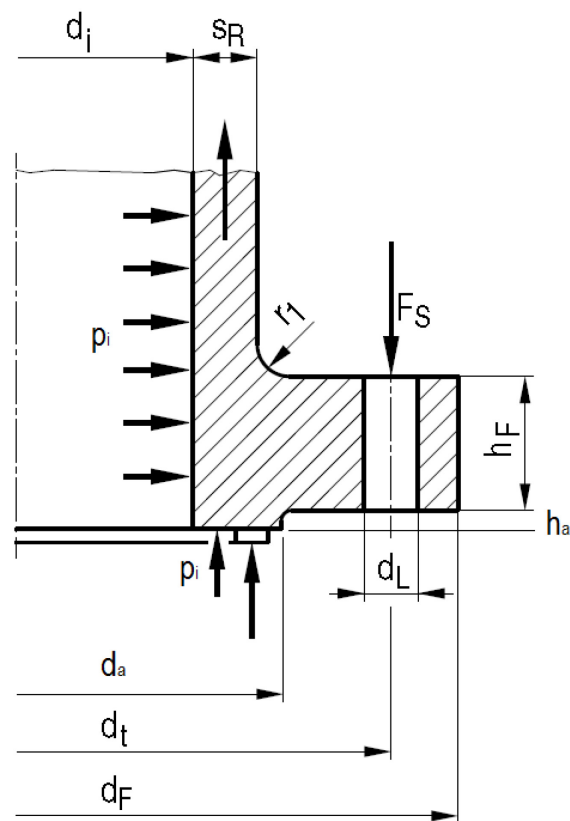


Table 5.1. Flange data

Type	$d_i$	$d_t$	$d_F$	$d_L$	$d_a$	$s_R$	$h_F$	$h_a$	$r_1$
DN150 / 6''	155.4	250	300	17.5	229.4	4.85	18	2	6

Eight M16 expansion bolts had to be considered. With respect to the available material characterisation data the material was assumed to be also 20MnMoNi5-5. Geometry and preload force data are contained in the schematic drawing Figure 5.2 and Table 5.2. The preload should be applied in a pressure free state at  $50^\circ\text{C}$ . A washer of 17 mm inner diameter, 30 mm outer diameter and 3 mm thickness made of 20MnMoNi5-5 should be modelled to transfer the load of the nut. Between flange, washer and bolt, an ideal heat transfer could be assumed (e.g. heat transfer coefficient of  $10\,000\text{ W/m}^2\text{K}$ ). The bolts could be either bonded to the flange or a contact model representing frictional contact (coefficient of friction 0.1) could be implemented.

Figure 5.2. Schematic drawing of bolt [4]

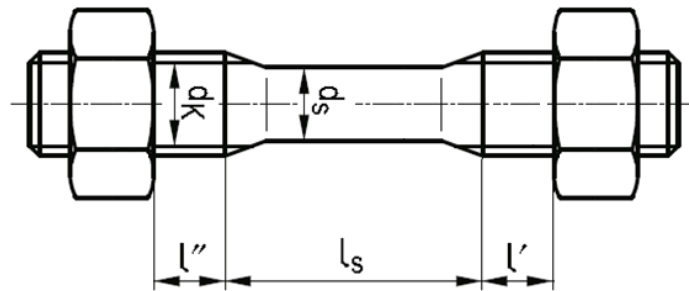


Table 5.2. Bolt data

Type	n	$F_s$ [N]	$d_k$ [mm]	$d_s$ [mm]	$l''$	$l_s$ [mm]	$l'$
M16	8	60 000	13.55	12	$\approx l'$	32	$\approx l''$

The behaviour of the gasket is a crucial point in the determination of the leak. In practice, a wide variety of gasket materials is in use (graphite, soft metal, hard metal, polyimide, etc.). In the main task, a hard metal gasket characterised by material data of 20MnMoNi5-5 was assumed. It was further assumed to be held in position by a small edge (see the schematic drawing Figure 5.3).

Figure 5.3. Schematic drawing of the gasket after arising of a gap [4]

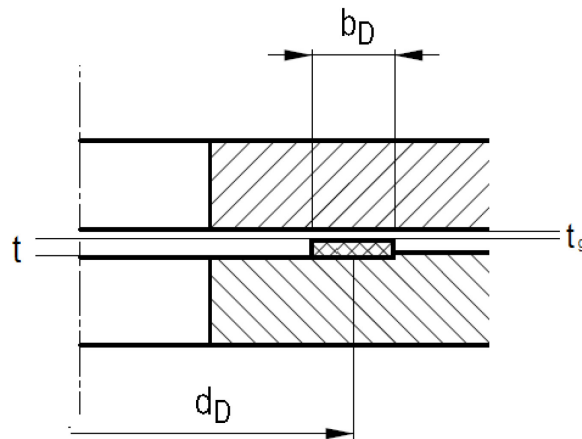
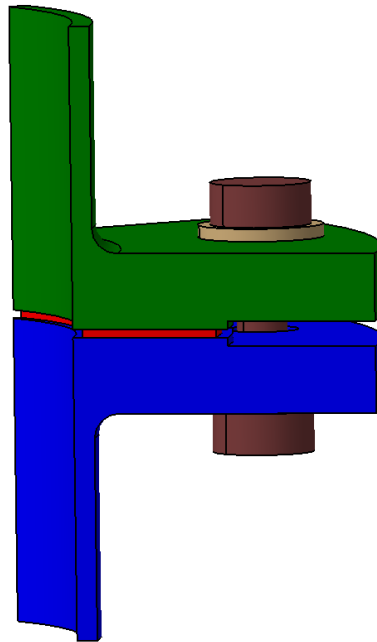


Table 5.3. Gasket data

Type	$d_D$ [mm]	$b_D$ [mm]	$t$ [mm]
Steel	192	32	2

Figure 5.4 shows a CAD model of the flange assembly, which is attached in a folder with files of CATIA V5 and STEP format (total model and part models).

Figure 5.4. CAD model of the assembly



Due to increasing steam temperature gasket, bolts and flanges will relax due to creep until the clamping force may vanish and a gap may arise between gasket and flange.

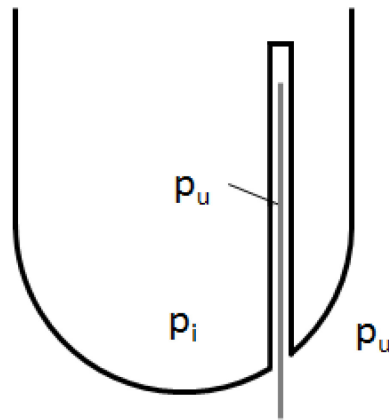
As result of the benchmark, the time history of the temperature gradient between inner diameter  $d_i$  and outer diameter  $d_F$  at the gasket-near side of a flange (bottom in Figure 5.1), the course of the clamping force as stress integral over the gasket surface and the size of the potentially arising gap  $t_g$  between gasket and flange both at the inner and outer radius of the gasket should be quantified.

In the parametric studies the participants had the opportunity to change parameters concerning sensitivity. We suggested for example to allow a radial deformation of the gasket by omitting the edge, which holds the gasket in position or assuming a different gasket material. In case of a graphite gasket, a blowout may be possible when the clamping force and the friction at the flange surface falls below a critical value, which will increase the leakage drastically.

#### 5.1.2.2 *Local failure of a reactor core instrumentation pipe*

In the second part, the buckling failure of a reactor core instrumentation tube (see Figure 5.5) under high temperatures and external pressure should be calculated. The tube was assumed to be made of 20MnMoNi5-5. The outer diameter was chosen 17 mm and the wall thickness 2 mm. The difference pressure was 7.1 MPa. The temperature of the tube rises with 0.2 K/s starting from 300 °C. A thermal calculation was not required in this case.

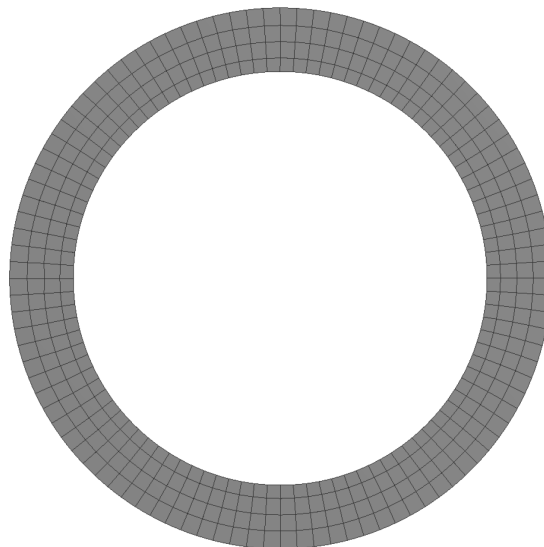
**Figure 5.5. Schematic view of a reactor core instrumentation pipe**



The time and temperature of buckling failure should be calculated either with analytical methods (e.g. von-Mises-formula) or numerical methods (FE).

If numerical methods were used, the instrumentation pipe could be modelled in 2D assuming plane stress conditions (see Figure 5.6). For the calculation an initial minimal imperfection (e.g. in form of a small geometric flattening) may be required.

**Figure 5.6. Example of an FEM model**



In the frame of a parametric study the participants had the opportunity to change parameters concerning sensitivity e.g. to assume the tube material to be made of X10CrNiNb18-9 and calculate the failure time / temperature.

### **5.1.3. Material data**

In this section material data of the ferritic and austenitic steel are presented.

### 5.1.3.1 Ferritic steel 20MnMoNi5-5

Data of the ferritic steel 20MnMoNi5-5 were already described in the first benchmark (see chapter 3.1.2).

### 5.1.3.2 Austenitic steel X10CrNiNb18-9

Data of the austenitic steel X10CrNiNb18-9 were already described in the second benchmark (see chapter 0).

### 5.1.4. Task matrix

The tasks of the third COSSAL benchmark on analysis of local failure and leakage of BWR components in a high-pressure core melt scenario are summarised in Table 5.4.

**Table 5.4. Task matrix of the third COSSAL benchmark**

<b>Main tasks (MT)</b>
<ul style="list-style-type: none"> <li>• MT 1 – Local failure of a flange connection Calculate the course of the thermal gradient, the clamping force and the potential gap at the inside and outside radius for a hard metal gasket.</li> <li>• MT 2 – Local failure of an instrumentation pipe Calculate time and temperature of buckling failure of a core instrumentation tube.</li> </ul>
<b>Tasks of parametric studies (PS)</b>
<ul style="list-style-type: none"> <li>• PS-A Vary parameters of MT 1 to study sensitivity, e.g. assume a possible radial deformation of the gasket or a different gasket material.</li> <li>• PS-B Vary parameters of MT 2 to study sensitivity, e.g. assume the tube to be made of X10CrNiNb18-9.</li> </ul>

## 5.2. Comparison of analysis results on boiling water reactor components

In the following sections, the participants' contributions to the COSSAL BWR Benchmark are summarised. The documentations provided by the participants (/INS17b/, /JRC17/, /GRS17b/) are attached in Appendix 5. These documents include details on the analysis models and applied boundary conditions. The participants were given the opportunity to modify their calculations after discussion of preliminary results during the workshop. Here, only results of the last iteration are shown, but identified and corrected user errors are discussed.

### 5.2.1. Local failure of a flange connection

Figure 5.7 gives an overview of the models used in the benchmark task. Different approaches regarding symmetry and pipe length can be clearly identified. During the comparison it had to be clarified that the asked result data referred to a full flange/gasket respectively to a flange region with only one bolt. The meshing type and sizing differs between the participants, but mesh studies done by at least two participants revealed no

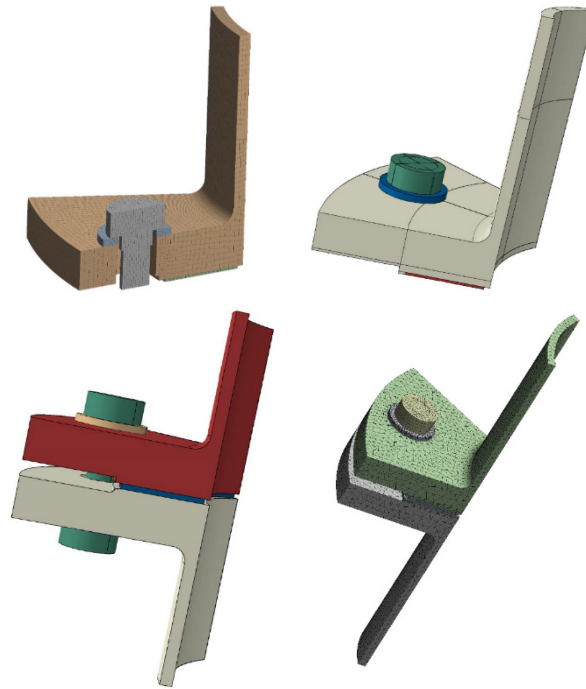
significant influence. Table 5.5 shows further boundary conditions with special emphasis on differences between participants and importance regarding suspected influence on the calculation.

**Table 5.5. Overview about different/important boundary conditions**

	Participant 1	Participant 2 (Model A)	Participant 2 (Model B)	Participant 3
<b>FEM Code</b>	ANSYS Mechanical	ABAQUS	ABAQUS	ANSYS Mechanical
<b>Symmetry, circumferential</b>	1/16	1/8	1/8	1/8
<b>Symmetry, axial</b>	1/2	1/2	1/1	1/1
<b>Thermal calculation</b>	steady state	transient	transient	steady state
<b>Rad. heat exchange bolt/hole considered</b>	no	yes	yes	no
<b>Thermal properties of contacts considered</b>	yes, unidirectional	yes, bidirectional	yes, bidirectional	yes, unidirectional
<b>Non-linear geometry effects</b>	yes	yes	yes	yes
<b>Pipe longer than given in problem statement</b>	74.1 mm = $2.7 * \sqrt{d_i * sR}$ (values see Table 5.1)	CAD file value + 40 mm = 90 mm	no	2 * CAD file value = 100 mm
<b>Top/bottom-end axial constraint</b>	free/free (symmetry)	free/free (symmetry)	fixed/free	fixed/free
<b>Bolt/Washer/Flange contact model</b>	frictional, $\mu = 0.1$	frictional, $\mu = 0.1$	TIE commands	frictional, $\mu = 0.1$
<b>Gasket vertical contact model</b>	frictional, $\mu = 0.1$	frictional, $\mu = 0.1$	frictional, $\mu=0.1$	frictionless
<b>Gasket radial constraint</b>	fixed	fixed	fixed	fixed
<b>Bolt preload</b>	Manually determined displacement	Bolt tool included in FEM code	Bolt tool included in FEM code	Bolt tool included in FEM code
<b>Loads on large (horiz.) face of gasket</b>	no	No	no	no
<b>Consideration of pipe-end-effect</b>	Stress (-55.15 MPa)	Stress (-55.152 MPa)	Stress (-55.152 MPa)	Force (-16832 N)
<b>Creep model stress dependency</b>	Norton	Norton	Norton	Garofalo
<b>Creep model temperature dependency</b>	One sampling point + Arrhenius	Coefficient interpol. + additional points	Coefficient interpol. + additional points	Coefficient interpol. + additional points



**Figure 5.7. FE models from Participant 1 (top left), Participant 2 Model A (top right), Model B (bottom left) and Participant 3 (bottom right)**



While in the problem statement, a unidirectional steady-state thermal calculation was asked, one participant took the influences of the thermal inertia and bidirectional effects of the contact on thermal calculation into account. Figure 5.8 and Figure 5.9 show the inner and outer thermal surfaces with contact to the fluid or atmosphere. While the inner surfaces are equal in all models, the outer surfaces differ regarding the area between the flanges and in the bolt hole.

**Figure 5.8. Inner thermal boundaries from Participant 1 (top left), Participant 2 Model A (top right), Model B (bottom left) and Participant 3 (bottom right)**

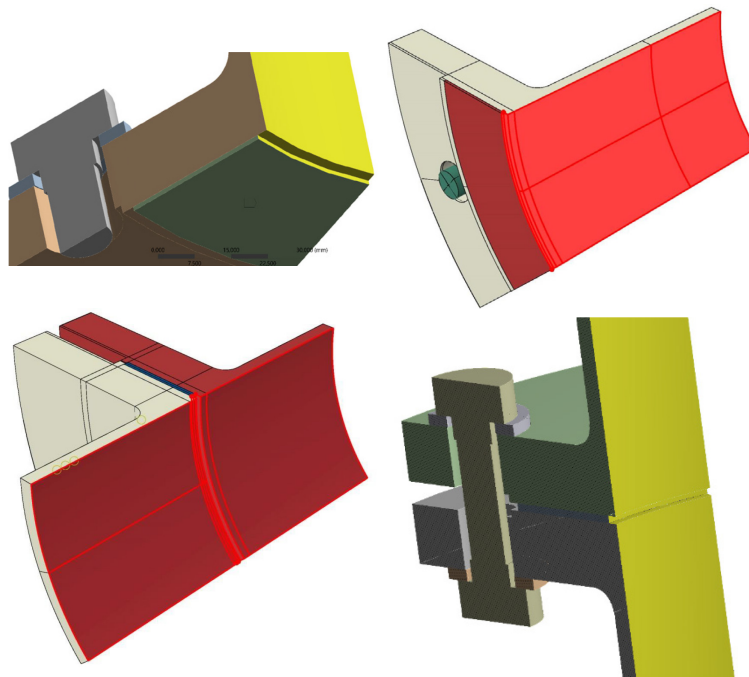


**Figure 5.9. Outer thermal boundaries from Participant 1 (top left), Participant 2 Model A (top right), Model B (bottom left) and Participant 3 (bottom right)**

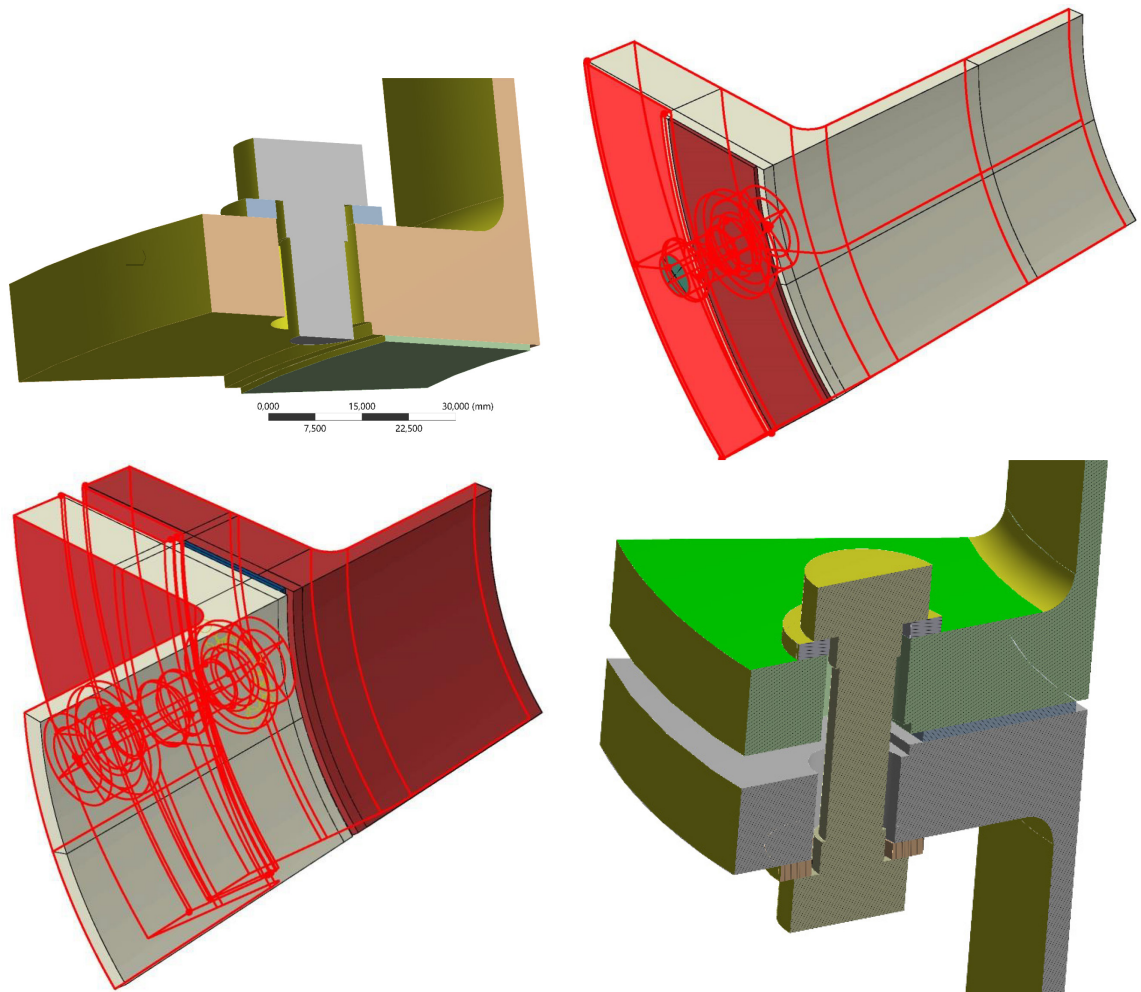
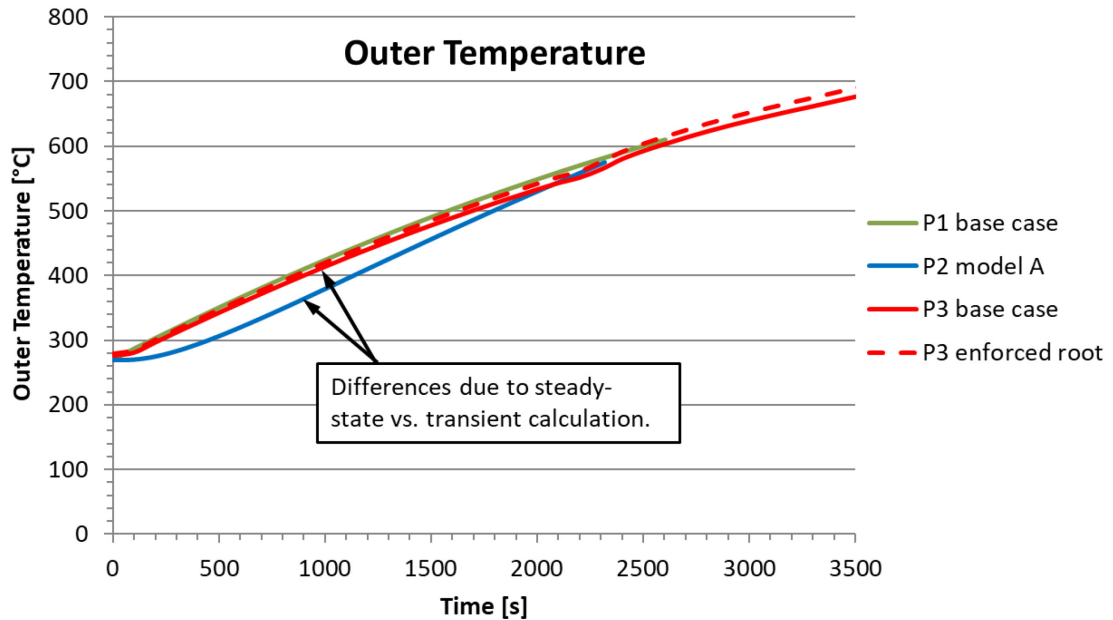
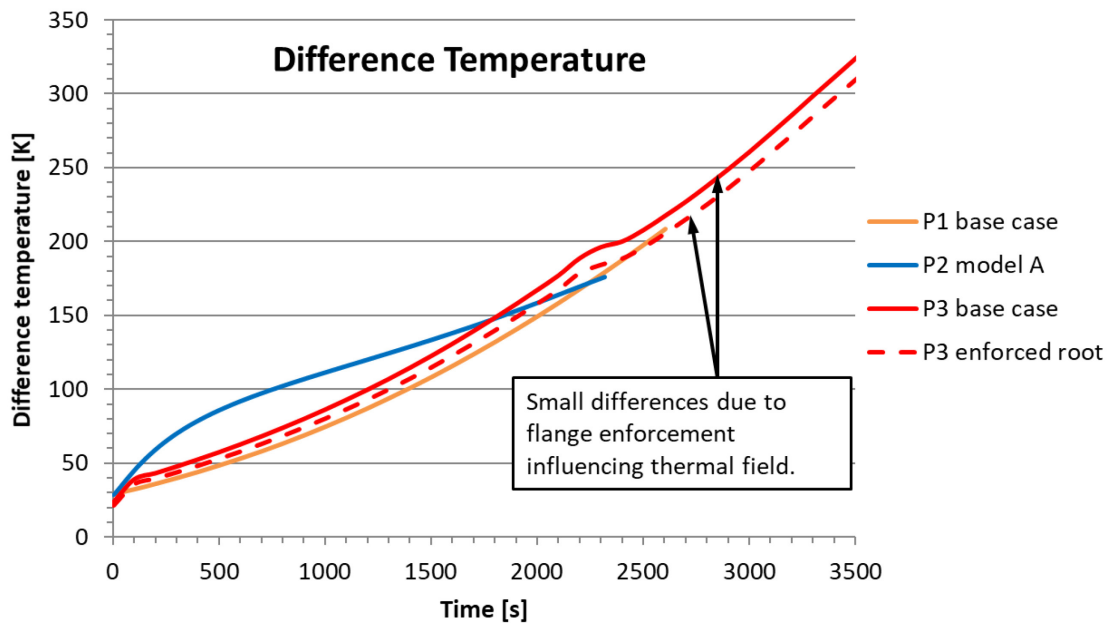


Figure 5.10 and Figure 5.11 show the calculated histories of the outer temperature, measured at the gasket-near edge, and the radial difference temperature over the flange.

**Figure 5.10. History of the outer temperature, measured at the gasket-near edge**



**Figure 5.11. History of the radial difference temperature over the flange**



The results of participant 1 and 3 are good in line despite different external boundary surfaces, which might be an indication that the temperature field is determined mainly by the heat transfer at the inside. The influence of thermal inertia, considered by participant 2

is larger than initially expected and might be non-negligible for best estimate calculation. Small differences are caused by the enforcement of the flange root, since heat transfer from pipe to flange body is slightly improved.

The main differences in the participant's mechanical model refer to the creep material modelling, the model fixation, the use of contact models and the application of bolt preload.

During the comparison of preliminary results, it was noticed that in the FE codes ABAQUS and ANSYS, temperature inter-/extrapolation of creep strain rates was done by inter-/extrapolating the coefficients of the creep relation before applying it to the creep formula.

$$\dot{\epsilon}_c(T, \sigma) = \left( \frac{T - T_2}{T_1 - T_2} * (A_1 - A_2) \right) * \sigma^{\left( \frac{T - T_2}{T_1 - T_2} * (B_1 - B_2) \right)}$$

This can lead to creep rate values much larger than the creep rate values calculated at the adjacent temperature support points. A more detailed description of the problem is given in /JRC17/. The problem was faced differently by the participants: Participant 1 used only the temperature support point near the suspected failure/onset of significant creep together with a temperature-dependency described by an Arrhenius-relationship derived from adjacent data. Participant 2 solved the problem by introducing several additional support points using an automated script. Participant 3 used the Garofalo-description of the stress dependency, which is much less affected by the problem. As an additional solution it was further discussed to generate a new set of coefficients for the creep relationship, keeping the coefficients in a narrow band and validating the interpolation behaviour.

Figure 5.12 and Figure 5.13 show the histories of the outer and inner gap. The inner gap starts with an offset of about 0.7 mm, which is due to the simplification in the problem statement taking hard steel as gasket material.

Figure 5.12. History of the outer gap (maximum gap along gasket outer edge)

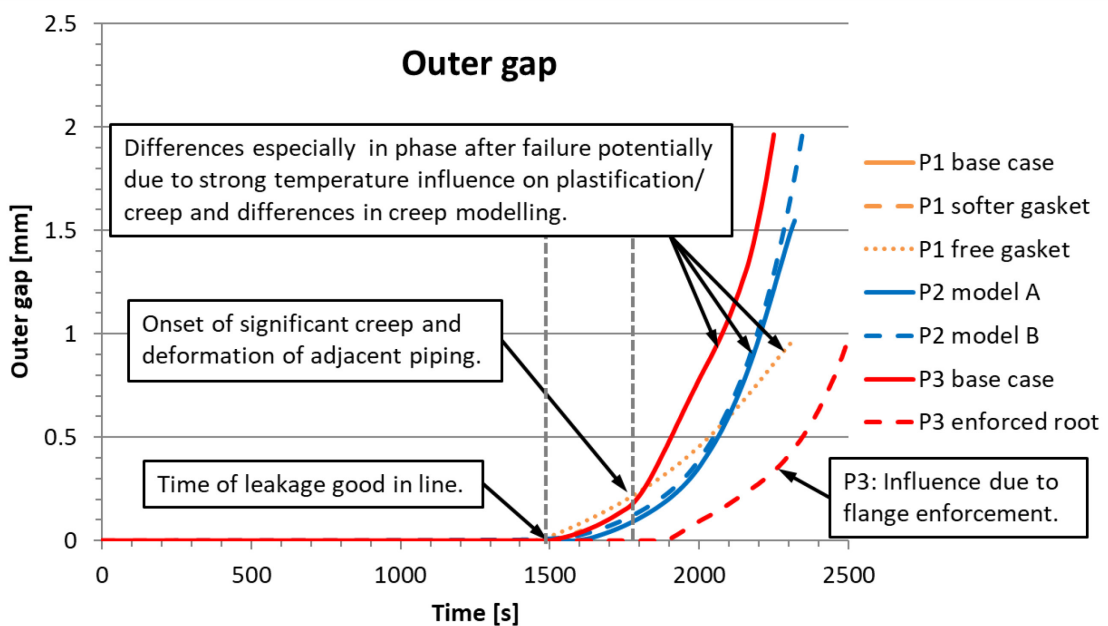
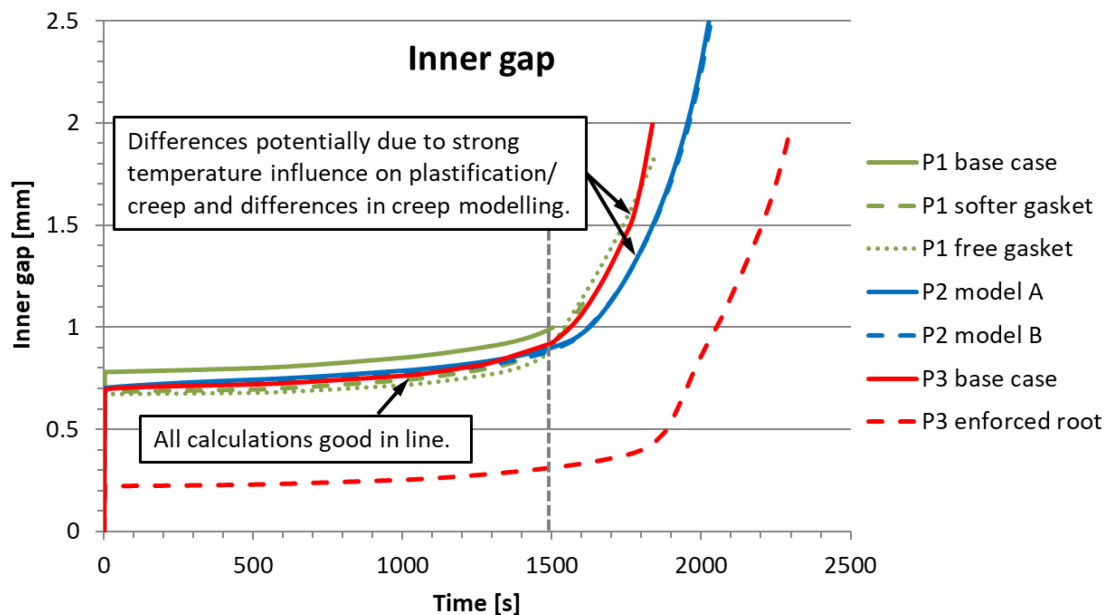


Figure 5.13. History of the inner gap (maximum gap along gasket inner edge)



It can be seen that until time of leakage and even until onset of significant creep and deformation of the adjacent pipe, all base case calculations are good in line. The later difference may be contributed to the different creep material modelling or differences in the temperatures due to transient modelling. The failure times defined as appearance of an outer gap, are also good in line (see Table 5.6). The parametric study with enforced flange root shows a significantly later failure.

Table 5.6. Failure times defined by arising outer gap

P1 base case	P1 softer gasket	P1 free gasket	P2 model A	P3 base case	P3 enforced root
1 503	1 473	1 403	1 570	1 500	1 900

Since the pipe given in the problem statement was rather short and an influence of the fixation could not be precluded, it was extended in the models by different amounts. Caused by the different use of axial symmetry the fixation in axial direction differs between a fixed/free and a free/free arrangement.

As contact model, mainly frictional contact with  $\mu = 0.1$  was used. The use of TIE contacts by one participant for the bolt and frictionless contacts by one participant for the gasket may be without influence here, since on the one hand a radial movement of the bolt was observed after failure and due to the problem statement simplifications, there was no significant friction induced tension on gasket surfaces.

For the application of the bolt preload, both special tools integrated in FE codes and manual displacement corresponding were used.

Figure 5.14 and Figure 5.15 show the reported bolt force and clamping force. While the bolt force refers to one bolt, the clamping force refers to the whole gasket. Different

calculation methods for the gasket force (e.g. integration of stresses, force balance) may explain a certain scatter of the reported gasket forces. The base case calculations of the bolt force are good in line. The enforcement of the flange root prevents a force relief between bolt and flange by rotation of the flange body. In the reported clamping forces, the influence of the use of axial symmetry (calculations of participant 2) and the influence of a 10 % reduced gasket Young's modulus, respectively a gasket with free radial motion (calculations of participant 1) can be observed.

Figure 5.14. History of the bolt force

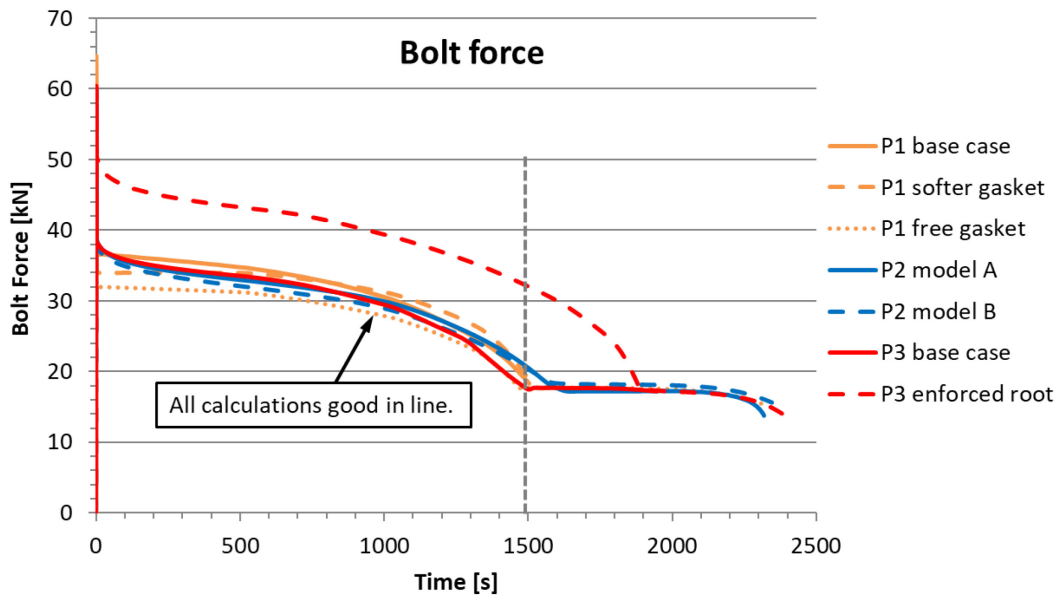


Figure 5.15. History of the clamping force

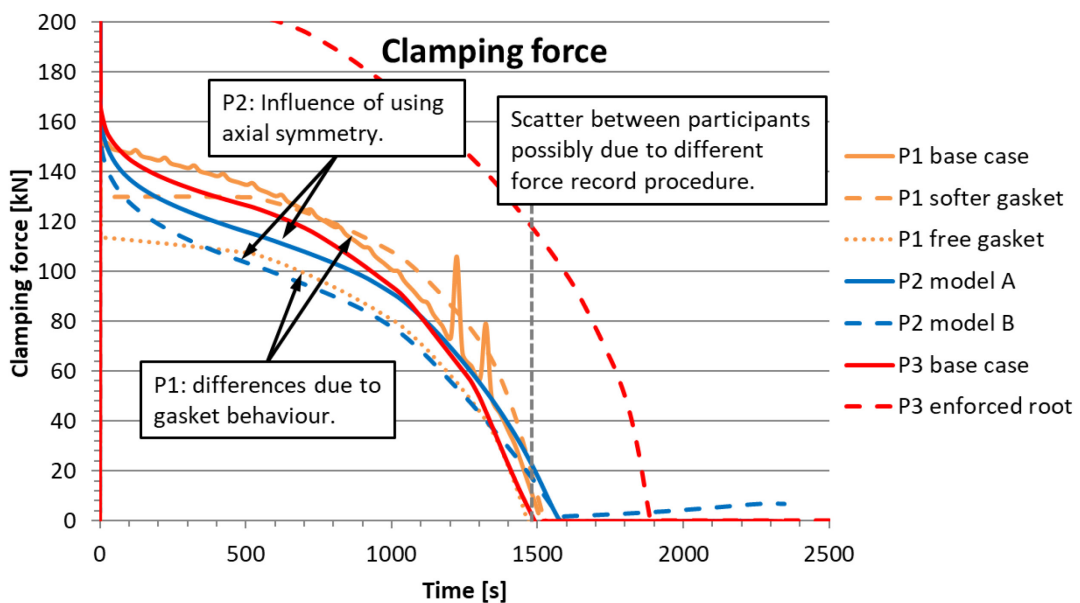


Figure 5.16 and Figure 5.17 show the history of the inner gap and the bolt force during following steps: (1) application of the pretension at a temperature of 50 °C, (2) application of inner pressure and axial force, (3) heating up to 300 °C.

Figure 5.16. History of the inner gap during the load application phase

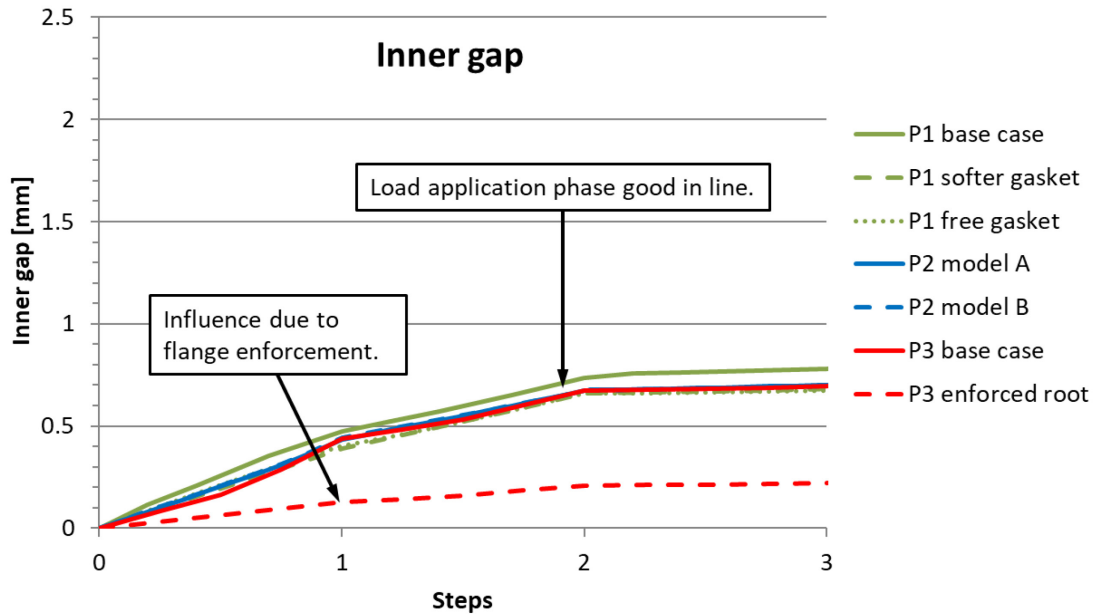
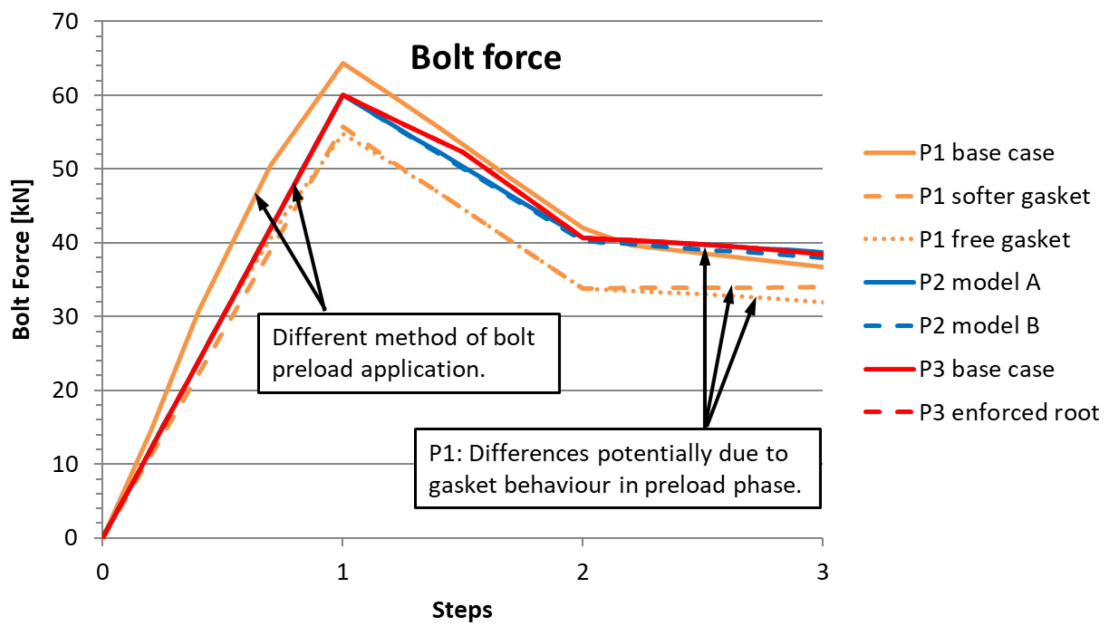


Figure 5.17. History of the bolt force during the load application phase





The reported values during the steps are good in line, which is an indication that the preload is correctly applied. Minor differences may origin from different methods of preload application or the different gasket behaviour in the parametric studies of participant 1.

The failure mode of the calculated flange is significantly influenced by geometry and lines of action of the forces. The radial position of the bolt determines its temperature history and thus its relaxation behaviour. After a certain relaxation of the bolt pretension due to creep, the momentum, which is built first mainly between bolt and gasket and later mainly between bolt and axial force at the pipe ends, leads to a rotational deformation, which further relaxes the forces and finally results in an arising outer gap. For the enforced flange this mechanism is suppressed to a certain extent, but the rotation is supported here by the later radial deformation of the upstream pipe due to bulging. In case of a flange design with bolts penetrating the gasket, the momentum load on the bolt would be much lower and the failure mechanism might change. Different gasket materials, e.g. with lower tensile strength or temperature resistance may also evoke other failure modes.

In summary, lessons learnt from the benchmark comparisons and the discussions during the workshop are:

- For creep material models, interpolation procedures in FE codes shall be validated, e.g. by generating “material model maps”.
- Physical dimensions used for comparison shall be clearly defined (specified location/global maximum, inside/outside, vector/equalised scalar, maximum/averaged, area of symmetric/full model).
- Thermal inertia effects and feedback loop of the mechanical calculation on thermal contacts might not be negligible.
- Care should be given to the process of preload application and the sequence of steps.
- The distance between model boundaries and the area of interest shall be chosen large enough to prevent mutual influence.
- Effects that were not considered in the benchmark, but may play a crucial role include: Consideration of heat exchange between bolt and hole, heating of the gasket/bolt due to premature leakage flow, loads on the large (horizontal) faces of the gasket once a gap arises, potentially leading to a hysteresis.
- In general, for a flange in the examined scenario, several failure modes are possible depending on geometry, radial positions of the bolts, lines of action of the forces and gasket material.

### ***5.2.2. Local failure of a reactor core instrumentation pipe***

The benchmark part on local failure of a reactor core instrumentation pipe was finished by only one participant. The participant used two different models, one based on the analytic linear-elastic von-Mises buckling formula and one based on a 2D FE model considering plasticisation and short-term creep effects. For details, see /GRS17b/. Subsequently, selected results are given.

**Table 5.7. Calculated failure times**

<b>Model</b>	<b>Failure time [s]</b>	<b>Failure temperature [°C]</b>
Von-Mises	4 980	1 296
2D FE	3 320	964

The main conclusions are:

- Plasticisation and short-term creep effects are not negligible and might significantly influence the failure time.
- Future investigations should have a closer look on the difference between short-term creep behaviour under tension and compression loading situation and the leak area of the arising gap.

## 6. Evaluation of the COSSAL workshop

A workshop on the Components and Structures under Severe Accident Loading (COSSAL) activities was held in February 2018 at Gesellschaft für Anlagen- und Reaktorsicherheit (GRS) in Cologne. In addition to the comparison and discussion of the benchmark results, seven plenary lectures were presented, reflecting the status of activities within the participating organisations. The agenda of the workshop is given in Appendix 7. Participants were from organisations listed in Table 6.1.

**Table 6.1. Organisations that participated in the Workshop**

Nuclear Energy Agency (NEA)	France
Institut de Radioprotection et de Sûreté Nucléaire (IRSN)	France
Kiwa Inspecta	Sweden
Joint Research Centre (JRC) Petten	European Union
ÚJV Řež	Czech Republic
Materials Testing Institute University of Stuttgart (MPA Stuttgart)	Germany
Federal Office for the Safety of Nuclear Waste Management (BfE)	Germany
Gesellschaft für Anlagen- und Reaktorsicherheit (GRS)	Germany
United States Nuclear Regulatory Commission (US NRC)	United States
Central Research Institute of Electric Power Industry (CRIEPI)	Japan

The main conclusions of the plenary lectures and the discussions during the workshop are:

- Mode, time and location of failure of a nuclear power plant (NPP) pressure barrier strongly determine the progress of the accident and the magnitude of radioactive release to the environment.
- Crucial components for high-pressure failure are the reactor pressure vessel (RPV) (high-pressure melt ejection, direct containment heating), steam generator tube (containment bypass), main coolant line/surge line (secondary damage due to energy release) and small early leaks (early influence on thermal-hydraulic state).
- An insufficient or inadequate consideration of failure models for the integrity assessment of components in thermal-hydraulic analysis, e.g. in Lumped Parameter Codes, such as MELCOR or ATHLET-CD can cause invalidate analysis results in

the further stage of the accident. Therefore, developers and users of such codes should be aware of the scope, the correct use and the reliability of the built-in structure mechanical failure models.

- Large modelling efforts have been given to high-pressure RPV failure in the aftermath of the TMI accident and sophisticated FEM as well as analytical models are available. For local failure of flanges or instrumentation tubes, which are relevant for the analysis of the Fukushima Daiichi accident, so far only a few basic models exist.
- Structure mechanical analysis should be aware about the complex thermal and mechanical load situations during a severe accident scenario, to decide on the allocation of modelling efforts, since only the combination of the weakest part and highest load will determine the location of the pressure boundary failure.
- Failure of components under core melt accident loading is strongly influenced by geometry, temperature, stress and stress state.
- Scatters in creep data are caused by differences in chemical composition, heat treatment, manufacturing processes, testing lab.
- Available short-term creep data for steam generator tube material Alloy 800 (mod.) are not sufficient.
- A study on a station blackout scenario with reflux flow through steam generator tubes (SGTs) shows that failure time of SGT may be in the range of the main cooling line if secondary side is depressurised and 40% SGT wall thinning is assumed.
- Secondary stresses due to different thermal elongations relax with elevated temperatures so that often the simulation can be simplified using symmetric or cut-out models.
- Recalculations of the Fukushima Daiichi accident have shown that the calculated location of the pressure boundary failure strongly depends on the existence and accuracy of failure models. Thermal-hydraulic state variables, like the pressure history are crucially dependent on the size of early leaks, e.g. in instrumentation tubes and flanges.
- Although there is no consensus about the mechanism of depressurisation of the Fukushima Daiichi unit 1 pressure barrier yet, investigations show favorite candidates for depressurisation are leaks of safety and relief valve flanges and tubes of core instrumentation. Models in current severe accident analyses are rather simple. More information from future decommissioning is expected.
- For consideration of uncertainties in severe accident analysis simplified models are needed.
- Failure modes of the RPV can be contributed to three different pressure levels: fusion at low levels (3 – 20 bars), creep starting from the inner surface at medium pressure (~80 bars) and plasticity starting from the outer surface at high pressure (~160 bars).
- The Safety and Relief Valves (SRV) play an important role in the progress of high-pressure core melt accidents. Nevertheless, only few data on the behaviour in the hot state are available.

- In a plant- and site-specific uncertainty analysis of a short-term station blackout scenario rupture of SGT occurred in about 10 % of the calculations and produced source terms that are one to two orders of magnitude greater than for alternative paths. The most significant parameters influencing the likelihood of SGTR are the SV stuck open area fraction upon failure to close and the SG hottest tube thickness. The results show negligible early fatality risk, low source term and low latent cancer fatality. Long-term behaviour dominates the health effect risks.
- Up to now, the consideration of ageing effects is focused on operational loads and seldom considered at beyond-design stage.
- A Large-scale facility to prove in-vessel melt retention (IVMR) for WWER 1000 by external RPV cooling is built at ÚJV Řež.

The conclusions on the benchmark activities are included in Chapters 3, 4 and 5.

## 7. Summary and conclusions

The main tasks within the Components and Structures under Severe Accident Loading (COSSAL) project were a survey on analysis methods, material properties and failure criteria, a benchmark on a large-scale test with a pipe, benchmarks on components of selected pressurised water reactor (PWR) and boiling water reactor (BWR) pressure boundaries, and a workshop in February 2018 at Gesellschaft für Anlagen- und Reaktorsicherheit (GRS) in Cologne.

The answers to the questionnaire provide an overview about the knowledge and the work that has been performed in the participating organisations.

The analysis results on the large-scale test provided by the benchmark participants have been compared to measured data and assessed. The main observations are:

- It has been shown that a geometric non-linear calculation is necessary to account for the changed kinematic properties due to large deformations during the progressive failure process.
- A material law that considers non-linear material properties, i.e. creep and plasticisation effects, is necessary for an accurate simulation and prediction of the time of failure. Norton's Law, a modified Garofalo formulation and a Khachanov-Rabotnov Law were successfully used to describe creep properties of the employed material.
- Complex 3D Finite-Element (FE) models and axisymmetric 2D FE models with selected boundary conditions may show a good consistency with the test results regarding average radial deformation history. Furthermore, FE models (3D/2D) and simplified analytical methods give accurate predictions in failure time, if properly used.
- The asymmetry of the radial deformation could not be reproduced, since it may be influenced by small unknown deviations in geometry and material or rigid body motion of the assembly.
- The history of the axial deformation could not be reproduced. A reason might be that the radially asymmetric deformation might have influenced the displacement transducer measurements.
- The average wall thickness reduction after failure could be reproduced sufficiently. Nevertheless, local maxima at the location of failure were not calculated due to the neglect of effects in the late phase of failure that are not accessible to quasistatic modelling.
- The results show a high sensitivity on the temperature distribution that influences the creep process.

- The sensitivity on variations of pressure load and wall thickness are significant but much lower than the sensitivity from assumptions concerning the temperature distribution in the specimen.

The analysis results on the tasks given for PWR components under a station blackout scenario provided by the benchmark participants have been compared and assessed. All participants conclude that in the selected core melt scenario the main coolant line fails first, then the surge line and then the steam generator tube without damage. Failure of the steam generator tube with damage by wall thinning occurs at wall thickness smaller than about 15 % of the original wall thickness. Early failure of the steam generator tube with heating by circulating gas flow (reflux condenser) becomes more probable. Based on the discussions during the COSSAL Workshop in February 2018 at GRS in Cologne, the main influence factors concerning differences in calculated results are the following:

- Boundary conditions at the pipe end may have significant influence if not properly defined.
- Nonphysical effects at the boundaries prevent a solution convergence or lead to a nonphysical rise in values confused with failure.
- The method of thermal load application is crucial and can evoke transient distributions with thermal gradients, which effect stress gradients.
- The choice of a failure criterion may have a minor influence on the time of failure, if high rise of strains occurs.

The benchmark analysis results on the tasks given for BWR components under a scenario with increasing temperature and constant pressure based on best estimate thermal-hydraulic calculations of Fukushima Daiichi unit 3 have been compared and assessed. Based on the discussions during the COSSAL Workshop in February 2018 at GRS in Cologne the lessons learnt concerning differences in calculated results on the specified flange connection are:

- Attention should be given to the temperature interpolation of creep data in FE codes. In some cases, the coefficients of the creep relation were linearly interpolated before applying them to the creep relation instead of interpolating the results of the creep relation at the adjacent temperatures. This could lead to unphysically high creep strain rates.
- For creep material models, interpolation procedures in FE codes shall be validated, e.g. by generating “material model maps”.
- The use of symmetry can limit the choice of boundary conditions.
- Contact models between bolt, washer and flange body did have a minor influence in the considered scenario.
- Care should be given to the process of preload application and the sequence of steps.
- The distance between model boundaries and the area of examination shall be chosen large enough to prevent mutual influence.
- In general, for a flange in the examined scenario, several failure modes are possible depending on geometry, radial positions of the bolts and lines of action of the forces and gasket material.

- Plasticisation and short-term creep effects are not negligible and might significantly influence the failure time.

Effects that were not considered in the benchmark on a flange connection, but may play a crucial role might include:

- heat exchange between bolt and hole;
- thermal inertia effects;
- feedback loop of the mechanical calculation on thermal contacts;
- heating of the gasket/bolt due to premature leakage flow;
- loads on the large faces of the gasket once a gap arises.

The COSSAL results therefore show that FE methods are precise and robust for assessment of global failure but simplified analytical methods are partly adequate. They may give accurate predictions in failure time, if properly used and application limits are considered. FE models can be used for local failure and complex components, but currently the level of confidence might be lower than for global failure.

The behaviour of components under severe accident loading is important for the simulation of scenarios by system codes. Structure mechanical behaviour of components, and particularly the failure of components, has consequences on the thermal-hydraulic behaviour of severe accidents. Investigations on the pressure barrier of Fukushima Daiichi unit 1 emphasise this statement. Therefore, knowledge exchange about application limits of the failure assessment methods, the sensitivity of the results and recommendations on proper use should be improved. This could be achieved by future interdisciplinary activities. Furthermore, short-term creep data for pressure boundary steels are partly incomplete, especially for steam generator tube materials. Finally, the safety relevant topic “component behaviour under severe accident loading” includes challenging tasks, which in part need additional research activities, particularly on:

- assessment of local failure and integrity of complex components;
- size quantification of early leaks;
- assessment of local loads in RPV, piping and valves;
- consideration of ageing effects/pre-existing damage, e.g. cracks;

Furthermore, the main factors with the uncertainties should be specified for each case to allow the sensitivities of the results to be investigated.



## 8. References

- /GRS15/ Bläsius, C., Sievers, J., GRS, Germany: GRS contribution to COSSAL Task 3, August 2015.
- /GRS17a/ Arndt, J., Bläsius, C., Sievers, J., GRS, Germany: GRS contribution to COSSAL – PWR Benchmark, August 2017.
- /GRS17b/ Bläsius, C., Sievers, J., GRS, Germany: GRS contribution to COSSAL – BWR Benchmark, December 2017.
- /INS15/ Steingrimsdottir, K., Manngard, T., Gunnars, J., Storesund, J., Inspecta Technology AB: Results from Inspecta Technology (Task 3), November 2015.
- /INS17a/ Bonnaud, E., Andersson, D., Manngard, T., Gunnars, J., Inspecta Technology AB: COSSAL-Task 4.1: Failure analysis of primary-circuit components in a high-pressure core-melt scenario of a generic PWR during total station blackout, January 2017.
- /INS17b/ Andersson, D., Manngard, T., Bhatti, A., Gunnars, J., Inspecta Technology AB: COSSAL-Task 4.2: Analysis of local failure and leakage of BWR components in a high-pressure core-melt scenario, December 2017.
- /JAE15/ Katsuyama, J., Li, Yinsheng (Japan Atomic Energy Agency) Japan, Takakura, K (Nuclear Regulation Agency): COSSAL Benchmark Analysis (Task 3), September 2015.
- /JRC17/ Simonovski, I. and Baraldi, D., JRC Petten: Components and Structures under Severe Accident Loading (COSSAL) – BWR Benchmark (Task 4.2), 2017.
- /KTA13/ KTA 3201.2 Components of the Reactor Coolant Pressure Boundary of Light Water Reactors, Part 1: Materials and Product Forms, November 2013.
- /MPA88/ MPA University Stuttgart: Experiments on the failure of a main coolant line due to creep rupture under high sytem pressure, final report of project no. 15007712, 1988 (in German).
- /MPA90/ Maile K., A. Klenk, V. Obst, D. Sturm: Load carrying behavior of the primary system of PWR's for loads beyond the design limits. Nuclear Engineering and Design 119 (1990), pp. 131-137.
- /MPA99/ MPA University Stuttgart: Determination and modelling of material behavior of reactor steels under multiaxial loading in the temperature range from 400 °C up to 1 000 °C, final report of project no. 1501010, report number 8779 01 000, 1999 (in German).
- /MPA05/ MPA University Stuttgart: Description of the short-time creep rupture behavior at temperatures up to 1200 °C exceeding usual design on the basis of damage mechanisms, final report of project no. 1501257, report number 8306 000 000, 2005 (in German).

/NEA15/ Benchmark Study of the Accident at the Fukushima Daiichi Nuclear Power Plant (BSAF Project), Phase I Summary Report, NEA/CSNI/R(2015)18, 2015.

/PVA15/ Varpasuo, P., PVA Engineering Services, Finland: Contribution to COSSAL2015 Benchmark (Task 3), May 2016.

/VUJE15/ Hermanský, P., VUJE, Slovak Republic: VUJE Results (Task 3), 2015.